A CHEMOSTRATIGRAPHIC AND DETRITAL ZIRCON GEOCHRONOLOGICAL ANALYSIS OF UPPER CRETACEOUS STRATA: APPLICATIONS FOR DATING AND CORRELATING STRATA

BY

EDWARD MOREHOUSE

Submitted to the graduate degree program in Geology and the Graduate Faculty of the University of Kansas in partial fulfillment of the requirements for the degree of Master of Arts.

_____

Chairperson: Luis González

_____

Mike Blum

_____

Andreas Möller

Date Defended: May 5 2015

The Thesis Committee for EDWARD MOREHOUSE
certifies that this is the approved version of the following thesis:

A CHEMOSTRATIGRAPHIC AND DETRITAL ZIRCON GEOCHRONOLOGICAL ANALYSIS OF UPPER CRETACEOUS STRATA: APPLICATIONS FOR DATING AND CORRELATING STRATA

_____

Chairperson: Luis González

Date approved: May 13 2015

ABSTRACT

Rates of sedimentation, length of hiatus, temporal relationships and absolute age of strata are all difficult to determine in clastic non-marine and shallow marine environments due to their erosive and rapidly fluctuating depositional nature. High energy environmental conditions, erosion, and diagenesis make preservation of common chronological markers unlikely. Lack of chronological information results in the interpretation of sedimentation rates, length of hiatus/erosion, and genetic relationships based on chronological information obtained from strata bracketing the section of interest. Temporal relationships between strata and sequence stratigraphic interpretation can also be based on lithostratigraphic correlation to other dated sections. However, this can be highly unreliable when the lithological data is discontinuous, complex, or appearing homogeneous (e.g. shales or amalgamated sandstones). To provide chronostratigraphic control, this study demonstrates the utility of using high resolution organic carbon ($\delta^{13}C_{OM}$) stable isotope chemostratigraphy to better understand the timing of fluvial and shallow marine siliciclastic successions from a 200m thick section of Mid-Campanian Mesaverde Group strata. Because recognizable changes in the carbon cycle can occur in the 10's to 100's of the years, organic carbon chemostratigraphy has the potential to precisely date individual strata at a resolution greater than is achievable with $^{87}Sr/^{86}Sr$ techniques. Constraining the organic carbon isotopic data using detrital zircon geochronology allows better understanding of the relative and absolute timing of major periods of deposition, as well as the temporal relationships between strata. The studied rock units include: The Grassy highstand sequence set and Desert lowstand sequence set of the Desert Member of the Blackhawk Formation, the Castlegate Sandstone, and the Buck Tongue of the Mancos Shale.

Detrital zircon (U/Pb) radiometric and chemostratigraphic studies conducted east of Green River, Utah, reveal that the top of the Grassy highstand sequence set was deposited sometime between 76.9–77.2 ± 0.1 Ma. The Desert lowstand sequence set was deposited sometime between 76.2–76.9 ± 0.4 Ma. The lower Castlegate Sandstone was deposited sometime between 75.8–76.2 ± 0.4 Ma. The Buck Tongue of the Mancos Shale was deposited sometime between 75.2–75.8 ± 0.4 Ma. The Sego Sandstone was deposited at 73.3 ± 1.3 Ma. Duration of unconformities during lowstand incisional events is estimated to be 100–200 kyr based on global eustatic curves for the Campanian.

ACKNOWLEDGEMENTS

I am greatly indebted to Dr. Luis González for backing this project. This project would not have succeeded without his mentorship, encouragement, and financial support. This project would also not have been possible without Dr. Mike Blum. He has shared much of his time and expertise, provided access to the ExxonMobil Sego #2 core, and shared the detrital zircon dates. I am thankful to Dr. Diane Kamola for helping me in the field, and for taking time to share ideas. I also wish to thank my committee member, Dr. Andreas Möller for his encouragement, guidance in writing, and expertise.

I would like to thank Greg Cane and the University of Kansas Keck Paleoenvironmental and Environmental Stable Isotope Laboratory for the chemostratigraphic analyses and support during 2014-2015. I am very thankful for KUEA support from the Roscoe G. Jackson III Graduate Research in Geology Scholarship, the Alice Mitchel Jackson Award, the Department of Geology at the University of Kansas, and my parents for their financial support.

Field work would have taken several weeks without the hard work of Tucker Steen, Ty Tenpenny, and Matt Green, I am very grateful for their time. I am also deeply appreciative for the guidance in writing and the various expertise provided by Adam Jackson, Dr. Steve Hasiotis, Jeff Oalmann and Raymond Morehouse.

Most of all, I thank my wife Jaylyn for supporting me through it all. I could not have done it without her love and encouragement. I would also like to thank my sons Briggs, Finn, and Max for being there for me even though I was gone so much. They gave me the motivation to finish strong.

Table of Contents

INTRODUCTION

Rapid changes in depositional rate, the low probability of preserving chronological markers, variable provenance, and the unknown length of hiatuses and/or erosional events all combine to introduce large uncertainties in the reconstruction and quantification of the depositional history of fluvial systems (Miall 2014). Changes in ecosystem (e.g. Ripple & Bechsa 2004; Gurnell 2003; Polvi & Wohl 2012, 2013), climate (e.g. Vandenberghe 2003), tectonics (e.g. Willis 2000), and eustacy (e.g. Van Wagoner et al. 1988) can all have profound effects on fluvial system dynamics. Because of the variability and overlap between these different controls, it can be difficult to identify what the primary driving forces for sedimentation were for fluvial systems preserved in the rock record. In fluvial sequences lacking chronostratigraphic control, interpretations of depositional rates, temporal relationships, and fluvial system driving forces must rely on geochronological data bracketing the investigated strata. This interpolated geochronology is then applied throughout the study area and quantification of rates is approximated using modern analogs (e.g. Aschoff & Steel 2011; Miall 2014). While this is sometimes the only technique available due to lack of data, the interpolation of dates from outside the study area or studied interval magnifies already existing uncertainties in the study of high-energy environments caused by the abundance and unpredictable length of unconformities (Miall 2014). Therefore, in-situ chronostratigraphic understanding of the fluvial strata in question is immensely valuable if not necessary to untangle the depositional history and processes affecting a fluvial system.

Without chronostratigraphic information, temporal relationships between fluvial strata are based solely on lithostratigraphic correlation, and assumptions of factors controlling sedimentation (Blum & Törnqvist 2000; Blum 2013). Lack of geochronological data may also be

problematic when trying to apply current sequence stratigraphic methodologies to the non-marine environment, which is characterized by widespread deposition and erosion during all stages of base level change (Strong & Paola 2006, 2009). Base level change or cyclicity refers to changes in lowest level of flow in a body of water. Changes in base level commonly are the product of tectonic uplift or subsidence, and/or rise or fall in sea level. Revealing the primary factors governing incisional and depositional events can be difficult and result in differing interpretations of sequence stratigraphic frameworks **(Fig. 1)** (Adams & Bhattacharya 2005; Strong & Paola 2009; Blum et al. 2013). Because fluvial depositional and incisional events can occur throughout a complete base level cycle, using the current sequence stratigraphic approach (e.g. Van Wagoner 1995) alone does not allow fluvial strata to be distinguished as part of events associated with a specific period of the base level cycle (e.g. lowstand). Sequence stratigraphic methods also do not allow high-resolution chronological interpretation of the numerous events that produce incised valley fills (IVF) **(Fig. 2)**. Without high resolution seismic, or chronostratigraphic data, lapout relationships between one-dimensional data sources (e.g. outcrop or well) must be interpolated based on assumptions of rock relationships (Bhattacharya 2011). To determine if incisional and depositional events are truly driven by base level change, the chronostratigraphy must be understood so that local sedimentary events can be compared to regional tectonic events and dated changes in eustacy.

Since some of the driving forces affecting fluvial dynamics (e.g. climate change) are regional or global in scale, their impact can be reflected and recorded in many other stratigraphic successions (Jarvis et al. 2002, 2006). Geochemical markers that are regional in scale can provide the means for high-resolution correlation of strata in close proximity (e.g. sedimentary

basin). Events that are global in scale afford the opportunity to correlate to precisely-dated successions anywhere regardless of depositional setting (Jarvis et al. 2002, 2006).

Organic carbon isotope chemostratigraphy is a technique that can resolve some of these problems or uncertainties by high-resolution correlation of individual strata. This includes the correlation of channel belt sand bodies, coal beds, paleosols, overbank deposits and other fluvial facies giving the ability to unambiguously identify coeval deposits and events. Correlation to well-dated reference curves (e.g. Jarvis et al. 2006) can allow application of absolute dates to sedimentary deposits and processes.

To test this technique, and in hopes of using it to construct a detailed chronostratigraphy, I have conducted a high-resolution organic carbon isotope analyses of well-known fluvial/shallow-marine siliciclastic rocks from the Book Cliffs, Utah. To constrain my isotopic data, I have utilized detrital zircon U-Pb geochronological data generated by two research groups led by Joel Saylor and Mike Blum. With these radiometric ages, I gain the ability to correlate to dated isotope curves with a higher level of confidence.

Geologic Setting

Non-marine and shallow-marine deposits within the well-studied Campanian siliciclastic formations of the Mesaverde Group, Utah, are well-exposed in outcrops in the Book Cliffs east of Green River **(Fig. 3)**. During the Campanian, the Cretaceous Western Interior Basin was flooded forming the Cretaceous Western Interior Seaway (KWIS) (Hampson 2010). This flooding was due to increased sea-floor spreading, which raised the global sea level (Gurnis 1993; Kaiho & Saito 1994). During the Campanian in Utah, rivers were flowing down from the Sevier orogenic belt to the west and depositing sediments across a wide coastal plain and into the

KWIS to the east (DeCelles 2004; Hampson 2010). Interpretations on how these sediments were deposited as strata and how these strata relate to each other genetically is what formed the backbone for the ExxonMobil fluvial sequence stratigraphic model put forth by Van Wagoner (1995). Many of these strata lack high-resolution chronological constraints, making quantification of depositional history difficult, and the sequence stratigraphic framework open to different interpretations (Miall 2014; Blum et al. 2013).

Stratigraphy

Outcrops of Upper Cretaceous strata from the Blackhawk Fm. up to the Neslen Fm. extend east of Green River from Tusher Canyon to Thompson Canyon. The stratigraphic nomenclature used in this study is a combination of sequence stratigraphic and lithostratigraphic units. The main lithostratigraphic units include the Mancos Shale (Mancos), Blackhawk Fm., Castlegate Sandstone (Castlegate), Sego Sandstone (Sego), and Nelsen Fm. These formations further subdivide into the Grassy and Desert Members of the Blackhawk Fm., and the Buck Tongue of the Mancos Shale (Hampson 2010). The Desert Member has been subdivided into sub-members by Van Wagoner (1991) into: the Grassy highstand sequence set (Grassy LSF) and the Desert lowstand sequence set (Desert FLV). The fluvial facies terminology used in this thesis follows that described in Blum et al. (2013).

For the purposes of this study the most basal formation discussed is the Mancos Shale. According to Hampson (2010), the Mancos Shale was deposited in a distal marine environment within the KWIS. Interfingering into this marine shale are several fluvial/marginal marine sandstone wedges, which have been interpreted to have been sourced from the Sevier Highlands to the east and deposited into the Western Interior Basin during the Late Cretaceous (Van

Wagoner 1995; Hampson 2010). Four of these progradational sandstone bodies and a shale inter-tongue make up the 200m thick section measured in this study: The Grassy LSF and Desert FLV of the Desert Member, the Castlegate, the Buck Tongue, and the Sego.

Above the Grassy LSF, and floored by an erosional unconformity, the Desert FLV consists of siltstone, medium-fine sandstone, coal and paleosol deposited within a well-studied incised valley fill (IVF) (Van Wagoner 1991). In some locations a fluvial erosional unconformity exists separating the top of the Desert Member from another well studied IVF, the Castlegate (Van Wagoner 1991). Similar in nature to the Desert Member IVF, the Castlegate contains siltstone, fine to medium-grained sandstone, coal and paleosol. Nearing the top of the Castlegate, the sandstone fines upward into the Buck Tongue. The Buck Tongue consists of siltstone and shale with an occasional fine sandstone bed, and has been interpreted to be a distal shoreface deposit resulting from base level rise (Van Wagoner 1995). Overlying the Buck Tongue is another progradational sandstone wedge, the lower Sego, which is the uppermost formation used in this study.

The grassy member of the Blackhawk, and Sego Sandstone have been dated using Ammonite zones and lithostratigraphic correlations proposed by Fouch et al. (1983) and Cobban et al. (2006) **(Fig. 4)**. These dates will be explored in more detail in the following chapter.

Prior Chronostratigraphic Work

A detailed and comprehensive biostratigraphic zonation based on ammonites, inoceramids, constrained by radiometric ages (e.g. Izett et al. 1988) has been constructed for the Late Cretaceous of the western interior of the United States by various authors (e.g. Gill & Hail 1975; Fouch et al. 1983; Cobban et al. 2006). Fouch et al. (1983) applied this biostratigraphic

framework to the Book Cliffs, and their report continues to serve as the chronostratigraphic foundation for stratigraphic and sedimentological studies (e.g. Hampson 2010; Aschoff & Steel 2011; Miall 2014). Based on this prior biostratigraphic work, Cobban dates the base of the Grassy Member at 80.58 ± 0.55 Ma, and the top of Sego at 80.58 ± 0.55 Ma and 75.19 ± 0.11 Ma respectively, based on correlation of dated ammonite zones (Aschoff & Steel 2011). Using an early biostratigraphic study from 1975 (Gill & Hail 1975), the top of the Blackhawk Formation has been estimated to be ~79 Ma, the Castlegate ~77 Ma, and the Buck Tongue ~75 Ma (Aschoff & Steel 2011). The data indicate that circa 4 Ma of depositional history are encompassed by the 160m of fluvial and marine sediments studied here.

It must be noted that the ammonites used to date strata between Green River and Thompson Canyon Utah were collected from locations outside my study area such as Price Canyon, Utah, and Grand Junction, Colorado. The strata in which these ammonites were found were then correlated across tens to hundreds of kilometers of temporally complex stratigraphy, using early lithostratigraphic data (Fouch et al. 1983; Cobban et al. 2006). Thus there are uncertainties introduced by the correlations across large distances. In this study I aim to improve the chronostratigraphy through the use of detrital zircon (DZ) data and stable isotope analysis. Much of this data was collected from within the study area or within a few kilometers.

Sequence Stratigraphy

Strata of the Desert Member, the Castlegate, Buck Tongue and Sego were placed in a sequence stratigraphic framework by Van Wagoner (1991), and have been used to exemplify sequence stratigraphic concepts (e.g. Van Wagoner 1991, 1995; Miall 1993; Yoshida et al. 1996; McLaurin & Steel 2000; Miall & Arush 2001). According to Van Wagoner (1991), the Desert

Member consists of one complete depositional sequence, containing one lowstand systems tract (LST), a transgressive systems tract (TST) and a highstand systems tract (HST). The Castlegate consists of one depositional sequence containing several nested IVF's (Van Wagoner 1991). Overlying the Castlegate, the Buck Tongue contains a TST and LSF. In determining systems tracts, Van Wagoner assumed constant fluvial discharge and sediment load. Quantitative absolute data of the duration of deposition of each formation is lacking as are estimates for the length of hiatus (non-deposition and erosion) (Miall 2014). Elapsed time between each sequence has been estimated to be 200–400k years (Van Wagoner, 1995).

Alternative Interpretations

Van Wagoner's sequence stratigraphic model (Van Wagoner et al. 1988), which served as the paradigm for fluvial-marine sequence stratigraphic interpretations, has been challenged by a number of researchers (e.g., Yoshida et al. 1998; Adams & Bhattacharya 2005; Anderson, 2005; Strong & Paola 2008; Martin et al. 2009; Bhattacharya 2011; Holbrook et al. 2012; Blum et al. 2013). Much of the difference in interpretation centers on whether or not a sequence boundary represents a geologically instantaneous, time-correlative surface that separates younger and older strata and/or on the correct placement/existence of sequence boundaries within a previous framework. Sequence boundaries are defined as regional-scale erosion surfaces, which formed during a period of complete sediment bypass and knickpoint migration during a fall in relative sea level (Van Wagoner et al. 1988). However, recent flume and field studies (e.g. Vandenberghe 2003; Strong & Paola 2008; Martin et al. 2009) indicate that previously interpreted fluvial sequence boundaries may fail to meet the criteria for definition as a sequence boundary. These studies have shown that regional fluvial erosion surfaces could form over the entirety of a relative sea level change cycle (Strong & Paola 2008), be forced by variation in

climate and not base level (Vandenberghe 2003), and represent periods of simultaneous deposition and erosion (Vandenberghe 2003; Strong & Paola 2008; Blum et al. 2013).

High Resolution Chemostratigraphy and Detrital Zircon Geochronology

High resolution carbon isotope chemostratigraphy, which captures quasi-instantaneous events that affect atmospheric CO_2 composition (Sundquist & Visser 2004), may be used as a chronostratigraphic tool similar in nature to strontium isotope stratigraphy (Elderfield 1986; McArthur et al. 1991) to better resolve the timing and the relationship between various events in high energy clastic non-marine and shallow marine deposits. It is well established that carbonate rocks and sedimentary organic matter carbon isotopic compositions have varied through time as a result of changes to the global carbon cycle producing globally correlatable signals (e.g. Kaufman et al. 1992; Jarvis et al. 2002, 2006). Differing from $^{87}Sr/^{86}Sr$ ratios whose variability is often unresolvable in timeframes less than 100kyr (McArthur et al. 1994), carbon cycling between the oceans near surface and atmosphere occurs much more quickly, within tens to hundreds of years (Sundquist & Visser 2004). Carbon cycling between the entirety of the ocean and atmosphere occurs within hundreds to thousands of years due to variations in the terrestrial biosphere, rates of organic carbon storage and exhumation, and variations in the abundance of reactive marine sediments (Sundquist & Visser 2004). In a broad sense, the $\delta^{13}C$ value of the ocean affects the entire carbon cycle, and is reflected in the isotopic composition of terrestrial plants and soils. Thus, the sedimentary organic matter preserved in the rock record should or could capture these rapid changes and be useful for correlating events.

U-Pb dating of detrital zircons (hereafter DZs) is a well-established radiometric method used for determining the provenance and maximum age of deposition of sediments and

sedimentary rock (e.g. Davis et al. 2003; Fedo et al. 2003; Gehrels 2011; Gehrels et al. 2011; Laskowski et al. 2013; May et al. 2013). Zircon is produced in a wide range of igneous and metamorphic rock types, and is exceptionally durable. Because of its durability, zircon abundance has increased in the Earth's crust over time to the extent that it is found in virtually every sedimentary deposit (Fedo et al. 2003). Although zircons occur in both plutonic and volcanic igneous rocks, the likelihood of finding a detrital grain that closely approximates the age of sediment deposition depends on the sediment being sourced from a region with active volcanism (Fedo et al. 2003). The western margin of North America is known to have been volcanically active during the Campanian, which makes DZs potentially useful for attaining maximum depositional ages on siliciclastic rocks (Bertog 2013). Whereas the overall spectrum of U-Pb ages on DZs from a single sample provides information on provenance, the youngest 3 statistically overlapping dates obtained are typically used to calculate maximum-depositional ages (hereafter MDA; Dickinson & Gehrels 2009), based on the assumption that the strata in question can be no older than the youngest zircons contained therein. In this thesis, MDAs are used to constrain chemostratigraphic profiles, and tie them to the chronologically-controlled global organic carbon reference curve for the Cretaceous (Jarvis et al. 2006) **(Fig. 5)**

My chemostratigraphic profiles match the global reference curve with some confidence due to constraints provided by MDAs from a dataset provided by Joel Saylor and Mike Blum. Using DZ geochronology and the dates drawn from the global reference curve has allowed me to absolute date individual depositional sequences at a 400kyr resolution. This resolution was estimated by Jarvis (2006) for the Campanian section of his reference curve based on an assumption of uniform depositional rates of chalk. These depositional rates were validated using strontium isotopes and comparisons with other Campanian aged chalk successions globally

(McArthur et al. 1993a,b). Using this uniform depositional rate of chalk, Jarvis then extrapolated depositional ages through his Campanian-aged chalk succession from the dated Campanian-Santonian and Campanian-Maastrichtian contacts (Ogg et al. 2004). Drawing upon studies on orbital cyclicity, biostratigraphy, tephrastratigraphy, and other methods, Jarvis was able to calibrate depositional age of his chalk succession further and ultimately achieve a 100-400kyr resolution (Jarvis 2006).

While dating depositional sequences with detrital zircon u/Pb ages, and chemostratigraphic correlation is possible, approximating the duration of missing rock record is more challenging. Identification of significant unconformities between strata is possible in the form of truncated chemostratigraphic timelines, but quantification of the duration of missing rock record is much more difficult to determine. Dates extrapolated from chemostratigraphic correlations form a time window during which deposition could have occurred, but not a well-defined point in time. Likewise, the detrital zircon U/Pb dates commonly available have low stratigraphic resolution, and errors too high (ca. 2-5 Ma) to precisely quantify the duration of rock record missing. However, the age correlation to Miller et al.'s (2005) sea level curve may make approximation of the duration of unconformities possible, assuming that the unconformity is the product of changes in eustacy **(Fig. 5)**. Jarvis (2006) made a strong case that change in global sea level is reflected by the organic carbon isotope composition of the Ocean. Falls in sea level expose and reintroduce buried “light” carbon making the oceans isotopic composition “lighter”, whereas a rise in sea level results in increased burial potential and removal of “light” carbon from the carbon cycle making the oceans isotopic composition “heavier”. If incisional events or the durations of unconformities are directly connected to the duration of eustatic fall, then the drop in eustacy should approximate the duration of unconformity. This can be tested by

examining the dated global sea level curves and the changing isotope composition across unconformities and throughout strata.

It must be noted that while the techniques stated about may allow us to approximate duration of major unconformities, fluvial systems are defined by erosion and reworking down to finer scale than can currently be reconciled. It is highly unlikely with the technology available that many of the smaller erosional events found in fluvial systems could ever be resolved (e.g. bounding surfaces in trough cross stratification). Until technology advances to stage that individual laminae can be dated, quantification of total "missing time" in the rock record will have to rely on the application of studies of modern analog systems to the available geochronological data (e.g. Miall 2014).

METHODS

Outcrop Studies

The Book Cliffs strata used for the chemostratigraphic portion of the study are located east of Green River, Utah and west of Thompson, Utah. The Sego #2 drill core, acquired from Sego Canyon by ExxonMobil served as the primary stratigraphic and geochemical source for this study. The drill core study was accompanied by outcrop studies in Thompson and Blaze Canyons, which are located near the Sego #2 well bore (**Fig. 3**). Tusher Canyon chemostratigraphic data produced previously by Cornwell (2012) is also used in this study. These canyons were chosen because they are distal or proximal representations of the strata found in the core, and they contain outcrops with long sections of rock accessible for sampling. Outcrop sections were measured and described at a 10 cm scale using a Jacob's staff and Brunton® compass. Sedimentary structures, grain size, lithology, fossils, and trace fossils were described. The sampling interval was approximately 20 cm vertically. Roughly 10 g of sample was collected from 4-6" within both outcrop and core using a portable hammer drill with 8" tungsten carbide masonry bits.

Detrital Zircon Dating

Detrital-zircon geochronological studies of Blackhawk to Sego strata from several locations in Utah are currently being conducted by two research groups led by Joel Saylor (University of Houston) and Mike Blum (formerly of ExxonMobil Upstream Research, now at the University of Kansas). They have given access to preliminary data, from which the time frame for chemostratigraphic data can be constrained.

Outcrops samples for DZ studies were collected by ExxonMobil Upstream Research and by the University of Houston from exposures within Horse, Tusher, and Thompson Canyons (**Fig. 3**): Bulk samples were collected within each exposure, from which zircons were separated using standard heavy liquid separation techniques. U-Pb analysis of between ~150-300 zircons per sample was conducted by Laser Ablation Inductively Coupled Plasma Mass Spectrometry (LA-ICP-MS). Samples collected by ExxonMobil Upstream Research and by the University of Houston were analyzed at the Arizona Laserchron Center: A complete description of analytical procedures is provided in **Appendix D;** Laserchron 2015.

Following Dickinson and Gehrels (2009), the most robust MDA is defined as the mean of at least three youngest grains that overlap at 2σ uncertainty interval. I am including all youngest grains that overlap at 2σ uncertainty interval to address the larger uncertainty of our zircon ages. In order to maintain this technique, I am excluding samples which contain less than three grains overlapping from the final geochronological results. Understanding there is still uncertainty, some samples will have MDA's that are significantly older than actual depositional age constrained by other means, whereas others have MDAs that are consistent with, or younger than, depositional ages assigned previously (Fouch et al. 1983; Cobban et al. 2006).

While not the focus of this study, it is worthy of mention that the detrital zircon data provided to us contains provenance information in addition to MDAs. Frequency and age distribution of zircon grains can be used as a provenance indicator, as certain-aged grains are known to have originated from specific geographic locations (Fedo et al. 2003). These grains are often reworked and transported from basin to basin due to tectonic uplift and subsidence before ultimately making their way to marine sediments. Therefore, careful analysis of the zircon assemblage can provide some insight on the long term provenance of strata. (e.g. Dickinson & Gehrels 2008a,b, 2009; May et al. 2013; Laskowski et al. 2013).

Chemostratigraphy

All analyses were conducted at the University of Kansas Keck Paleoenvironmental and Environmental Stable Isotope Laboratory (KPESIL). 1218 ~10g samples were collected, either pulverized directly from the rock using a hammer drill, or as hand samples. Approximately 1–2 g of each sample was ground into powder using an ore grinder and mortar and pestle (if not already pulverized), and then oven-dried at 45°C for 24–48 hours. Decarbonation was accomplished by the introduction of 40 ml of 1.65 M hydrochloric acid to digest and remove all carbonate material, followed by rinsing with deionized-distilled water until the supernatant reached neutrality. Samples were then oven-dried at 45°C for 1–2 weeks, weighed and re-homogenized with a mortar and pestle. Sample weight lost during decarbonation is assumed to be all carbonate in the sample.

Following the decarbonation procedure, 903 samples were analyzed for TOC and organic carbon $\delta^{13}C$ values. Depending on the concentration of carbon within the sample, 0.05–75 mg of sample was weighed out and encapsulated in tin foil, and then combusted at 1060°C using a

Costech Elemental Analyzer connected via a CONFLO III to the inlet of a ThermoFinnigan MAT 253 continuous-flow mass spectrometer. The analysis resulted in $\delta^{13}C$ values for both bulk sedimentary organic carbon and total organic carbon. All data is reported relative to V-PDB. Instrument precision was monitored and maintained during each run using three different reference standards: DORM, USGS-24 and ANU. Quality control was achieved each run using the following reference standards: DORM, Montana Soil, and Peach Tree Leaves.

RESULTS

ExxonMobil Sego #2 Research Core

Stratigraphy

Approximately 150 m of section was measured from the Sego #2 research core supplied by ExxonMobil, which had once served as an integral component of Van Wagoner's study of Book Cliff sequence stratigraphy (Van Wagoner et al. 1990) (**Fig. 6)**. The drill core was extracted from a well located in Sego Canyon, and encompasses strata from the Upper Blackhawk to the Neslen Fm. For the purposes of my study, we measured and sampled up to the Sego contact. The drill core also came with matching well logs, which have been used in the discussion to aid in my interpretation of facies and sequence stratigraphy. The core has been measured at a 10cm scale with the base of the core (878.29' depth being referenced as 0.0 m). At the base of the Sego 2 core, what has been interpreted as the Grassy LSF extends from 0.0–49.0 m and consists of upward-coarsening shales and sandstones (Van Wagoner 1991). This section is heavily bioturbated; trace fossils include *Chondrites*, *Ophiomorpha*, *Skolithos*, and *Thalassinoides* **(Fig. 7)**. Interbedded within the shales are occasional medium- to fine-grained sandstone beds characterized by hummocky cross stratification (HCS). These sandstone beds increase in thickness toward the top of the interval. In the middle of the Grassy LSF, at 30.0 m, there is a 1.5 m thick sandstone that has been calcified into a dense, impermeable hardcap. At approximately 49.5 m, there is an erosional surface A. (**Fig. 8)**. Above the erosional surface there is an abrupt change to sandstone containing much less mud and silt, no trace fossils, and trough cross stratification instead of HCS. At 52.6m is an erosive surface B, previously interpreted as fluvial (Van Wagoner 1991), which separates the Grassy LSF from the Desert FLV **(Fig 8)**.

The Desert FLV of the Desert Member consists of stacked heterolithic deposits with thin layers of siltstone and thick sandstone beds containing trough cross bedding, small coal specks, and root traces. This deposit spans 12.4 m and culminates in a 0.5 m thick coal bed at 62.2 m. Directly above this coal are meters-thick sandstone bodies containing pieces of wood, flasered-beds and HCS. At 69.6 m there is another erosional surface, separating the Desert FLV of the Desert Member from the overlying Castlegate Sandstone.

The Castlegate consists of medium- to fine-grained sandstone alternating from sections of fine-grained sandstone containing double mud drapes, what has been interpreted as sandstone-siltstone tidal bundles **(Fig. 9)**, and flasered cross beds, and medium-grained sandstone containing large scale trough cross stratification, rip up's, and woody debris. The Castlegate Sandstone gradually fines upward from 85.0 m to a surface at 86.1m, previously described as the Buck Tongue contact, where fissile shale and siltstone becomes the dominant lithology (**Fig. 10)**. The Buck Tongue interval contains three upward coarsening shales, which contain abundant cm-thick fine sandstone and very little evidence of bioturbation. At 133.0 m there is another fluvial erosional surface separating the Buck Tongue from the overlying Sego Sandstone, which consists of several stacked fluvial and marine deposits not described in this project.

Organic Carbon Chemostratigraphy

From the base of the section up to approximately 14.5 m the $\delta^{13}C$ value is quite uniform at -25.5‰ ±0.5 **(Fig. 6)**. Above 14.5 m to ~50 m the $\delta^{13}C$ signal increases in variability and shifts to an average of ~ -26.5‰ ±1.0. Two prominent positive excursions are located at 43.0 m (+2.1‰) and 46.2m (+2.6‰). Moving up the section, other notable excursions are located at 53.0 m (+1.5‰), 55.0 m (+2.1‰), 60.0 m (+2.3‰), 62.6 m (-0.8‰), 63.2 m (-0.8‰), 66.2 m (-

1.8‰), 72.6 m (-1.8‰), and 77.6 m (-1.8‰), From 79.4 m to 82.0 m is a double peak 4.0‰ negative and positive excursion pattern. Above this event, at the Buck Tongue flooding surface, isotopic composition remains relatively unchanging at ~27.0‰ ±0.5 until the Sego Sandstone unconformity.

TOC and % Carbonate

The sandstones from 0.0 m to approximately 30.0 m, below the calcified caprock, contain ~2.0% TOC **(Fig. 6)**. Above the calcified zone at 30.8m, TOC drops to ~0.1% except for small beds of organic rich shale, paleosols or coal which contain up to 56.7% TOC. High variability (0.1-56.7%) in the rocks TOC continues up to the Castlegate/Buck Tongue contact, above which, TOC remains steady at ~1.6%.

From 0.0 m, Carbonate weight percent is approximately 15.0% up to a 1.2 m thick calcified zone at 30.8 m where carbonate makes up ~55% of the rock. Above this calcified zone, carbonate makes up ~20% of the rock until the Desert FLV contact at 49.8 m, where there is an abrupt shift from calcite to silica cementation. The sandstone remains siliceous until 61.6 m where there is a jump in carbonate cement to over 31.1%. Following this spike, carbonate cement remains present up in concentrations of ~10.0% through the coal and hummocky cross bedded sandstone increasing in concentration to ~20.0% until the contact with the Castlegate. At the Desert-Castlegate contact there is another abrupt drop in carbonate cement to 6.6% at 71.0 m. Carbonate weight percent increases and decreases abruptly from 20.0% to 2.0% up through different sandstone bodies within the Castlegate. Above the Castlegate/Buck Tongue contact carbonate makes up a consistent ~10.0%.

Thompson Canyon

Stratigraphy

The base of the Thompson Canyon measured section begins in the Grassy LSF of the Desert Member. From 0.0–10.2 m the drill core is made up of two, fine-grained HCS beds, divided by a 0.5m shale bed **(Figs. 11 & 12)**. At 10.2 m is an erosional surface separating the Grassy LSF from the Desert lowstand sequence set. The base of the Desert Member consists of medium-fine sandstone, truncated by an erosional surface at 11.2 m, above which is a ~8 m section of inclined heterolithic strata, which fines upward to a siltstone plug and coal bed. Large organism tracks and soft sediment deformation are abundant at the top of the heterolithic strata interval, below the clay plug. Above the coal bed is more medium-fine sandstone strata exemplified by HCS, as well as mud drapes and wood debris. From 24.6-27.8 m the section could not be measured, but is inferred to be similar to the overlying unit of siltstone/sandstone and contains thin coals, roots, and lenticular sandstone bodies, which extends from 27.8 to 30.4 m. This unit has previously been interpreted as the basal unit of the Castlegate Sandstone (Van Wagoner 1995). Above 30.4 m the remaining interval consists of m-grained sandstone with large pieces of wood with *Teredolites*, current ripples, and mud drapes.

Organic Carbon Chemostratigraphy

Isotopic composition averages around -26.2‰ ±0.5 from the base of the section to 9.0 m, when there is a +3.0‰ excursion ending at -23.6‰ at 10.2 m **(Fig. 12)**. From 10.0–15.0 m the isotopic composition is highly variable, but forms a convex right pattern starting at -23.6‰, decreasing to -26.8‰ and then increasing again to -23.2‰ at 15.2 m. Immediately following is a -4.0‰ excursion ending at -27.05‰ at 16.2 m. Above this event, isotopic composition forms a

concave right pattern (E3) starting at -27.1‰ at 16.2 m, increasing to -23.2‰ at 19.0 m and decreasing again from 16.2‰ to -28.2‰ at 20.6 m. Above 20.6 m isotopic composition returns to an average of -26.2‰ ±0.5 up to the Castlegate contact, where it shifts to heavier values of ~ -25.0‰. Above this, isotopic composition forms a pattern from 33.6–35.8 m consisting of two +2.0‰ positive peaks at the base followed by -4.0‰ negative shift and two -2.0‰ negative peaks at the top.

TOC and % Carbonate

From the base of the section, TOC averages low at ~0.1%, but begins increasing at 16.8 m from 1.0% to 21.2% in the coal bed at 18.2 m. TOC then drops off again to ~0.1% from 18.6–24.6m where the section was not measurable. From 28.0–30.0m TOC averages ~2.0%, maxing out at 29.8% in the coals at 29.8 m. Above 30.2 m, in the sandstone, TOC drops off again to ~0.1%.

From the base of the section, carbonate weight percent averages ~8.0% until the just below the Desert Member contact where it abruptly increases to 28.8% at 10.2 m and then falls to 1.5% above the contact at 10.4 m. Carbonate content gradually increases ~30.0% in the inclined heterolithic strata, dropping again abruptly to ~8.0% at the 18.8 m contact with the HCS beds. At 28.0 m carbonate averages 35.0% until the contact with the medium-grained sandstone at 30.2 m where it abruptly drops to 0.9%. From 30.2–36.6m, carbonate increases gradually to ~17.0%

Blaze Canyon

Stratigraphy

The base of the Blaze Canyon section begins at the Grassy LSF/Desert FLV contact **(Figs. 13 & 14)**. The Grassy LSF at this location could not be measured and sampled due to inaccessibility of the vertical cliff face, but consists of +10.0 m thick fine grained sandstone with clearly visible HCS. The base of the measured section, 0.0–1.4 m, consists of fine sandstone, siltstone interbeds with abundant *Ophiomorpha* traces. The interval 1.4–8.0 m consists of upward fining heterolithic strata, with medium-fine sandstone and siltstone interbeds, current ripples and lenticular sandstone bodies. From 8.0–8.5 m on the outcrop is grey colored nodular silty sandstone, and an abundance of root traces. From 8.5–10.4 m the silty sandstone continues to fine upward to a 0.5m thick clay plug capped with a 0.5m thick woody coal. Above the coal, from 10.4–12.2 m is an erosional surface topped with medium-fine sandstone shaped into low angle structures and HCS. Another erosional surface occurs at 12.2 m, above which to the top of the measured section at 27.1 m are three, stacked, medium-grained sandstones separated by thin siltstone or coal beds. The sandstone contains abundant woody debris and flaser beds, as well has planar-laminar cross-stratification and current ripples. Only the stratigraphically lowest coal bed was sampled at 15.8m.

Chemostratigraphy

Isotopic composition from 0.0 m starts at -27.8‰, which rapidly increases to -24.8‰ at 0.6 m and then returns to an average of -26.0‰ up until 7.2 m **(Fig. 14)**. From 7.2–10.0 m is a convex right curve (E1) in isotopic composition. A 2.0‰ negative excursion to -27.6‰ (E2) occurs at 10.2 m. Composition then begins a concave right curve, increasing until 12.2 m when it

is truncated by the erosional surface. Above the erosional surface composition steadily decreases from -23.5‰ at 12.6 m to -27.3‰ at 19.0 m. Isotopic composition then varies little from an average of 26.5‰ until the end of the section at 24.0 m

TOC and % Carbonate

The base of the section, 0.0 m contains 0.1% TOC which then increases to 3.7% at 0.8 m before decreasing again to 0.1% at 1.4 m, which is an erosional contact **(Fig. 14)**. From 1.6– 3.0 m TOC remains very low, an average of 0.1%. TOC gradually increases to 6% from 2.6–3.4 m before decreasing again to 0.1%. In the coal bed from 10.2–10.4 m TOC averages 56.0%. Above the erosive surface on top of the coal, except for one coal bed that was sampled at 15.6 m, which was 33.4%, TOC remains at an average low of 0.1 %.

Carbonate weight percent averaged ~10.0% from the base of section up to 2.8 m where it abruptly increases to 28.6% **(Fig. 14)**. From 2.8–8.6m carbonate decreases gradually to around 15.0% and then there is a sudden break and it drops to 3.6% at 8.8 m. Carbonate averages 2.0% up to the coal bed at 10.2 m where it jumps to 9.5% before entering the sandstone above at 10.6 m. From 10.6–22.0 m carbonate gradually increases from ~1.0% to ~10.0%, where there is a break at 22.2 m and it drops to 1.6%. From 22.2 m to the top of the section carbonate weight percent smoothly increases to ~20.0%.

Tusher Canyon

Measured sections and chemostratigraphic data collected by Cornwell (2010) were used for the Tusher Canyon portion of my study **(Fig. 15)**.

Detrital Zircon Dating

Research groups led by Joel Saylor and Mike Blum have processed and analyzed bulk sediment samples for zircon U/Pb analysis. Samples were collected from outcrop locations within Thompson, Horse, and Tusher Canyons. Strata studied included the Grassy LSF and Desert FLV of the Desert Member of the Blackhawk Formation, the lower Castlegate Sandstone, and the Sego Sandstone.

Results of DZ geochrological studies can be subdivided in two categories. First, the total assemblage of U-Pb ages has been plotted graphically (**Fig. 16**). From this graphic, several patterns of age signatures emerge. Frequency and value of the U-Pb ages can be used as indicators of provenance and source terrain of the samples. Second, several samples provided enough young zircons to define MDAs for many of the strata used in this study in addition to strata outside of the study scope (**Fig. 17; Appendix E,F,G.**).

Detrital Zircon MDAs

Grassy LSF of the Desert Member of the Blackhawk Formation

From Tusher Canyon sample BC-01, 148 zircons were analyzed, yielding a youngest single zircon age of 81.9 ± 2.3 Ma (**Fig. 15; Appendix F**). The next two youngest grains have dates of 88.5 ± 1.7 Ma. and 89.6 ± 3.4 Ma respectively. Since their uncertainties do not overlap with the youngest grain, they have been disregarded in average calculation of MDA. MDA for sample BC-01 relies on the single date of 81.9 ± 2.3 Ma.

Desert FLV of the Desert Member of the Blackhawk Formation

From Thompson Canyon sample: 70314-21, 306 zircons were analyzed, yielding a youngest single zircon age of 76.9 ± 4.9 Ma (**Appendix E**). The next two youngest grains are 90.6 ± 3.1 Ma. and 91.7 ± 2.8 Ma. Since their uncertainties do not overlap with the youngest grain, they have been disregarded in average calculation of MDA. MDA for sample 70314-21 relies on a single age: 76.9 ± 4.9 Ma.

From Horse Canyon samples: BC-10, and BC-11, 141 and 192 zircons were analyzed respectively (**Appendix F**). BC-10 and BC-11 yield youngest single zircon ages of 76.0 ± 2.8 Ma, and 76.2 ± 3.0 Ma. Mean weighted averages of the seven youngest grains in BC-10 yields an MDA of 77.2 ± 2.1 Ma and five youngest grains in BC-11 yields an MDA of 78.9 ± 2.7 Ma.

From Tusher Canyon samples: BC-03 and 70514-30, 141 and 304 zircons were analyzed respectively (**Appendix E, F**). BC-03 yields a youngest single zircon age of 79.0 ± 2.0 Ma. Mean weighted averages of eight youngest grains for BC-03 yields a MDA of 79.6 ± 1.6 Ma.

Youngest single zircon age for sample 70514-30 yields 71.9 ± 4.6 Ma. The next two youngest grains for 70514-30 are 78.5 ± 3.1 Ma and 81.5 ± 3.7 Ma. Since their uncertainties do not overlap with the youngest grain, they have been disregarded in average calculation of MDA. MDA for sample 70514-30 relies on a single age: 71.9 ± 4.6 Ma.

Middle to Upper Castlegate Sandstone

From Horse Canyon sample BC-09, 327 zircons were analyzed yielding a youngest single zircon age of 72.6 ± 3.9 Ma (**Appendix G**). The mean weighted average of the twelve youngest grains yields a MDA of 75.9 ± 2.0 Ma.

Sego Sandstone

From Thompson Canyon samples: 70214-20 and 70414-25, 303 and 309 zircons were analyzed respectively (**Appendix E**). Youngest single zircon ages of 75.2 ± 3.2 Ma and 73.7 ± 3.3 Ma. were obtained from 70214-20 and 70414-26. Mean weighted averages for 4 youngest grains from 70214-20 yields an MDA of 77.3 ± 4.0 Ma, and six youngest grains from 70414-26 yields an MDA of 75.9 ± 2.8 Ma

DISCUSSION

The organic carbon isotopic composition in fluvial and deltaic near-shore sediments is the product of a complex array of organic matter sources and the environmental processes affecting their isotopic composition and depositional processes (e.g. reworking of ancient carbon, microbial remediation, oxidation, etc.). The resulting signature can at times be considerably noisy and absolute values can vary from site to site, yet distinct events (spikes) and patterns are still discernible between facies and locations and are independent of TOC. In this study, high-resolution sampling has been used to increase the possibilities of capturing regional and global signatures among the noisy record. The result, discussed below, is the ability to recognize and correlate dozens of isotopic excursions in the non-marine and shallow marine deposits of the 3 outcrops and a drill core spaced over 200 square kilometers.

Detrital Zircon Geochronology, Chemostratigraphic Global Correlation and Revised Ages for the Blackhawk, Castlegate, Buck Tongue and Sego Sandstone

The high-resolution carbon isotope chemostratigraphic data collected from my measured sections allows for identification of a number of regional and global scale isotopic excursions or events. These excursions/events are interpreted based on the correlative overall isotopic pattern and/or relative placement of isotopic "spikes". The chemostratigraphic profile generated for my study was correlated to the Late Cretaceous carbonate carbon reference curve generated from chalk successions in England **(Fig. 18)** (Jarvis et al. 2006). Dates are based on correlation to Jarvis et al.'s (2006) global Cretaceous organic carbon reference curve. Jarvis et al. (2006) accomplished a stratigraphic resolution of between 100-400kyr through the Cenomanian-

Campanian, which was validated against corresponding pelagic successions located in Germany, France, Spain and Italy.

To accomplish such a highly defined chronostratigraphy, Jarvis et al. (2006) assumed near constant deposition rates of chalk. This assumption was validated by strontium isotope data (McArthur et al. 1993a,b), and correlation to coeval successions located in northern Germany. The Campanian chalk succession Jarvis et al. (2002) used to generate the global curve is 246 m thick, yielding a sedimentation rate of 2 cm per kyr^{-1}. This rate of sedimentation is typical of Late Cretaceous chalk. Bracketing this succession are the dated Santonian/Campanian boundary at 83.5 ± 0.5 Ma and the Campanian/Maastrichtian boundary at 71.3 ± 0.5 Ma (Ogg et al. 2004). The Campanian chalk succession ages were further constrained in Jarvis et al. (2006) by incorporating ammonite, inoceramid bivalve, and planktonic foraminifera biostratigraphy (Gale et al. 2002), and bentonite tephrastratigraphy (Wray 1999). My correlation to the global reference curve is constrained by the DZ data provided by Joel Saylor and Mike Blum, which was collected from within the vicinity of my study area. Differences between my correlation to the dated global Late Cretaceous $\delta^{13}C$ reference curve and many of the detrital zircon MDA's fall within the uncertainty **(Fig. 19)**.

I suggest, based on my data, that these deposits formed 2 Ma earlier than the prior work indicated (e.g. Hampson 2010; Aschoff & Steel 2011; Miall 2014), and that the time encompassed by the measured succession is shorter. Subtracting the Buck Tongue age from the Grassy LSF age implies that deposition of strata from the upper Desert Member to the top of the Buck Tongue occurred over a period of ~2.5 Ma, instead of ~4 Ma **(Fig. 19)**. Differences between my data and the prior chronostratigraphic work are likely due to prior dating methods relying on a sparse fossil record and potentially uncertainties in correlation of biostratigraphy

over 100's of kilometers of temporally complex terrain. Approximation of the timespan during which sediments were deposited can be accomplished using the constrained $\delta^{13}C$ global chemostratigraphic correlations **(Fig. 18).** I am not able to pinpoint the exact age of strata. This is because the isotopic record for the Book Cliffs is disrupted by numerous unconformities and thus a complete match to the seemingly continuous chalk record (Jarvis et al. 2006) is impossible. In agreement with Miall (2014), it must be noted that actual depositional time represented by the strata could be but a minute fraction of my correlative timespan, and the bulk of the rock record is lost as unconformities. Correlation to the global curve **(Fig. 18)** indicates that the Grassy LSF was deposited sometime within a time span of ~600 kyr from 76.6–77.2 ± 0.4 Ma. This rate is in agreement with previous interpretations of depositional time made by Van Wagoner (1995). The Desert FLV was deposited sometime within a time span of ~300 kyr from 76.3–76.6 ± 0.4 Ma. The Castlegate Sandstone was deposited sometime within a time span of ~500 kyr from 75.8–76.3 ± 0.4 Ma. The Buck Tongue was deposited within a timespan of ~600 kyr from 74.9–75.8 ± 0.4 Ma. These ages give a much better approximation of the duration of which these sequences take to develop than what was previously available. The maximum depositional ages determined by DZ geochronology are in good agreement with these chemostratigraphic ages, but because their errors can encompass millions of years, are useful mainly for bracketing a zone on Jarvis et al's (2006) global reference curve for correlation purposes.

Provenance of Blackhawk and Castlegate Zircon

The detrital zircon data provided by the ExxonMobil Upstream Research group (**Fig. 16**), for the Blackhawk Fm. through the Sego Sandstone show a several patterns of age signatures that has been identified in previous studies of Cretaceous strata in the western interior (e.g. Dickinson & Gehrels 2008a,b, 2009; May et al. 2013; Laskowski et al. 2013). One primary population

group consists of zircons that were ultimately derived from (a) the Mid-continent anorogenic granites (ca. 1.5-1.3 Ga), and magmatism associated with the (b) Grenville (ca. 1.25-0.95 Ga) and (c) Appalachian orogenies (ca. 500-300 Ma): this assemblage represents a signature that was initially derived from the Appalachian cordillera, and transported by river systems to the Paleozoic passive margin of western North America during the late Paleozoic and early Mesozoic, then eroded from the Sevier orogeny during the Cretaceous. A second important population group is derived from (a) the paleo-Proterozoic Yavapai-Mazatzal orogeny (ca. 1.6-1.8 Ga), best exposed along the Mogollon Rim of Arizona, and (b) the Mesozoic Sierra Nevada magmatic arc (ca. 275-55 Ma), located to the west of the Sevier fold and thrust belt. This population group may have a recycled component as well, but is also the source for zircons used to define MDA. Regardless, these two population groups characterize many DZ populations that have been described from the Western Interior foreland basin (e.g. Dickinson & Gehrels 2008a,b, 2009; May et al. 2013; Laskowski et al. 2013).

Driving force for Desert Member and Castlegate incised valley fill development

Revised, precise dating of strata has allowed me to identify the primary driving force behind incision and deposition within the Desert and Castlegate IVF is glacio-eustatic in origin through temporal correlation to the global Phanerozoic sea level curve **(Fig. 20)**. In the sea level curve of Miller et al. (2005), rapid Campanian-aged shifts in base level recorded by strata deposited along the New Jersey margin correlate to similar shifts recorded by strata in the Bahamas, northwest Europe, the U.S Gulf Coast, and Russia. These shifts in eustacy occurred over very short periods of time (<100 kyr), likely due to sporadic periods of glaciation in the otherwise greenhouse world (Miller et al. 2005). Jarvis et al. (2002) found that many positive and negative excursions were directly related to changes in eustacy. Rise in sea level leads to

enhanced organic matter preservation and burial resulting in a shift to more positive values, whereas a fall in sea level erodes and reintroduces stored carbon resulting in a shift to more negative values (Jarvis 2002). I see this relationship between isotopic composition and eustacy occurring in many of my studied successions.

Using the sea level curve of Miller et al. (2005) with my new geochronological data and examining the positive and negative shifts in organic carbon composition has allowed us to make interpretations of sea level in my area. Around 77.2 Ma, based on Miller et al's (2005) sea level curve global sea level rapidly dropped ~25 m contributing to incision of the Desert Member paleovalley floor forming the Desert sequence boundary **(Fig. 20)**. This drop in eustatic sea level is reflected in an overall negative trend in $\delta^{13}C$ values in the Grassy LSF leading up to the Desert FLV erosional unconformity **(Fig. 18)**. As eustacy rebounded about 15 m, Desert FLV non-marine and marine strata were then deposited in this new incised valley sometime between 76.2–76.9 Ma. Another ~25 m eustatic drop occurred around 75.9 Ma, contributing to the erosion and formation of the Castlegate sequence boundary. Sea level rebounded and the Castlegate sands were deposited between 75.8–76.2 Ma **(Fig. 20)**. The Desert and Castlegate eustatic rises are reflected by two positive shifts in $\delta^{13}C$ as depleted organic matter is removed from the carbon cycle due to burial **(Fig. 18)** (Jarvis et al. 2006). Around 75.8 Ma sea level rose approximately 45 m, flooding over the top of the Castlegate and pushing the shoreline hundreds of kilometers to the west **(Fig. 20)**. It was in this distal setting that the bulk of the Buck Tongue was deposited between 75.2–75.8 Ma **(Fig. 18)**.

According to the isopach maps of Van Wagoner (1995), the Castlegate IVF ultimately incised to a maximum depth of ~120 m. This depth, compared to the eustatic record of a ~40 m drop, indicates that forces beyond increased gradient due to sea-level fall are responsible for

erosion of the valley. To erode that deeply, tectonic uplift and climate, not eustacy, likely played the major roles in determining the level of incision of the Castlegate IVF.

Regional Chronostratigraphic Correlations, Facies and Sequence Stratigraphic Reinterpretations

For regional correlation, the four sections have been hung on the Buck Tongue flooding surface. Seventeen different isotopic spikes, some which can be correlated across all four measured sections, have been identified **(Fig. 21)**. For ease of discussion these spikes have been grouped together into five correlatable events, (E1 to E5). The basal unit, the Grassy LSF, which is laterally continuous from the Sego #2 wellbore to Tusher canyon, exhibits an upward coarsening profile of amalgamated HCS beds and bioturbated siltstone. Many of these beds contain a marine trace fossil assemblage indicating conditions below fair weather base. These features and interpretation of the well logs suggest that the Grassy LSF was deposited in a progradational LSF environment **(Fig. 22)**. Event 1 (E1) ties a section of these strata in Thompson Canyon to the Sego well bore location indicating a period of simultaneous deposition of marine sands along the coast of the KWIS.

At the top of the Grassy LSF is an erosional surface interpreted by Van Wagoner (1995) as the Desert Member Sequence Boundary, separating the underlying Grassy LSF strata from Desert FLV fluvial strata above. Differing from Van Wagoner's (1995) previously interpreted facies, the top section of the Grassy LSF in the Sego #2 core has been reinterpreted as a deltaic deposit **(Fig. 22)**. The base of the deltaic sandstone is distinguished by a scour surface, which undercuts into the underlying heavily deformed LSF strata. The surface is further marked by abrupt shift from calcite to siliceous cementation. Event 2, which is continuous through the

fluvial strata in Tusher, Blaze, and Thompson Canyons, dips below the previously interpreted sequence boundary in the Sego #2 core **(Fig. 21)**. As I am considering these events to be time correlative, this invalidates the previously interpreted sequence boundary. The isotope event indicates that the deltaic sands were deposited at the same time as the fluvial strata updip, and the sequence boundary is actually below the deltaic sands. This hypothesis is further strengthened by eastward flowing paleocurrents for the Desert FLV fluvial (Van Wagoner 1995) **(Fig. 23**). These paleocurrents were collected from Sagers Canyon, which is 7km SE of the Sego #2 borehole. This current direction infers that the fluvial strata found in the other sections to the west, was updip from the deltaic deposit in Sego, and that the fluvial system was depositing sediment while at the same time prograding and cannibalizing its own delta **(Fig. 23)**.

It must be noted that Event 2 (E2) correlates channel belts sands between all four sample locations, and that given the length (25 km) and width (5 km) of the sampling area, it is possible that the channel sandstone sampled at each location belong to separate channel belts deposited at different times. However my chemostratigraphic data's strong correlation suggests that all four deposits were formed at roughly the same time. A possible explanation for this is that there were multiple active channels, depositing sediments at roughly the same time across the 5km study area.

Above the fluvial erosion surface (previously interpreted as the Desert FLV sequence boundary in the Sego #2 core), the Desert FLV fluvial strata consists of medium-fine grained channel belt sandstone, silty channel fills, and organic-rich swamp or mire deposits **(Fig. 21)**. The medium to fine grained sandstone, abundance of siltstone, inclined heterolithic strata marked by ripples and trough cross stratification, siltstone plugs, and tidal indicators suggest that the Desert FLV was deposited in a tidally influenced meandering stream environment. Abundant

large animal tracks, roots, and coals infer that the coastal plain onto which the Desert FLV was deposited was fertile. Paleocurrent directions collected for the Desert FLV and Castlegate fluvial strata indicate an Eastward to South-Eastward flow direction (Van Degraaff 1972; Van Wagoner 1995). The Desert FLV fluvial fines upward to paleosols and swamp deposits, which are overlain by a scour surface and LSF sandstone in Blaze and Thompson Canyons and at the Sego well bore location, but not in Tusher Canyon. This erosional surface between the Desert FLV and the lower-shoreface sandstone has been interpreted as a transgressive surface of erosion (TSE). The TSE has previously been interpreted to form due to a rise in base level followed by a marine transgression over the top of the Desert FLV fluvial. The Desert FLV marine is made up of amalgamated HCS beds and siltstone interbeds. Event 3 **(E3 in Fig. 21)** ties these marine deposits in Sego and Thompson Canyons, but is truncated by the Castlegate Sequence Boundary somewhere between Blaze and Thompson Canyons. The TSE does not continue updip to Tusher Canyon because it also is truncated by the Castlegate Sequence Boundary.

Previously interpreted by Van Wagoner (1995), the Castlegate Sequence Boundary separates LSF from fluvial in Blaze, Sego, and Thompson Canyons and fluvial from fluvial in Tusher Canyon. The Castlegate fluvial differs from the Desert FLV fluvial by being made up of coarser sandstone, less siltstone, and larger cross stratification. Because of the tidal structures in the Sego core, the Castlegate is interpreted to be tidally influenced. This study does conclude the Castlegate's fluvial system type. Events 4 and 5 tie together Castlegate channel sandstones in Sego, Thompson and Blaze Canyons. Event 4 crosses Van Wagoner's Castlegate Sequence Boundary 2, invalidating it **(Fig. 21)**.

The Castlegate fines upward from siltstone and fine sandstone interbeds to muddy siltstones and shale at what has been interpreted as the Buck Tongue contact. The Buck Tongue

consists of 3 upward shallowing parasequences of shale, interpreted to be deposited in a lower-shoreface to offshore environment. Isotopic composition is stable at ~-26.7‰ ±0.5‰. The flat trend in isotopic composition could reflect the relatively flat global isotope trend during this time **(Fig. 10)**.

The chemostratigraphy has helped guide my interpretation of both sequence stratigraphy and facies, which was especially useful in the Sego #2 core. It can be exceedingly difficult to determine facies when only provided a 4" visual of the rock. Using the chemostratigraphy in outcrop also proved useful in Blaze Canyon, where a thin section of sandstone previously interpreted as LSF (Van Wagoner 1995) was correlated to fluvial strata in Tusher Canyon **(Fig. 23)**. I have interpreted this sandstone as fluvial, because Timeline 2, which is a strong correlation, would have been truncated had the TSE penetrated all of the way to the coal **(Fig. 21)**. My interpretation of the Desert FLV data infers simultaneous deposition and erosion and would seem to follow Van Wagoner's (1995) model B **(Fig. 1)**. Interpretation of the Castlegate is inconclusive as to which model it follows. A possibility put forth by Hoffmeister (2011) is that Castlegate paleocurrents are actually directed toward the south, and therefore it would be unlikely to find Castlegate fluvial and deltaic deposits prograding to the east. Further study, strategically sampling the Castlegate on a north-south transect, may be able to shed more light on this matter.

Sources of Uncertainty

It must be noted that this study's findings rely on several assumptions, and thus there is some inherent uncertainty. The general problems faced in chemostratigraphic correlation are similar to the problems faced by petrophysicists correlating well logs. Chemostratigraphic interpretation can be erroneous if the isotopic curve has been disrupted by erosion, and no longer temporally complete. Variability in the duration or magnitude of isotopic excursions can also be warped by changes in the depositional rate compressing or expanding the recorded time and/or diluting the primary event signal.

The exact processes that produced the organic carbon composition of the samples are unknown. First and foremost is the possibility of exhumation and reworking of ancient organic carbon by erosion. Because of the regional correlatability between different facies, I submit that reworked ancient organic matter may be responsible for some of the noise and some of the overall shift in composition but that the more abundant fresh organic carbon fractionated in response to regional and global climate factors overwhelms any reworked organic carbon. It is possible that much of the older organic carbon was removed via oxidation and so makes up a minute fraction of the TOC. A follow up study to address this one could be to determine the fraction of old to new organic in deposits formed by modern river systems

Lastly, ground water penetration, microbial alteration (Macko & Estep 1984), diagenesis, and weathering may all have had some effect on the intra-granular carbon composition of the rock, again however, high correlatability between sections and different depositional facies, and the independence of $\delta^{13}C$ values from TOC concentrations, indicate that the original regional and global isotopic signal remains strong enough to recognize.

Utility of Sequence Stratigraphic and Facies Interpretation.

The data and correlation presented in this study clearly demonstrate that organic carbon isotopic excursions can be correlated across different facies, and are identifiable regardless of type of sediment and depositional environment. These cross-facies isotopic time lines challenge some of the chronostratigraphic assumptions associated with traditionally used lithostratigraphic units and surfaces such as the coal beds in Blaze, and Thompson Canyons, and the Sego #2 drill core, which the isotopic data reveals to be diachronous (e.g. **Fig. 21**).

I have demonstrated that isotopic time lines or events make excellent tools for testing sequence stratigraphic interpretations, as they cannot cross sequence boundaries (such as was the case in this study). Because the driving forces behind fluvial systems are so complex, and to avoid controversy, future sequence stratigraphic interpretation should utilize some form of quantitative analysis, (e.g. DZ geochronology, chemostratigraphy) to constrain timing, driving force, and to test the validity of interpreted sequences and surfaces. Sequence stratigraphic interpretation between cores and outcrops has also been shown to be hazardous as predicted by Bhattacharya (2011), onlap geometries cannot be determined in one-dimensional data, and facies can be difficult to interpret in core. Further study is required to test if stable isotopes are useful in determining temporal relationships between terraces within an IVF **(Fig. 2)**.

In this study organic carbon isotope time lines have allowed for the identification of erosional vs. non-depositional surfaces (e.g., the lower Castlegate Sequence Boundary). Truncation of correlative isotopic excursions, allows recognition of erosional events in a similar manner as truncation of sedimentary structures and units. The presence or absence of isotopic pattern truncations helps with recognition of non-deposition vs. erosion surfaces. The use of

isotopic timelines can be particularly useful when studying visually-appearing homogenous rocks, where it is difficult to discern unconformities or hiatuses.

CONCLUSIONS

Lack of precise chronological constraint requires that assumptions be made that introduce large uncertainties in temporal or sequence stratigraphic study of sedimentary strata. Fluvial and shallow marine strata can become some of most difficult temporal problems facing chronostratigraphers. This difficulty caused by the fluvial realm being characterized by erosion and unconformity (Miall 2014), and sedimentology driven by numerous overlapping and episodic factors (e.g. tectonics, climate, eco-system, eustacy). Not only is the terrain temporally complex, but the preservation potential of chronological markers is very low.

Without chronological constraint or other empirical data to guide interpretation, sequence stratigraphic interpretation is model driven. A model's accuracy is limited to the perfection of the model and its inputs. Different assumptions using the same model can result in multiple sequence stratigraphic interpretations fitting the same dataset (Bhattacharya 2011; Blum et al. 2013). Multiple interpretations stagnates the advance of stratigraphy because authors become mired in debate defending their interpretations and terminology (Wilson 1988). A great example of this and the focus of this study is the sequence stratigraphic framework and model developed in the 1980's and 1990's to place strata into genetic packages bounded by unconformities and their correlative conformities (e.g. Van Wagoner et al. 1990; Van Wagoner 1991, 1995; Yoshida & Willis 1996; Yoshida & Miall 1998; Yoshida 2000).

This study attempts to addresses these problems by using detrital zircon and organic carbon isotopes to more empirically revisit a previously interpreted sequence stratigraphic framework (Van Wagoner 1995). Going further, this study validates the use of high-resolution chemostratigraphy to make regional, relative-age chronostratigraphic correlations between

successions of high energy non-marine and marine clastic deposits. The chemostratigraphic profiles generated for this study represent the most finely resolved organic carbon isotope analysis of fluvial and shallow marine strata ever conducted.

My interpretation were based on the assumption that changes in watershed-scale climate and ocean chemistry, which is recorded as variations in the organic carbon isotope composition of organic matter, occurs at time scales shorter than 1000 years. This assumption is strengthened by the remarkable similarity in isotope trends between strata within individual channel belt sand bodies. This stratigraphic isotope record allows the correlation of fluvial and nearshore rocks by their $\delta^{13}C$ values alone. Because these isotopic signals are driven by regional and/or global events, rather than local events, rocks sharing identical isotopic composition patterns infer that they are roughly time equivalent. Correlations between different facies can be interpreted to imply simultaneous deposition. Truncation of regionally extensive correlations indicates the presence of an unconformity. These time lines are useful for examining sequence stratigraphic surfaces and units, and have been used in this study to facilitate the shifting of a previously interpreted sequence boundary (e.g. Van Wagoner 1995; Blum et al. 2013). In the future, more strategic sampling locations and intervals should be used to test other sequence stratigraphic concepts and frameworks.

Despite the DZ geochronology's high errors, knowing maximum deposition age allows correlation to the Global Late Cretaceous global reference curve with a higher level of confidence than blind "wiggle matching". Based on the success in finding young detrital zircons probably closely matching the age of deposition, further DZ work should be done throughout the Book Cliffs. High resolution chemostratigraphy was successfully used to make global correlations between high energy non-marine and marine siliciclastic deposits and dated deep-

water carbonate successions (Jarvis et al. 2006). Maximum DZ depositional ages overlapped with chemostratigraphic ages. The DZ geochronology and chemostratigraphic global correlations were used to make inferences of the absolute timing of deposition of each depositional sequence at a temporal resolution never before achieved.

This study was initiated with no hypothesis in mind. It was rooted in the idea that correlatable trends in organic carbon isotope composition infer a temporal relationship between strata. I have demonstrated high-resolution chemostratigraphy indeed has potential to be a powerful tool for solving chronostratigraphic problems. Further research is required to address many uncertainties in the technique such as identifying what specifically is driving trends in organic carbon stable isotopes in the non-marine, validating my global correlation, and determining if my stratigraphic interpretation is correct. While I have demonstrated chemostratigraphy's utility, addressing some of the uncertainties that have been raised over the course of this study is essential to push organic carbon isotope usage into the mainstream.

REFERENCES

Adams, M.M., and Bhattacharya, J.P., 2005, No change in fluvial style across a sequence boundary, Cretaceous Blackhawk and Castlegate Formations of central Utah, U.S.A.: Journal of Sedimentary Research, v. 75, p. 1038–1051.

Aschoff, J.L., and Steel, R.J., 2011, Anomalous clastic wedge development during the Sevier–Laramide transition, North American Cordilleran foreland basin, USA: Geological Society of America, Bulletin, v. 123, p. 1822–1835.

Bertog, L.J, 2013, Timing of onset of volcanic centers in the Campanian of western North America as determined by distal ashfalls: Open Journal of Geology, v. 3, p. 121–133.

Bhattacharya, J.P., 2011, Sequence stratigraphy of fluvial–deltaic wedges: a 20 year perspective from the Cretaceous Interior Seaway of North America: Sedimentology, v. 58, p. 120–169.

Blakey, R.C., 2011, Paleogeography and geologic evolution of North America, http://jan.ucc.nau.edu/rcb7/nam.html (last accessed April 2015).

Blum, M.D., and Törnqvist, T.E., 2000, Fluvial responses to climate and sea-level change: a review and look forward: Sedimentology, v. 47, p. 2–48.

Blum, M.D., Martin J., Milliken K., and Garvin M., 2013, Paleovalley systems: Insights form Quaternary analogs and experiments: Earth-Science Reviews, v. 116, p. 128–169.

Buehler, H.A., Weissmann, G.S., Scuderi, L.A., Hartley, A.J., 2011, Spatial and temporal evolution of an avulsion on the Taquari River distributive fluvial system from satellite image analysis. Journal of Sedimentary Research, v. 81, p. 630–640.

Cobban, W.A., Obradovich, J.D., Walaszcyk, I., and McKinney, K.C., 2006, A USGS zonal table for the Upper Cretaceous Middle Cenomanian-Maastrichtian of the western interior of the United States based on ammonites, inoceramids, and radiometric ages: U.S. Geological Survey: Open-File Report 2006-1250, p. 47.

Cornwell, C.F., 2012, Sequence stratigraphy and chemostratigraphy of an incised valley fill within the Cretaceous Blackhawk Formation, Book Cliffs, Utah: M.S. Thesis, University of Kansas. 65 p.

Davis, D.W., Williams, I.S., and Krogh, T.E., 2003, Historical development of U-Pb geochronology: in Hanchar, J.M., and Hoskin, P.W.O., eds., Zircon: Reviews in Mineralogy and Geochemistry, v. 53, p. 145–181.

DeCelles, P.G., 2004, Late Jurassic to Eocene evolution of the Cordilleran thrust belt and foreland basin system, western USA: American Journal of Science, v. 304, p. 105–168.

Dickinson, W.R., and Gehrels, G.E., 2008a, Sediment delivery to the Cordilleran foreland basin: Insights from U–Pb ages of detrital zircons in Upper Jurassic and Cretaceous strata of the Colorado Plateau: American Journal of Science, v. 308, p. 1041–1082.

Dickinson, W.R., and Gehrels, G.E., 2008b, U–Pb ages of detrital zircons in relation to paleogeography: Triassic paleodrainage networks and sediment dispersal across southwest Laurentia: Journal of Sedimentary Research, v. 78, p. 745–764.

Dickinson, W.R., and Gehrels, G.E., 2009, U–Pb ages of detrital zircons in Jurassic eolian and associated sandstones of the Colorado Plateau: Evidence for transcontinental dispersal and intraregional recycling of sediment: Geological Society of America Bulletin, v. 121, p. 408–433.

Elderfield H., 1986, Strontium isotope stratigraphy: Palaeogeography, Palaeoclimatology, Palaeoecology, v. 57, p. 71–90.

Fedo, C.M., Sircombe, K.N., and Rainbird, R.H., 2003, Detrital zircon analysis of the sedimentary record: Reviews in Mineralogy and Geochemistry, v. 53, p. 277–303.

Fouch, T.D., Lawton, T.F., Nichols, D.J., Cashion, W.B., and Cobban, W.A., 1983, Patterns and timing of synorogenic sedimentation in Upper Cretaceous rocks of central and northeast Utah: Mesozoic paleogeography of the west-central United States: Society for Sedimentary Geology, Rocky Mountain Section, Second Rocky Mountain Paleogeography Symposium 2, p. 305–336.

Gale, A.S., Hardenbol, J., Hathway, B., Kennedy, W.J., Young, J.R. and Phansalkar, V., 2002, Global correlation of Cenomanian (Upper Cretaceous) sequences: evidence for Milankovitch control on sea level: Geology v. 30, p. 4–291.

Gehrels, G.E., Valencia, V., and Ruiz, J., 2008, Enhanced precision, accuracy, efficiency, and spatial resolution of U-Pb ages by laser ablation–multicollector–inductively coupled plasma–mass spectrometry: Geochemistry, Geophysics, Geosystems, v. 9. Q03017

Gehrels, G.E., Valencia, V., and Pullen, A., 2006, Detrital zircon geochronology by Laser-Ablation Multicollector ICPMS at the Arizona LaserChron Center: Geochronology: Emerging Opportunities, Paleontology Society Short Course: Paleontology Society Papers, v. 11, p. 10.

Gehrels, G.E., 2011, Detrital zircon U-Pb geochronology: Current methods and new opportunities in tectonics of sedimentary basins: Recent Advances, John Wiley & Sons, Ltd, p. 1–44.

Gehrels, G.E., Blakey, R., Karlstrom, K.E., Timmons, M.J., Dickinson, B., and Pecha, M., 2011, Detrital zircon U-Pb geochronology of Paleozoic strata in the Grand Canyon, Arizona: Lithosphere, v. 3, p. 183–200.

Gill, J.R., and W.J. Hail, Jr., 1975, Stratigraphic sections across Upper Cretaceous Mancos Shale–Mesaverde Group boundary, eastern Utah and western Colorado: U.S. Geological Survey Oil and Gas Investigation Chart OC-68.

Gurnell, A.M., 1998, The hydrogeomorphological effects of beaver dam-building activity: Progress in Physical Geography v. 22, p. 167–189.

Gurnis, M., 1993, Phanerozoic marine inundation of continents driven by dynamic topography above subducting slabs: Nature, v. 364, 589–593.

Hampson, G.J., 2010, Sediment dispersal and quantitative stratigraphic architecture across and ancient shelf: Sedimentology, v. 57, p. 96–141.

Hoffmeister, K., 2011, Forebulge influence on deposition of the Cretaceous Castlegate Sandstone, Book Cliffs, Utah, U.S.A.: M.S. Thesis, University of Kansas, 107 p.

Izett, G.A., Cobban, W.A., Dalrymple, G.B., and Obradovich, J.D., 1998, 40Ar/39Ar age of the Manson impact structure, Iowa, and correlative impact ejecta in the Crow Creek Member of the Pierre Shale (Upper Cretaceous), South Dakota and Nebraska: Geological Society of America Bulletin, v. 110, p. 361–76.

Jarvis, I., Mabrouk, A., Moody, R. T. J. and De Cabrera, S. C., 2002, Late Cretaceous (Campanian) carbon isotope events, sea-level change and correlation of the Tethyan and Boreal realms: Palaeogeography, Palaeoclimatology, Palaeoecology, v. 188, p. 215–48.

Jarvis, I., Gale, A.S., Jenkyns, H.C., and Pearce, M.A., 2006, Secular variation in Late Cretaceous carbon isotopes: a new $\delta^{13}C$ carbonate reference curve for the Cenomanian-Campanian (99.6-70.6 Ma): Geological Magazine, v. 143, p. 561–608.

Kaiho, K., Saito, S., 1994, Oceanic crust production during the last 100 Myr: Terra Nova v. 6, p. 376–384.

Kaufman, A.J., Knoll, A.H., and Awramik, S.M., 1992, Biostratigraphic and chemostratigraphic correlation of Neoproterozoic sedimentary successions; upper Tindir Group, northwestern Canada, as a test case: Geology, v. 20, p. 181–185.

Laskowski, A.K., DeCelles, P.G., and Gehrels, G.E., 2013, Detrital zircon geochronology of Cordilleran retroarc foreland basin strata, western North America: Tectonics, v. 32, p. 1027–1048.

Macko S. A. And Estep M. L. 1984, Microbial alteration of stable nitrogen and carbon isotopic compositions of organic matter: Organic Geochemistry, v. 6, 787–790.

Martin, J.M., Abreu, V., Neal, J., and Sheets, B., 2009, Sequence stratigraphy of experimental strata under known conditions of differential subsidence and variable base level: American Association of Petroleum Geologists Bulletin, v. 93, p. 503–533.

May, S.R., Gray, G.G., Summa, L.L., Stewart, N.R., Gehrels, G.E., and Pecha, M.E., 2013, Detrital zircon geochronology from the Bighorn Basin, Wyoming, U.S.A.: Implications for tectonostratigraphic evolution and paleogeography: Geological Society of American Bulletin, v. 125, p. 1403–1422.

McArthur, J.M., 1994, Recent trends in strontium isotope stratigraphy: Terra Nova, v. 6, p. 331–358.

McArthur, J.M., Howarth, R.W., and Bailey, T.R., 1991, Strontium isotope stratigraphy: LOWESS version 3: Best fit to the marine Sr-isotope curve for 0–509 ma and accompanying look-up table for deriving numerical age: The Journal of Geology, v. 109, p. 155–170.

McArthur, J.M., Thirlwall, M.F., Chen, M., Gale, A.S., and Kennedy, W.J., 1993a, Strontium isotope stratigraphy in the Late Cretaceous numerical calibration of the Sr isotope curve and intercontinental correlation for the Campanian: Paleoceanography, v. 8, p. 859–873.

McArthur, J.M., Thirlwall, M.F., Gale, A.S., Kennedy, W.J., Burnett, J.A., Mattey, D., and Lord, A.R., 1993b, Strontium isotope stratigraphy for the Late Cretaceous: A new curve, based on the English Chalk. High Resolution Stratigraphy: Geol. Soc. London Special Publication, v. 70, p. 195–209.

McLaurin, B.T., and Steel, R.J., 2000, Fourth-order nonmarine to marine sequences, middle Castlegate Formation, Book Cliffs, Utah: Geology, v. 28, p. 359–362.

Miall, A.D., 1993, The architecture of fluvial–deltaic sequences in the Upper Mesaverde Group (Upper Cretaceous), Book Cliffs, Utah, in Best, J.L., and Bristow, C.S., eds., Braided Rivers: Geological Society of London, Special Publication v. 75, p. 305–332.

Miall, A.D., 2014, The emptiness of the stratigraphic record: A preliminary evaluation of missing time in the Mesaverde Group, Book Cliffs, Utah, U.S.A.: Journal of Sedimentary Research, v. 84, p. 457–469.

Miall, A.D., and Arush, M., 2001, The Castlegate Sandstone of the Book Cliffs, Utah: Sequence stratigraphy, paleogeography, and tectonic controls: Journal of Sedimentary Research, v. 71, p. 537–548.

Miller, K.G., Kominz, M.A., Browning, J.V., Wright, J.D., Mountain, G.S., Katz, M.E., Sugarman, P.J., Cramer, B.S., Christie-Blick, N., and Pekar, S.F., 2005, The Phanerozoic record of global sea-level change: Science, v. 310, p. 1293–1298.

Ogg, J.G., Agterberg, F.P. and Gradstein, F.M. 2004, The Cretaceous Period: A Geologic Time Scale: Cambridge University Press, p. 83-344.

Polvi, L.E., and Wohl, E., 2012, The beaver meadow complex revisited: The role of beavers in post-glacial floodplain development: Earth Surface Processes and Landforms, v. 37, p. 332–346.

Polvi, L.E., Wohl, E., 2013, Biotic drivers of stream platforms: BioScience, v. 63, p. 439–52.

Ripple, W.J., and Beschta, R.L., 2004, Wolves, elk, willows and trophic cascades in the upper Gallatin Range of southwestern Montana, U.S.A.: Forest Ecology and Management, v. 200, p. 161–181.

Strong, N., and Paola, C., 2006, Fluvial landscapes and stratigraphy in a flume: The Sedimentary Record, v. 4, p. 3–7.

Strong, N., and Paola, C., 2009, Valleys that never were: time surfaces versus stratigraphic surfaces: Journal of Sedimentary Research, v. 78, p. 579–593.

Sundquist, E.T. and K. Visser, 2004, The geological history of the carbon cycle: Biogeochemistry, Treatise on Geochemistry, v. 8, p. 425–472.

Vandenberghe, J., 2003, Climate forcing of fluvial system development: An evolution of ideas: Quaternary Science Reviews, v. 22, p. 2053–2060.

Van Degraaff, F.R., 1972, Fluvial–deltaic facies of the Castlegate Sandstone (Cretaceous), east-central Utah: Journal of Sedimentary Petrology, v. 42, p. 558–571.

Van Wagoner, J.C., Posamentier, H.W., Mitchum, R.M., Vail, P.R., Sarg, J.F., Loutit, T.S., and Hardenbol, J., 1988, An overview of the fundamentals of sequence stratigraphy and key definitions: Society for Sedimentary Geology Special Publication, v. 42, p. 39–45.

Van Wagoner, J.C., Mitchum, R.M., Campion, K.M., and Rahmanian, V.D., 1990, Siliciclastic sequence stratigraphy in well logs, cores, and outcrops: Concepts for high-resolution correlation of time and facies: American Association of Petroleum Geologists, Methods in Exploration, v. 7, p. 1–55.

Van Wagoner, J.C., 1991, High-frequency sequence stratigraphy and facies architecture of the Sego Sandstone in the Book Cliffs of western Colorado and eastern Utah: American Association of Petroleum Geologists, Field Conference Guidebook, Tulsa, unpaginated.

Van Wagoner, J.C., 1995, Sequence stratigraphy and marine to nonmarine facies architecture of foreland basin strata, Book Cliffs, Utah, U.S.A.: American Association of Petroleum Geologists, Memoir 64, p. 137–223.

Willis, A.J., 2000, Tectonic control of nested sequence architecture in the Sego Sandstone, Neslen Formation, and Upper Castlegate Sandstone (Upper Cretaceous), Sevier Foreland Basin, Utah, U.S.A.: Sedimentary Geology, v. 136, p. 277–317.

Wilson, R.C.L., 1988, Sequence stratigraphy: A revolution without a cause: Geological Society of London Special Publication, v. 143, p. 303–314.

Wray, D.S., 1999, Identification and long-range correlation of bentonites in Turonian–Coniacian (Upper Cretaceous) chalks of northwest Europe: Geological Magazine, v. 136, p. 361–71.

Yoshida, S., Miall, A.D., and Willis, A., 1998, Sequence stratigraphy and marine to non-marine facies architecture of foreland basin strata, Book Cliffs, Utah, U.S.A- Discussion: American Association of Petroleum Geologists, Bulletin, v. 82, p. 1596–1606.

Yoshida, S., Willis, A., and Miall, A.D., 1996, Tectonic control of nested sequence architecture in the Castlegate Sandstone (upper Cretaceous), Book Cliffs, Utah: Journal of Sedimentary Research, v. 66, p. 737–748.

Yoshida, S., 2000, Sequence and facies architecture of the Upper Blackhawk Formation and the Lower Castlegate Sandstone (Upper Cretaceous), Book Cliffs, Utah, USA: Sedimentary Geology, v. 136, p. 239–276.

FIGURES

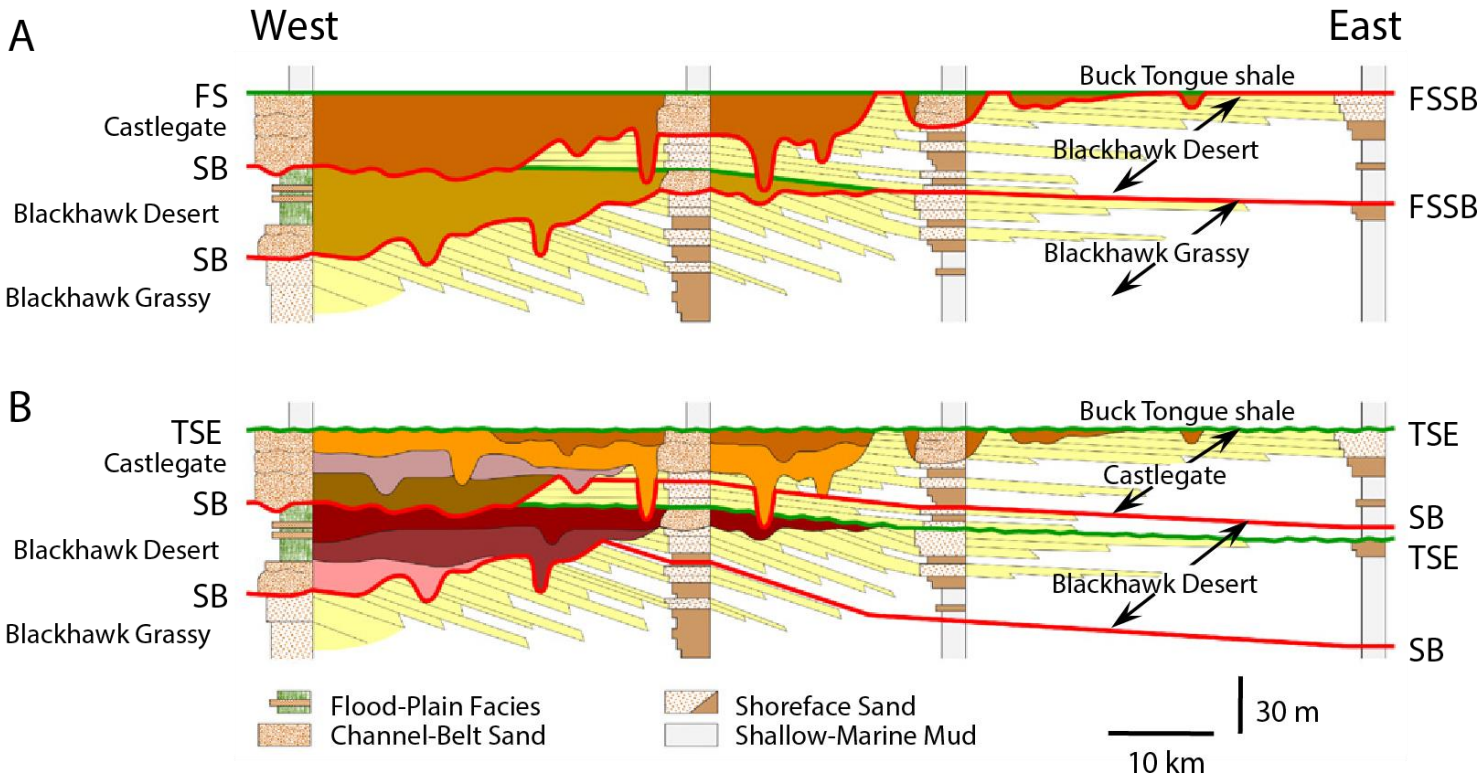
A
West
East
FS
Castlegate
SB
Blackhawk Desert
SB
Blackhawk Grassy
Buck Tongue shale
Blackhawk Desert
Blackhawk Grassy
FSSB
FSSB
B
TSE
Castlegate
SB
Blackhawk Desert
SB
Blackhawk Grassy
Buck Tongue shale
Castlegate
Blackhawk Desert
TSE
SB
TSE
SB
Flood-Plain Facies
Channel-Belt Sand
Shoreface Sand
Shallow-Marine Mud
30 m
10 km

Figure 1: Sequence stratigraphic models for Upper Blackhawk Fm. and Castlegate Sandstone stratigraphy: Model A is based on complete bypass and erosion of the incised valley fill (IVF), forming an unconformity, which separates two different genetic units. Flooding surfaces (FS) and sequence boundaries (SB) merge downdip. Model B assumes simultaneous incision and deposition, with fluvial systems cutting through their own deltas. Wave and tidal erosion remove the flooding surface and form a transgressive surface of erosion. Green lines represent flooding surfaces or transgressive surfaces of erosion, Red lines represent sequence boundaries, (From Blum et al. 2013, models originally from Van Wagoner, 1995)

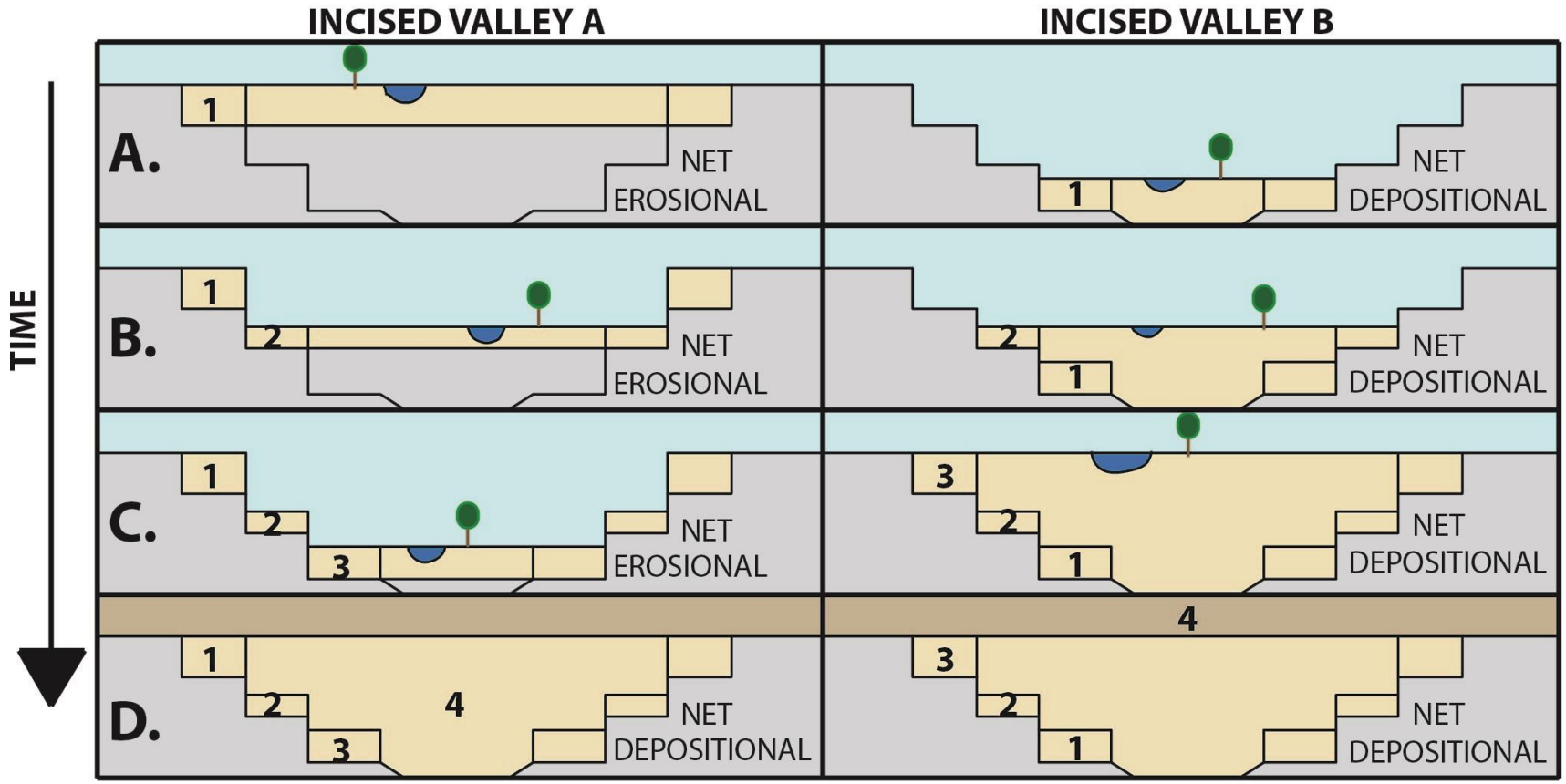
INCISED VALLEY A
INCISED VALLEY B
TIME
A.
B.
C.
D.
1
2
3
4
NET EROSIONAL
NET DEPOSITIONAL

Figure 2: Simplified illustration depicting how an IVF's deposits relative ages can be interpreted in two ways. Without knowledge of the timing and driving force behind IVF development, it is impossible to determine the correct timing sequence. Deposit 1 is youngest, Deposit 4, oldest.

Figure 3: Map depicting modern sample locations east of Green River, Utah and in respect to their Cretaceous paleogeographic location. Red dots indicate sampling locations for organic carbon, yellow are for detrital zircons. (Modified from Blakey 1996)

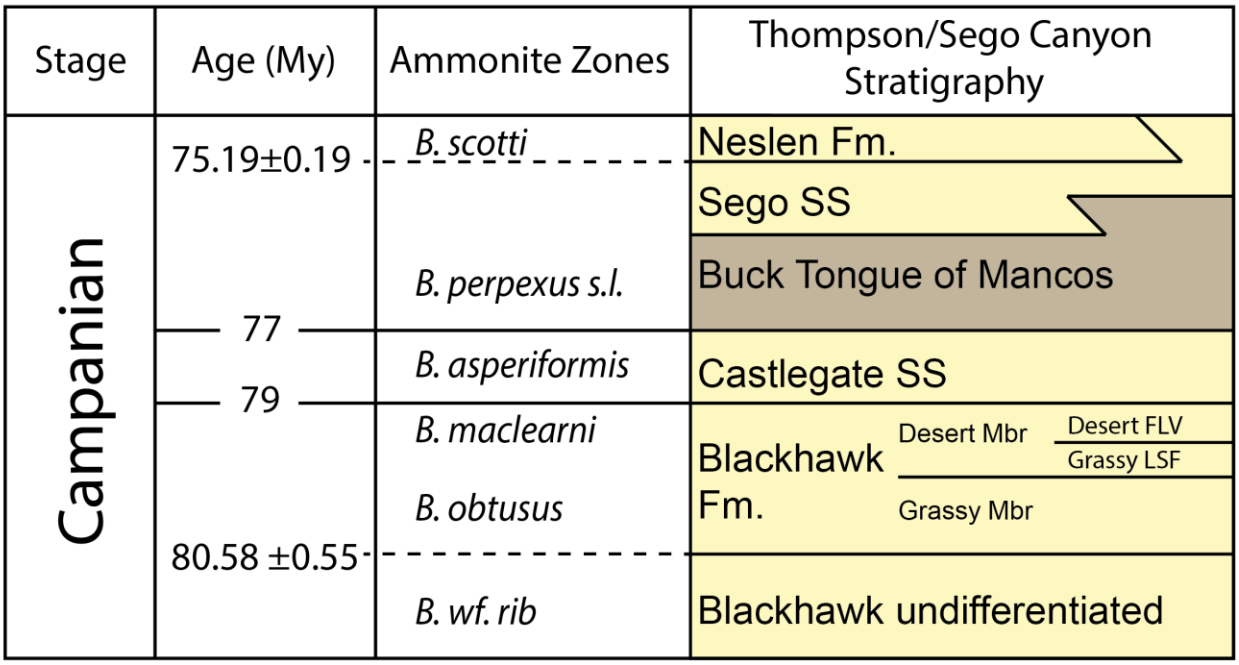
Stage
Age (My)
Ammonite Zones
Thompson/Sego Canyon Stratigraphy
Campanian
75.19±0.19
B. scotti
Neslen Fm.
Sego SS
B. perpexus s.l.
Buck Tongue of Mancos
77
B. asperiformis
Castlegate SS
79
B. maclearni
Blackhawk Fm.
Desert Mbr
Desert FLV
Grassy LSF
B. obtusus
Grassy Mbr
80.58 ±0.55
B. wf. rib
Blackhawk undifferentiated

Figure 4: Study area stratigraphy and biostratigraphy (Cobban et al. 2006), between Green River, UT, and Grand Junction, CO.

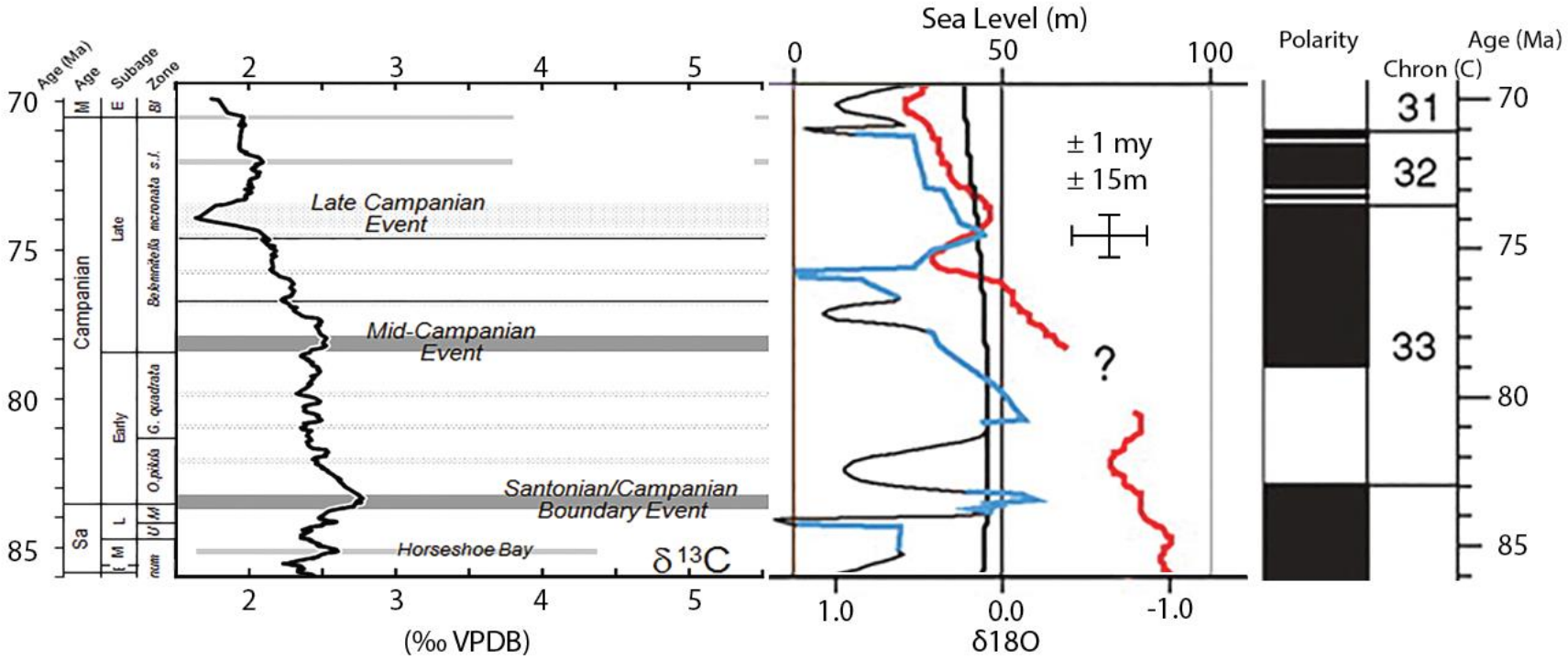
Age (Ma)
Age
Subage
Zone
70
75
80
85
M
Campanian
Sa
E
Late
Early
L
M
E
M
L
Bl
Bekomatella micronata s.l.
G. quadrata
O.pilula
Late Campanian Event
Mid-Campanian Event
Santonian/Campanian Boundary Event
Horseshoe Bay
δ13C
2
3
4
5
(‰ VPDB)
Sea Level (m)
0
50
100
± 1 my
± 15m
?
1.0
0.0
-1.0
δ18O
Polarity
Chron (C)
31
32
33
Age (Ma)
70
75
80
85

Figure 5: Cretaceous organic carbon isotope and sea level curves. Isotope curve was generated and validated using chalk successions in England, Europe and North Africa. Sea level curves were generated by back-stripping studies from New Jersey and other locations globally (Modified from Jarvis 2006 and Miller 2005).

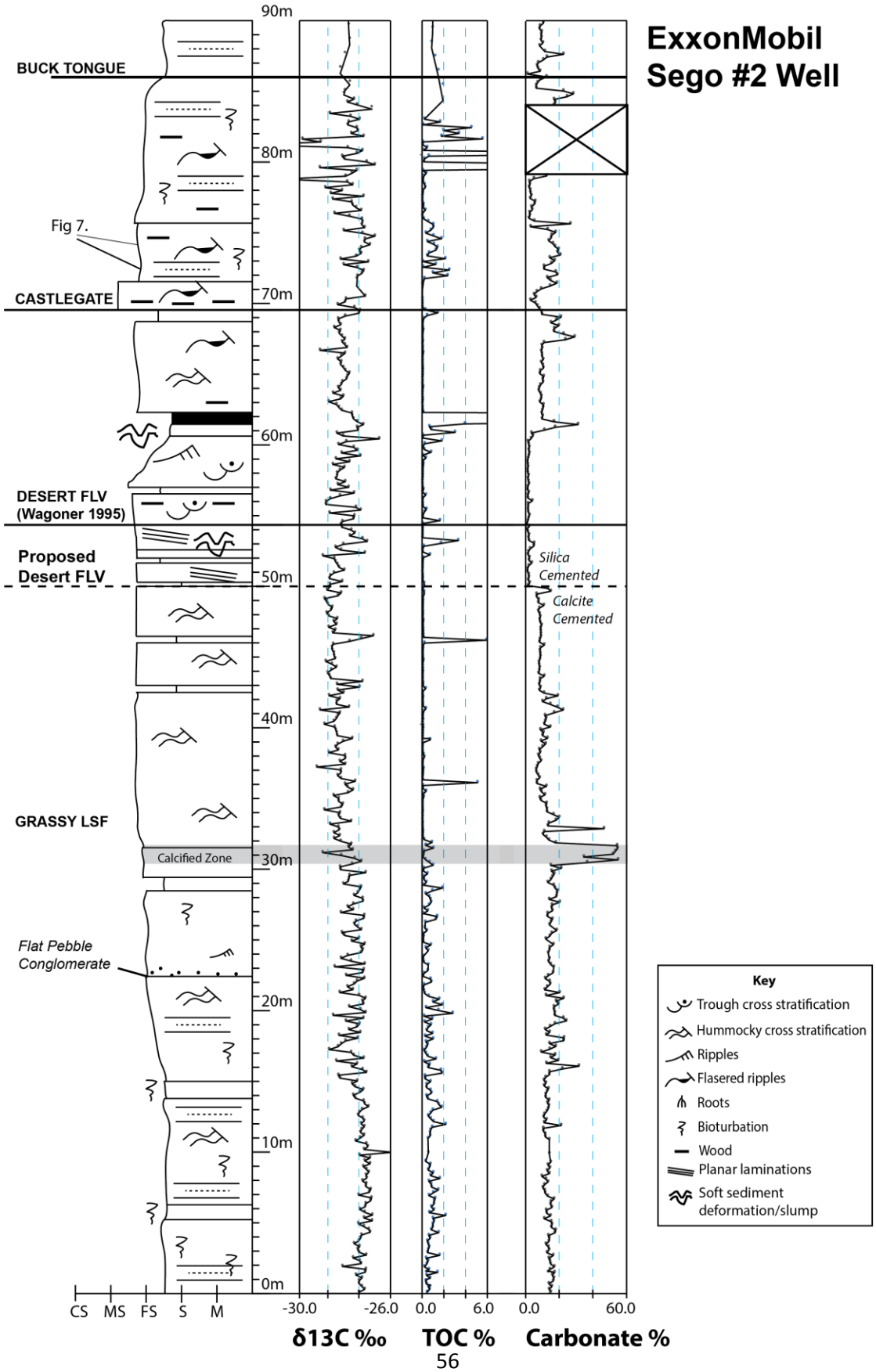
ExxonMobil
Sego #2 Well
BUCK TONGUE
CASTLEGATE
DESERT FLV
(Wagoner 1995)
Proposed
Desert FLV
GRASSY LSF
Calcified Zone
Flat Pebble
Conglomerate
Fig 7.
Silica
Cemented
Calcite
Cemented
90m
80m
70m
60m
50m
40m
30m
20m
10m
0m
CS
MS
FS
S
M
-30.0
-26.0
0.0
6.0
0.0
60.0
δ13C ‰
TOC %
Carbonate %
Key
Trough cross stratification
Hummocky cross stratification
Ripples
Flasered ripples
Roots
Bioturbation
Wood
Planar laminations
Soft sediment
deformation/slump

Figure 6: Sego #2 measured section. Three curves are: Organic carbon isotope composition, sample total organic carbon, and weight % carbonate of sample.

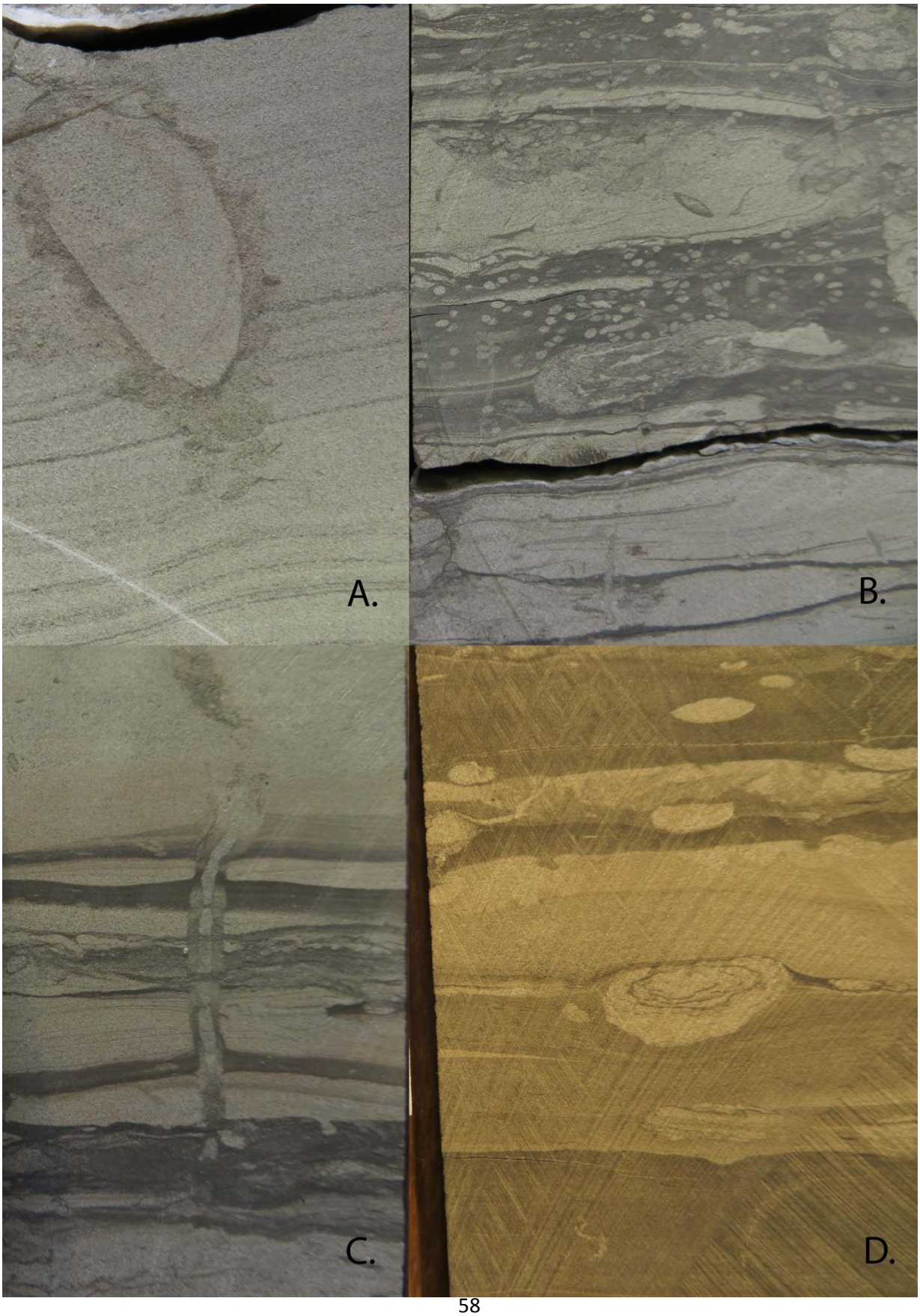
A.
B.
C.
D.

Figure 7: Sego #2 trace fossils from the Grassy LSF of the Desert Member: A: *Ophiomorpha*, B: *Chondrities, Rhizocorallium, Skolithos, Thalassinoides, Planolites, and Palaeophycus.* C: *Rosselia, Ophiomorpha, Palaeophycus, Planolites, and Cylindrichnus*, D: *Asterosoma, Thalassinoides, Lockeia, Helminthopsis.*

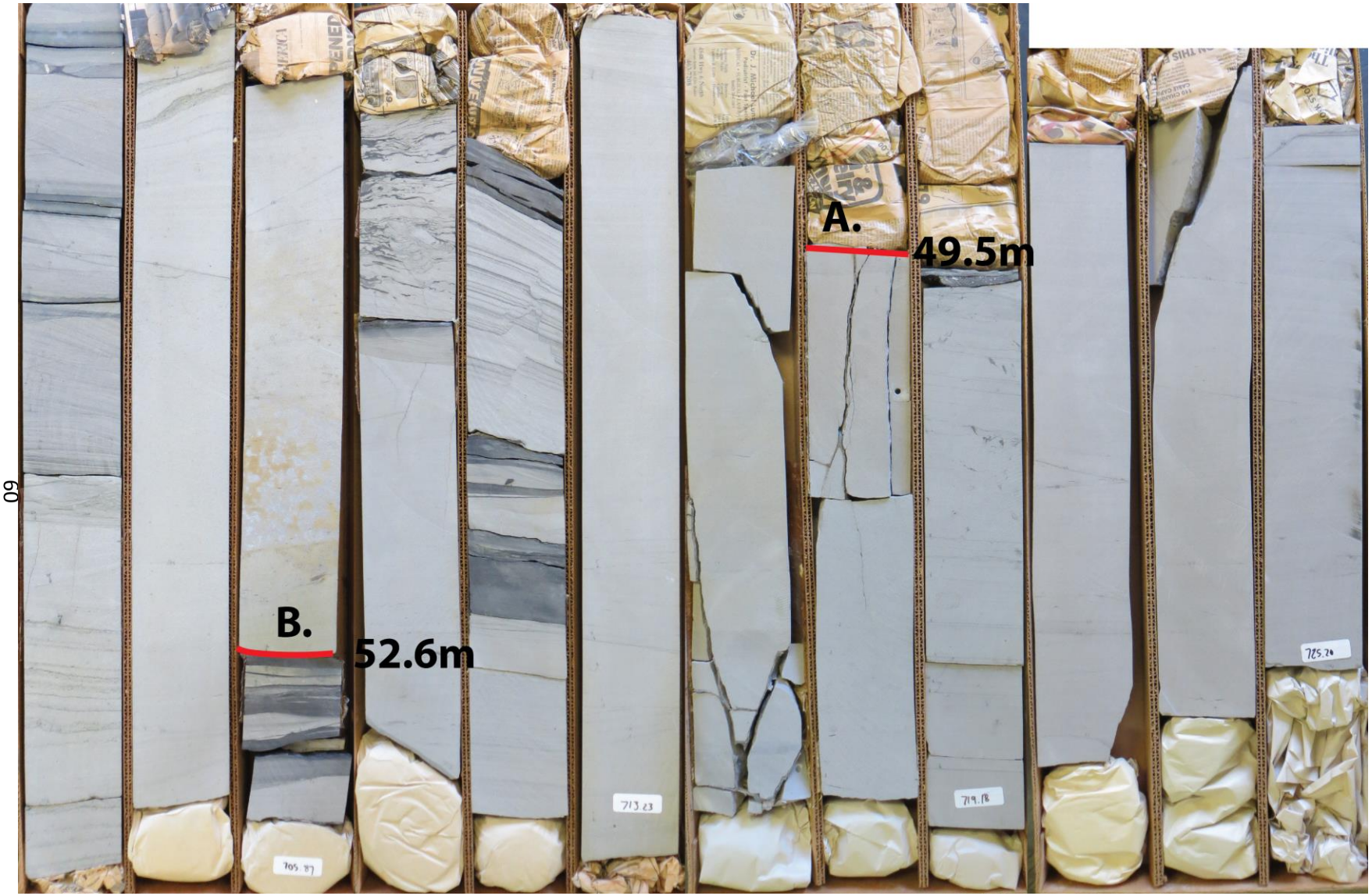

60

Figure 8: Photos of the Sego #2 core from 46.5m to 55.2m from the base of the core. Van Wagoner (1995) placed the Desert member SB at surface B. Cementation changes from calcite to siliceous near surface A., the strata above show slump structures, trough cross stratification and planar lamination.

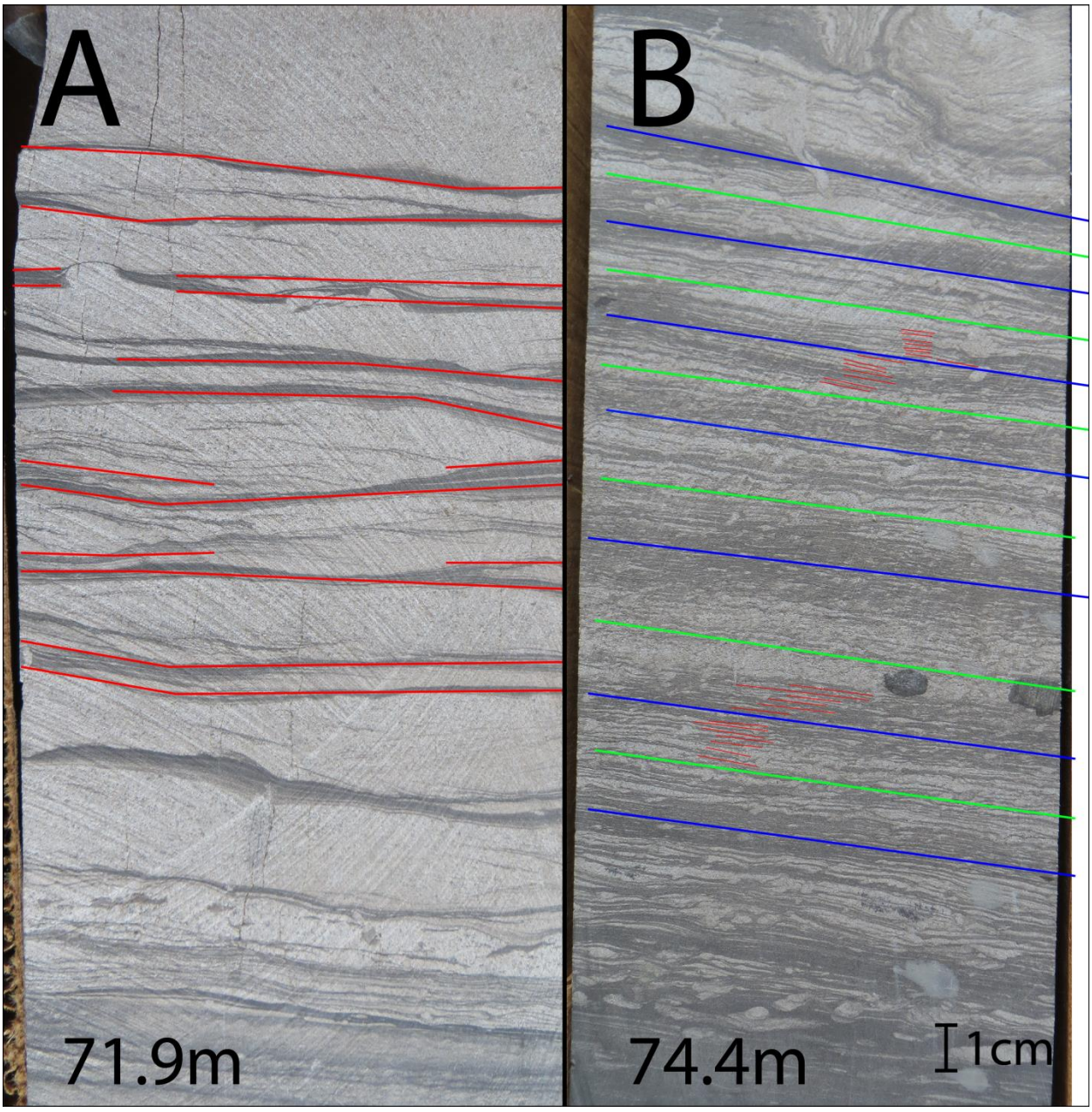
A
B
71.9m
74.4m
1cm

Figure 9: Castlegate sedimentary structures interpreted as tidal in origin: A. Double mud drapes deposited during the 2 periods of slack-water in one diurnal cycle. B. bundles of ~14 laminae or double lamina due to oscillation between spring and neap tide. Red = slack-water conditions. Blue = Neap tide apex. Green = Spring tide apex.

Sego #2: Buck Tongue Section

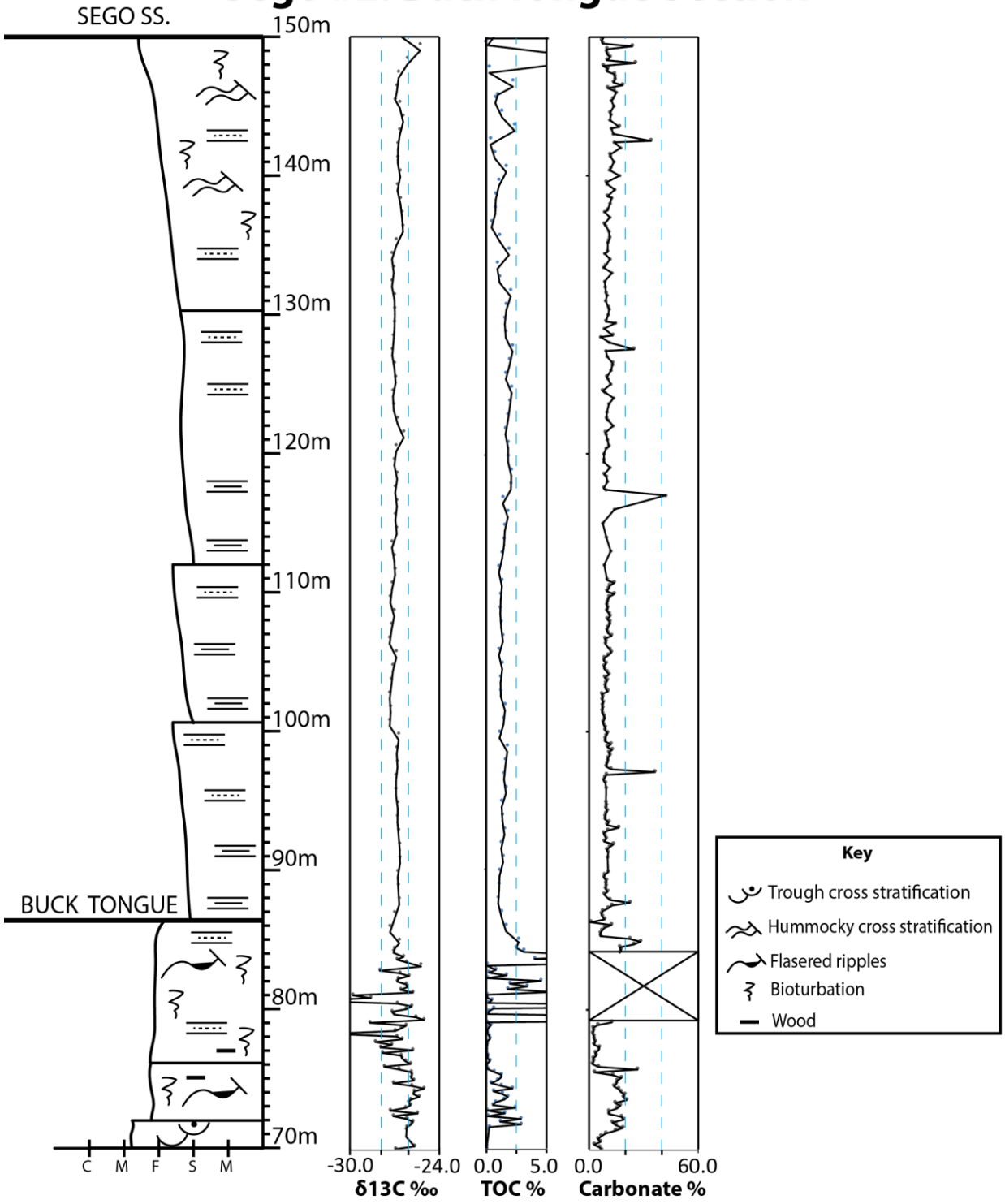

Figure 10: Buck Tongue Measured Section. The three curves are left to right: Organic carbon isotope composition, sample total organic carbon, and weight % carbonate of sample.

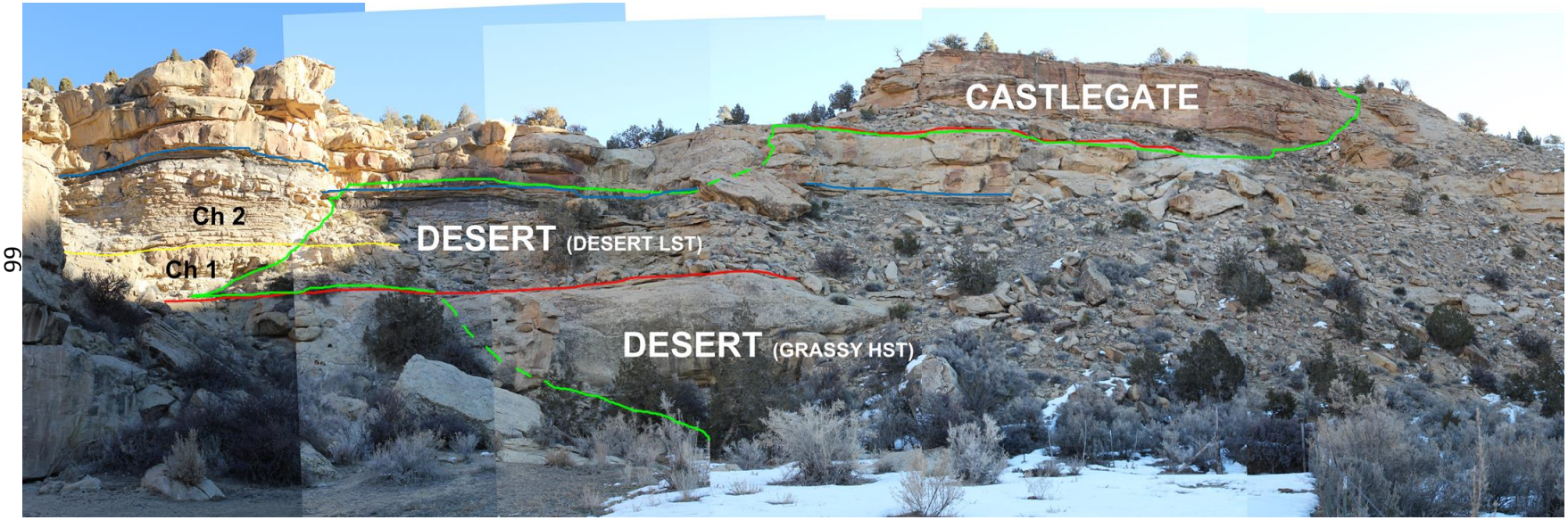
CASTLEGATE
Ch 2
Ch 1
DESERT (DESERT LST)
DESERT (GRASSY HST)

Figure 11: Thompson Canyon outcrop photomosaic. Green line is sampling path, Red lines denote sequence boundaries, blue lines: TSE, yellow lines: separate different channel sands. Ch 2 is an abandoned channel fill, complete with clay plug.

Thompson Canyon

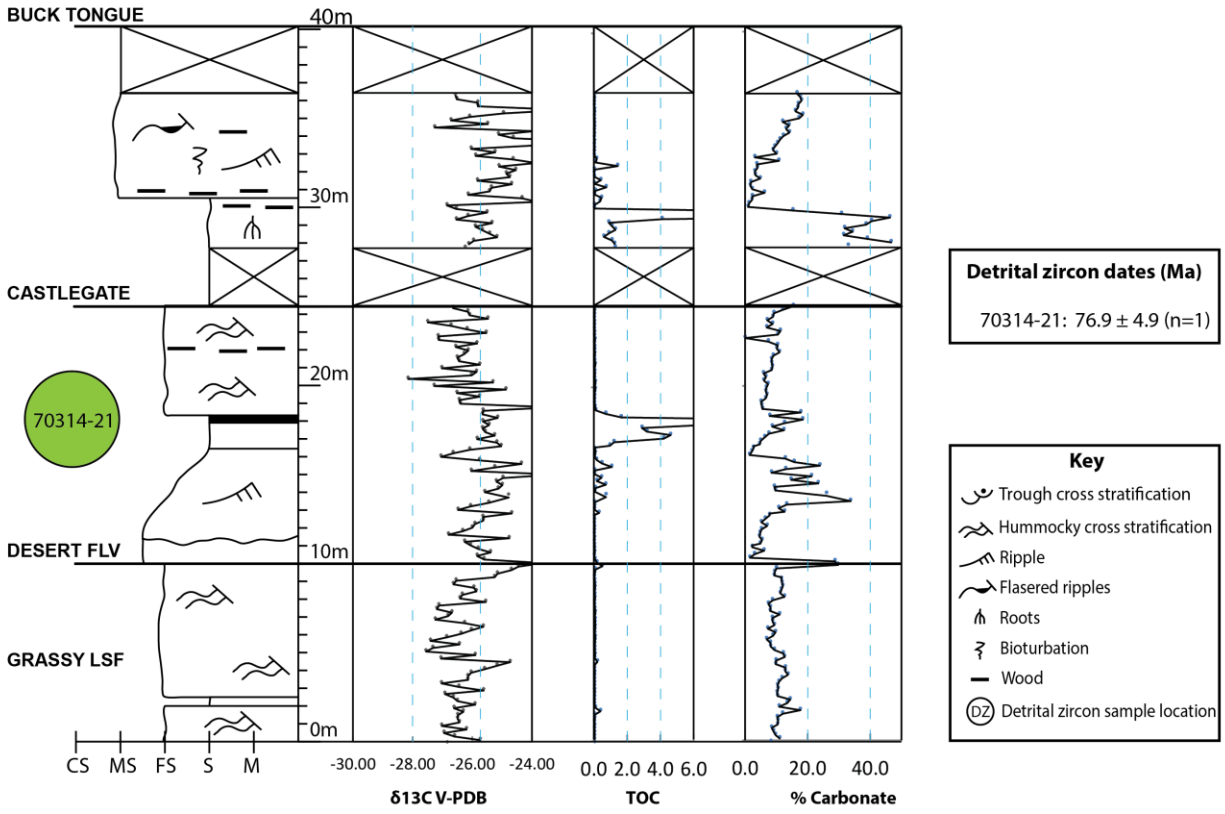

Figure 12: Thompson Canyon Measured Section. The three curves are left to right: Organic carbon isotope composition, sample total organic carbon, and weight % carbonate of sample. Detrital zircon dates represent MDA from a single anaysis (n=1)

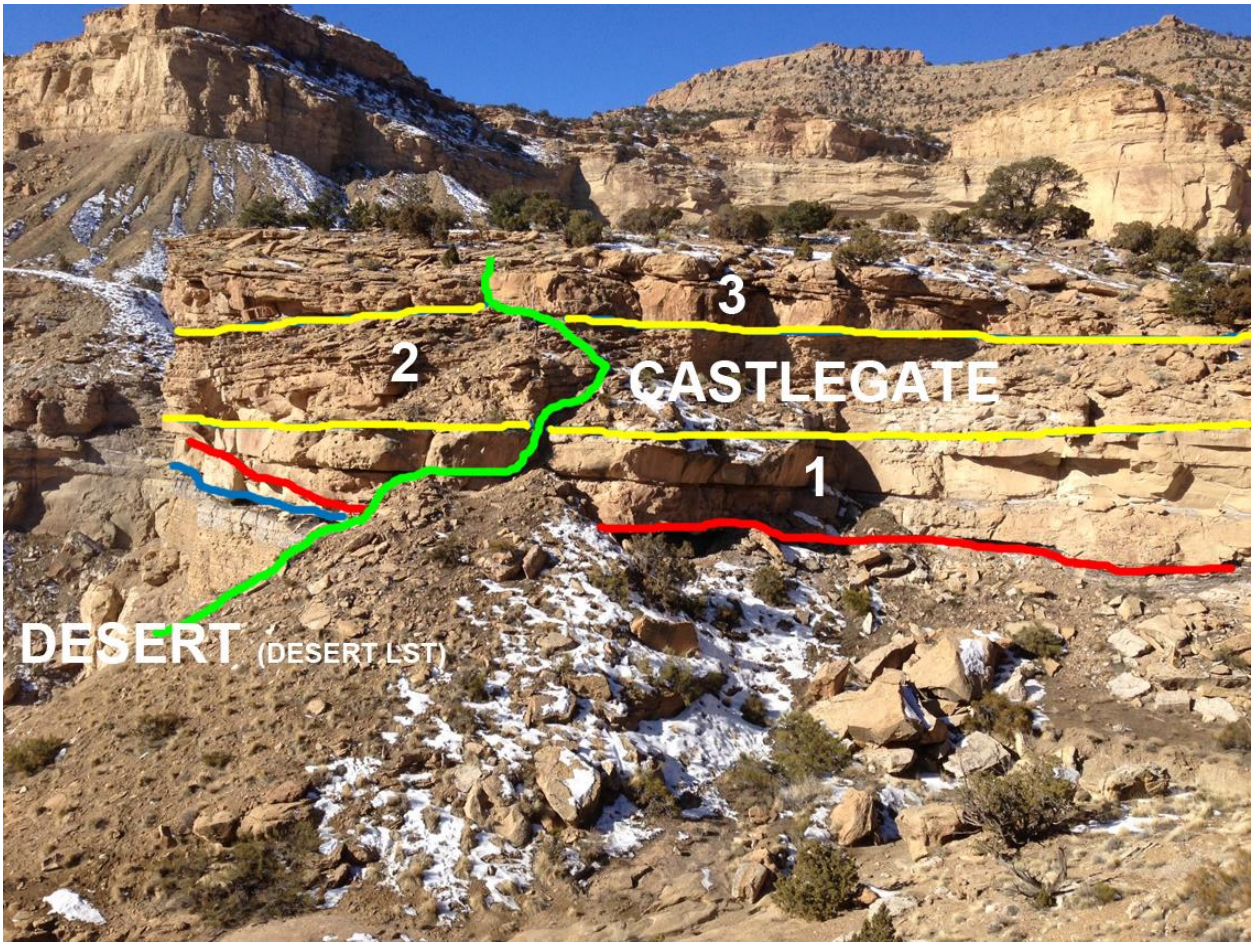
3
2
CASTLEGATE
1
DESERT (DESERT LST)

Figure 13: Blaze Canyon outcrop. Green: sampling path. Red is sequence boundary. Blue is TSE. Yellow: separates different channel sands.

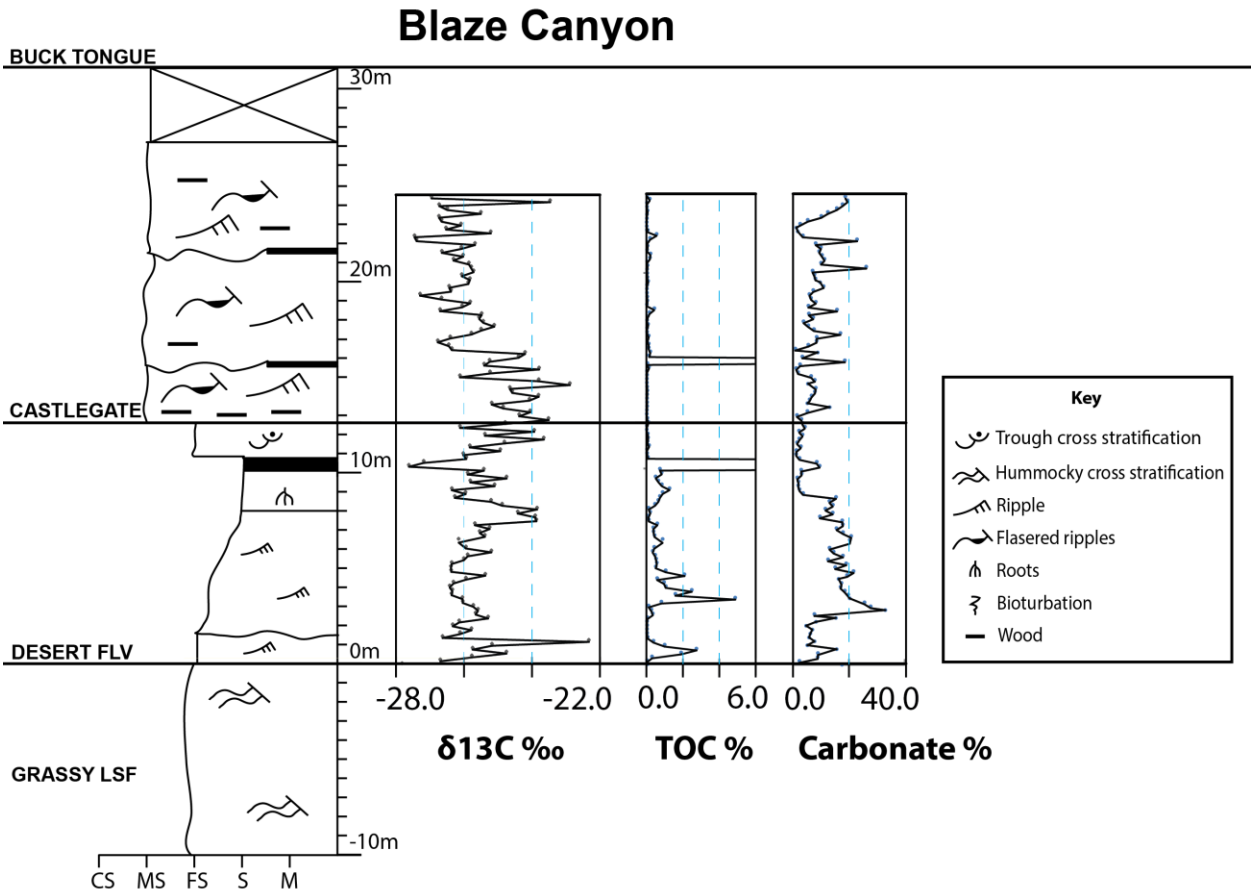
Blaze Canyon
BUCK TONGUE
CASTLEGATE
DESERT FLV
GRASSY LSF
30m
20m
10m
0m
-10m
CS
MS
FS
S
M
-28.0
-22.0
0.0
6.0
0.0
40.0
δ13C ‰
TOC %
Carbonate %
Key
Trough cross stratification
Hummocky cross stratification
Ripple
Flasered ripples
Roots
Bioturbation
Wood

Figure 14: Blaze Canyon Measured Section. The three curves are left to right: Organic carbon isotope composition, sample total organic carbon, and weight % carbonate of sample.

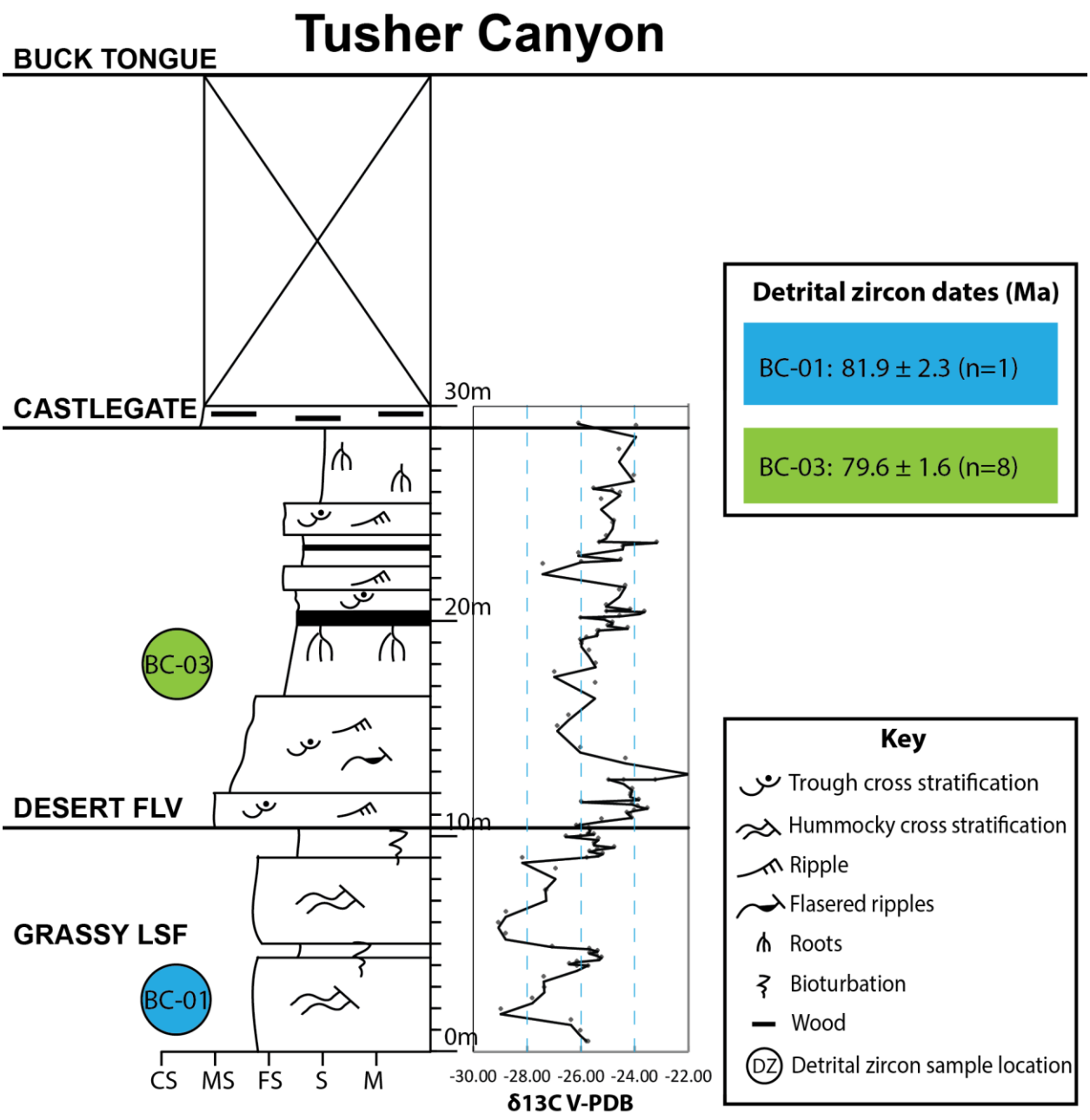
Tusher Canyon
BUCK TONGUE
CASTLEGATE
DESERT FLV
GRASSY LSF
BC-03
BC-01
30m
20m
10m
0m
CS
MS
FS
S
M
-30.00 -28.00 -26.00 -24.00 -22.00
δ13C V-PDB
Detrital zircon dates (Ma)
BC-01: 81.9 ± 2.3 (n=1)
BC-03: 79.6 ± 1.6 (n=8)
Key
Trough cross stratification
Hummocky cross stratification
Ripple
Flasered ripples
Roots
Bioturbation
Wood
DZ
Detrital zircon sample location

Figure 15: Tusher Canyon measured section (modified from Cornwell 2010). Single detrital zircon age from sample BC-01 yields an MDA of 81.9 ± 2.3 Ma. Averaged (n=3) detrital zircon age from sample BC-03 yields an MDA of 78.9 ± 3.4 Ma.

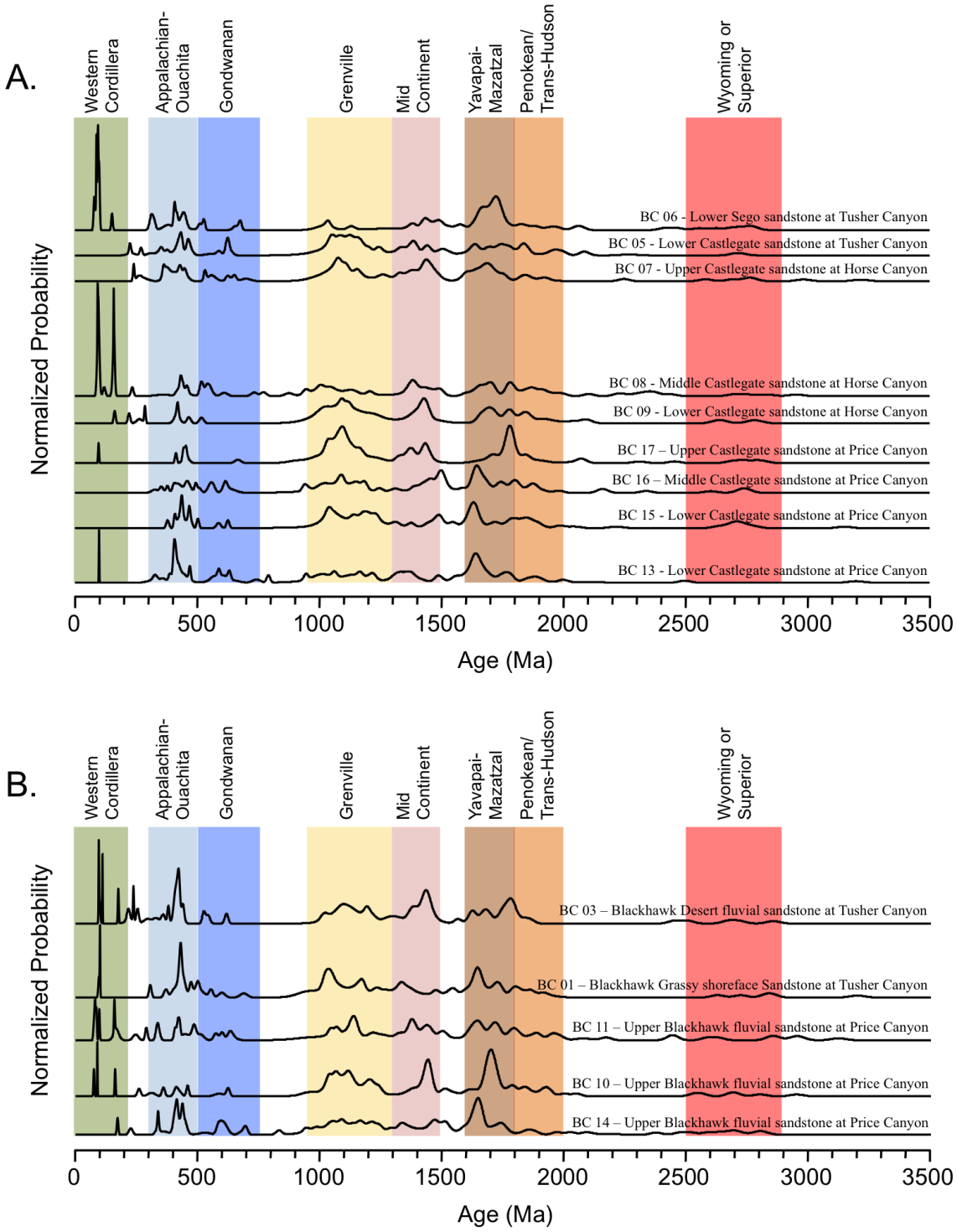
A.
Western Cordillera
Appalachian-Ouachita
Gondwanan
Grenville
Mid Continent
Yavapai-Mazatzal
Penokean/Trans-Hudson
Wyoming or Superior
Normalized Probability
BC 06 - Lower Sego sandstone at Tusher Canyon
BC 05 - Lower Castlegate sandstone at Tusher Canyon
BC 07 - Upper Castlegate sandstone at Horse Canyon
BC 08 - Middle Castlegate sandstone at Horse Canyon
BC 09 - Lower Castlegate sandstone at Horse Canyon
BC 17 – Upper Castlegate sandstone at Price Canyon
BC 16 – Middle Castlegate sandstone at Price Canyon
BC 15 - Lower Castlegate sandstone at Price Canyon
BC 13 - Lower Castlegate sandstone at Price Canyon
0
500
1000
1500
2000
2500
3000
3500
Age (Ma)
B.
Western Cordillera
Appalachian-Ouachita
Gondwanan
Grenville
Mid Continent
Yavapai-Mazatzal
Penokean/Trans-Hudson
Wyoming or Superior
Normalized Probability
BC 03 – Blackhawk Desert fluvial sandstone at Tusher Canyon
BC 01 – Blackhawk Grassy shoreface Sandstone at Tusher Canyon
BC 11 – Upper Blackhawk fluvial sandstone at Price Canyon
BC 10 – Upper Blackhawk fluvial sandstone at Price Canyon
BC 14 – Upper Blackhawk fluvial sandstone at Price Canyon
0
500
1000
1500
2000
2500
3000
3500
Age (Ma)

Figure 16: The detrital zircon data from the Blackhawk Fm. through the Sego Sandstone show several patterns of age signatures that have been identified in previous studies of Cretaceous strata in the western interior. One primary population group consists of zircons that were ultimately derived from (a) the Mid-continent anorogenic granites (ca. 1.5-1.3 Ga), and magmatism associated with the (b) Grenville (ca. 1.25-0.95 Ga) and (c) Appalachian orogenies (ca. 500-300 Ma): this assemblage represents a signature that was initially derived from the Appalachian cordillera, and transported by river systems to the Paleozoic passive margin of western North America during the late Paleozoic and early Mesozoic, then eroded from the Sevier orogeny during the Cretaceous. A second important population group is derived from (a) the paleo-Proterozoic Yavapai-Mazatzal orogeny (ca. 1.6-1.8 Ga), best exposed along the Mogollon Rim of Arizona, and (b) the Mesozoic Sierra Nevada magmatic arc (ca. 275-55 Ma), located to the west of the Sevier fold and thrust belt. These two population groups characterize many DZ populations that have been described from the Western Interior foreland basin

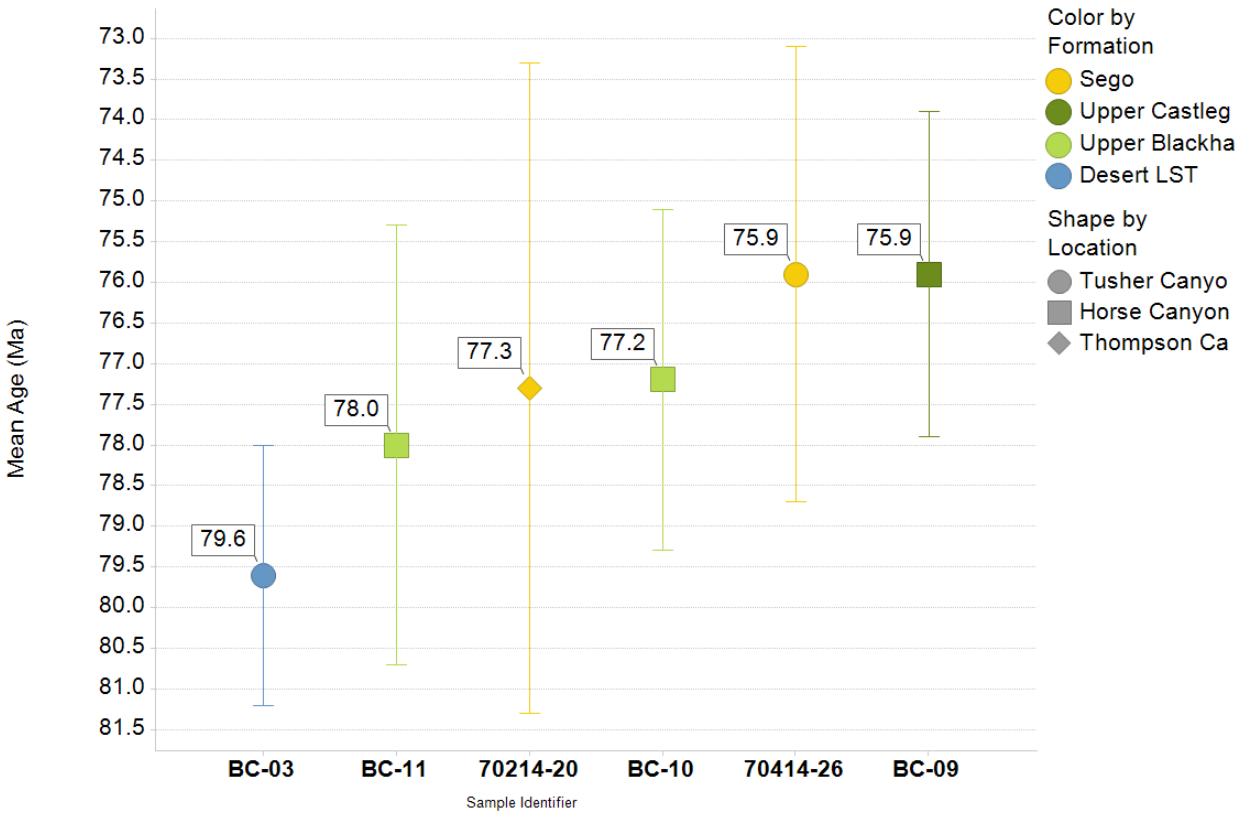

Figure 17. Weighted mean U-Pb age's (MDA) for Upper Blackhawk to Sego Sandstone strata from Tusher, Horse, and Thompson Canyons (Appendices F, G, and H). Samples containing less than three grains have been excluded. MDA's obey the stratigraphic superposition law, and thus can be used as indicators of age relative to one another, but because the errors overlap, there is considerable uncertainty that the dates are absolute dates.

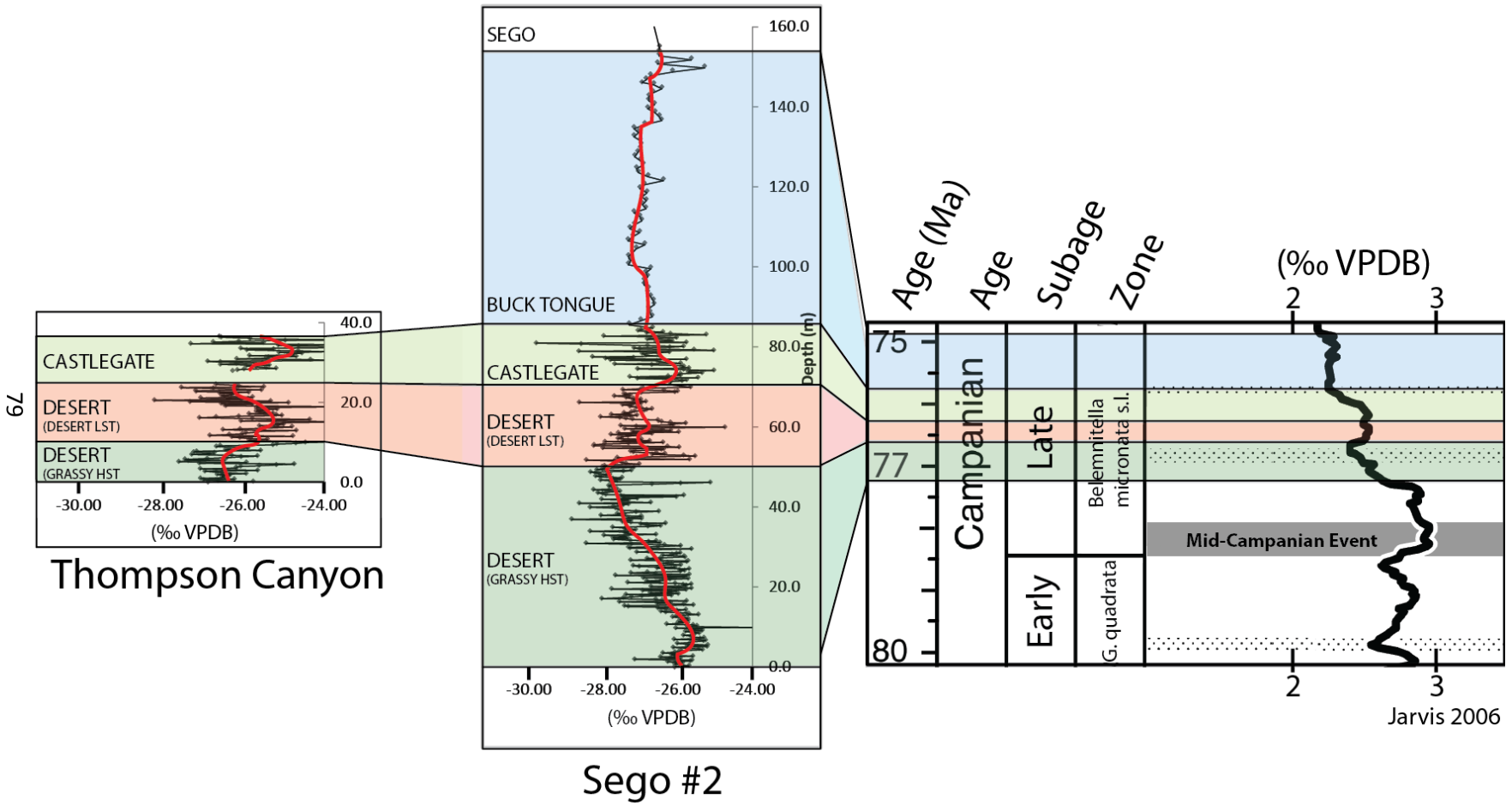
79
CASTLEGATE
DESERT
(DESERT LST)
DESERT
(GRASSY HST
40.0
20.0
0.0
-30.00
-28.00
-26.00
-24.00
(‰ VPDB)
Thompson Canyon
SEGO
BUCK TONGUE
CASTLEGATE
DESERT
(DESERT LST)
DESERT
(GRASSY HST)
160.0
140.0
120.0
100.0
80.0
60.0
40.0
20.0
0.0
Depth (m)
-30.00
-28.00
-26.00
-24.00
(‰ VPDB)
Sego #2
Age (Ma)
Age
Subage
Zone
75
77
80
Campanian
Late
Early
Belemnitella mucronata s.l.
G. quadrata
(‰ VPDB)
2
3
Mid-Campanian Event
Jarvis 2006

Figure 18: Global correlation between Sego and Thompson canyons and the global Cretaceous carbon isotope curve of Jarvis et al. (2006). Sego and Thompson data is overlain by interpreted formation contacts (black lines) (Van Wagoner 1995). It is worth noting that the positive excursion beginning just below the Desert LSF contact in Thompson Canyon is present above the same contact in the Sego #2 core. This indicates that it is possible that the Thompson Canyon Desert FLV sequence boundary is actually lower than interpreted, and that the positive excursion is held within deltaic sands cutting into underlying hummocky cross stratified (HCS) beds, similar to what was interpreted in the Sego #2 core. Further study should be done to test this hypothesis.

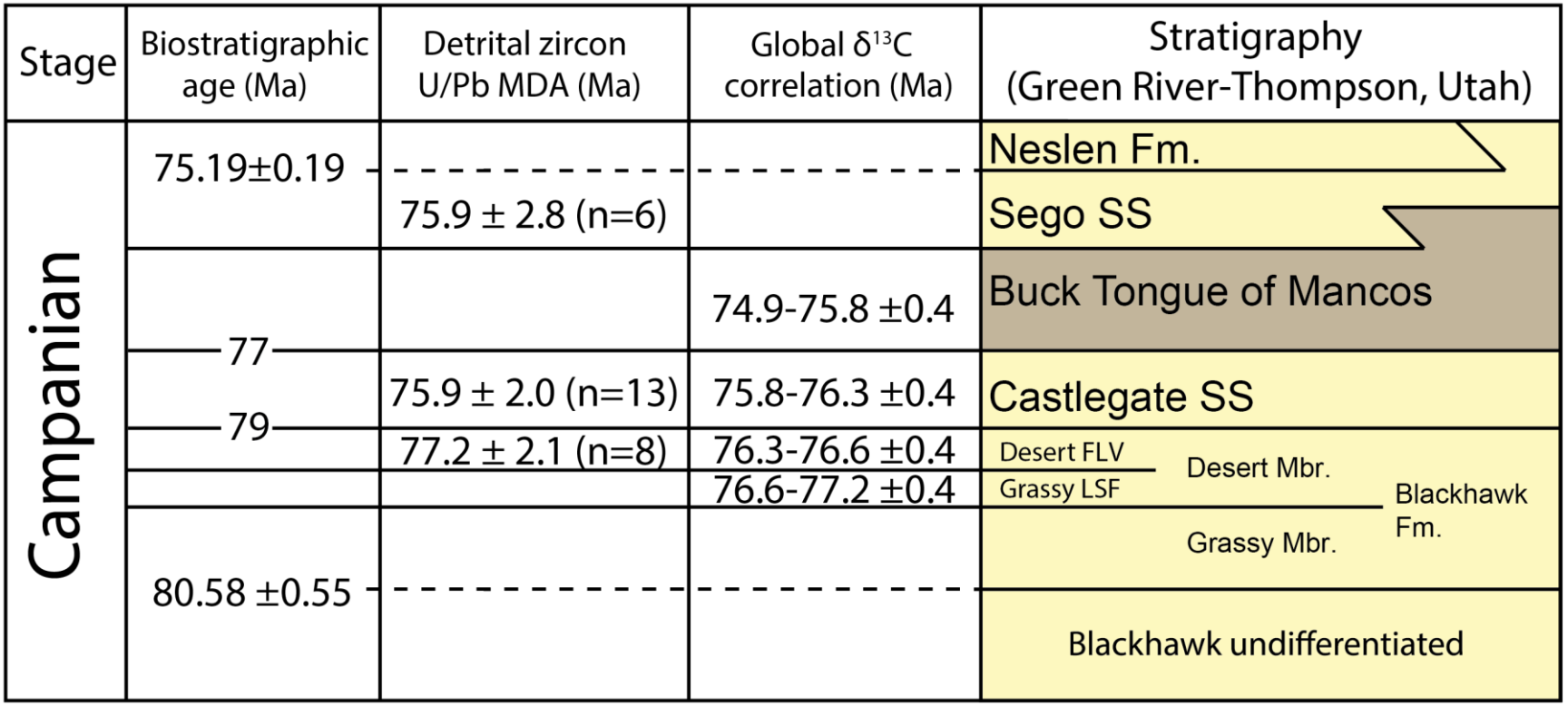
Stage
Biostratigraphic age (Ma)
Detrital zircon U/Pb MDA (Ma)
Global δ13C correlation (Ma)
Stratigraphy (Green River-Thompson, Utah)
Campanian
75.19±0.19
75.9 ± 2.8 (n=6)
Neslen Fm.
Sego SS
74.9-75.8 ±0.4
Buck Tongue of Mancos
77
75.9 ± 2.0 (n=13)
75.8-76.3 ±0.4
Castlegate SS
79
77.2 ± 2.1 (n=8)
76.3-76.6 ±0.4
Desert FLV
Desert Mbr.
Grassy LSF
76.6-77.2 ±0.4
Blackhawk Fm.
Grassy Mbr.
80.58 ±0.55
Blackhawk undifferentiated

Figure 19: Biostratigraphic ages come from radiometric dating of biostratigraphic zones and compiled are correlated across the western interior by Cobban et al. (2006) and Fouch (1983). DZ U/Pb dates and corresponding MDA's were generated by research groups led by Joel Saylor and Mike Blum (Appendices E, F, and G). Age based on chemostratigraphy is based on chemostratigraphic correlation to the global reference and extrapolation of Jarvis's dates and corresponding error. (**Fig. 18**) (Jarvis et al. 2006). Disagreement between the previous biostratigraphic ages and the new data is likely the result of lack of fossil data within the study area and correlation uncertainty compounded by distance and temporally complex stratigraphy.

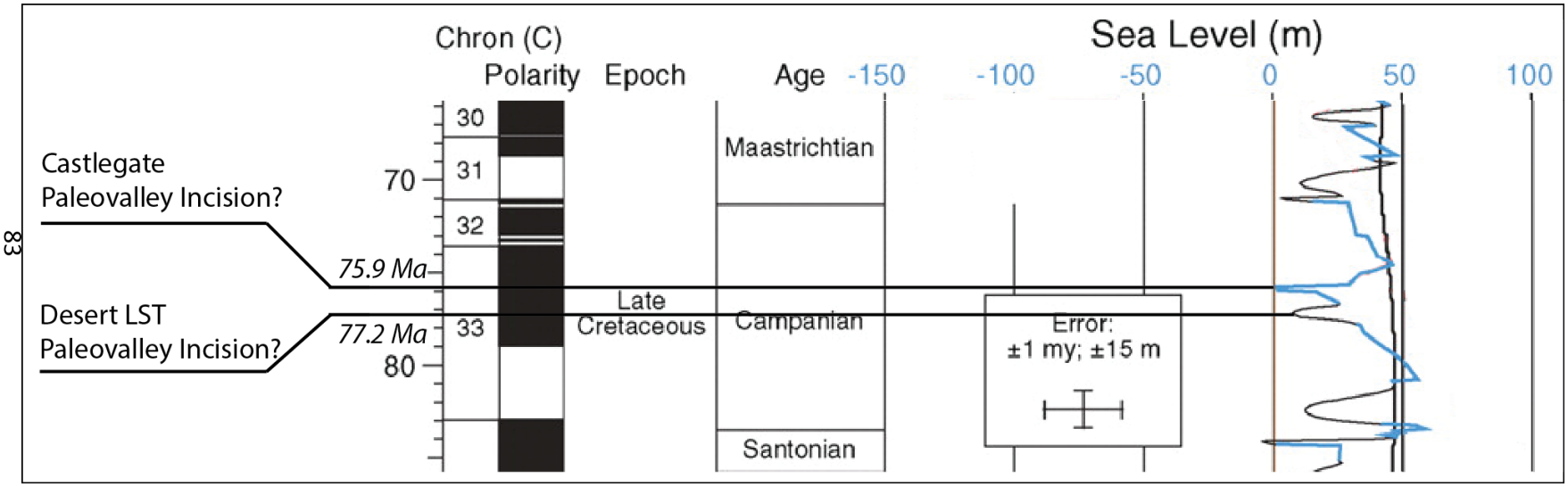
Chron (C)
Polarity
Epoch
Age
Sea Level (m)
-150
-100
-50
0
50
100
30
31
32
33
70
80
75.9 Ma
77.2 Ma
Maastrichtian
Campanian
Santonian
Late
Cretaceous
Error:
±1 my; ±15 m
Castlegate
Paleovalley Incision?
Desert LST
Paleovalley Incision?

Figure 20: Correlation of new ages of Castlegate and Desert FLV strata with the global sea level curve (Miller et al. 2005). Detrital zircon U-Pb geochronology and carbon isotope chemostratigraphy place Desert Member and Castlegate depositional and incisional events coincident with global sea level rises and falls. Isopach maps of the Castlegate IVF indicate that maximum incision was ~120m (Van Wagoner 1995), but the sea level curve only records a drop of ~40m during that time. These eustatic events are very rapid (100 kyr) and are likely responding to periods of rapid glaciation in an otherwise greenhouse world (Miller et al. 2005). Blue line: derived from basin backstripping studies in New Jersey, thin black line: basin backstripping globally, thick black line: long term sea level. (Modified from Miller et al. 2005)

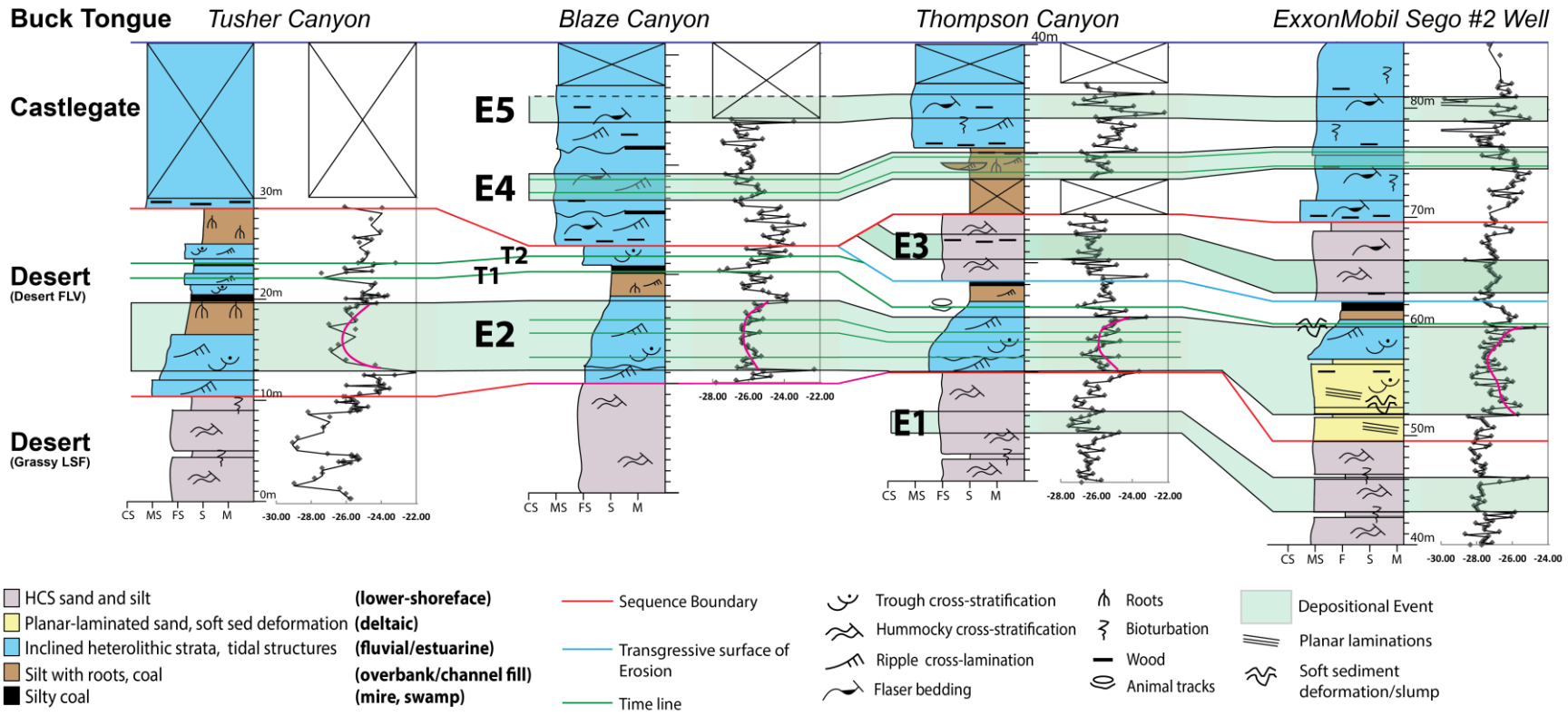
Buck Tongue
Tusher Canyon
Blaze Canyon
Thompson Canyon
ExxonMobil Sego #2 Well
Castlegate
Desert
(Desert FLV)
Desert
(Grassy LSF)
E5
E4
E3
E2
E1
T2
T1
30m
20m
10m
0m
40m
80m
70m
60m
50m
40m
CS MS FS S M
CS MS F S M
-30.00 -28.00 -26.00 -24.00 -22.00
HCS sand and silt (lower-shoreface)
Planar-laminated sand, soft sed deformation (deltaic)
Inclined heterolithic strata, tidal structures (fluvial/estuarine)
Silt with roots, coal (overbank/channel fill)
Silty coal (mire, swamp)
Sequence Boundary
Transgressive surface of Erosion
Time line
Trough cross-stratification
Hummocky cross-stratification
Ripple cross-lamination
Flaser bedding
Roots
Bioturbation
Wood
Animal tracks
Depositional Event
Planar laminations
Soft sediment deformation/slump

Figure 21: Regional correlation of the four chemostratigraphic and stratigraphic profiles from Tusher, Blaze and Thompson Canyons and the Sego #2 drill core. The four sections have been hung on the Buck Tongue contact and correlated based on previously interpreted stratigraphic contacts, and isotopic composition. Seventeen different isotopic excursions, some which are correlatable across all four measured sections, have been identified. These excursions have been grouped together into five correlatable events (E1-E5). Two excursions fall outside of these events and have been labeled T1 and T2. Sequence stratigraphic and facies interpretation has been modified from Van Wagoner (1995) based on results of my study. Comparison of the old framework against the new is shown in (**Fig. 23)**.

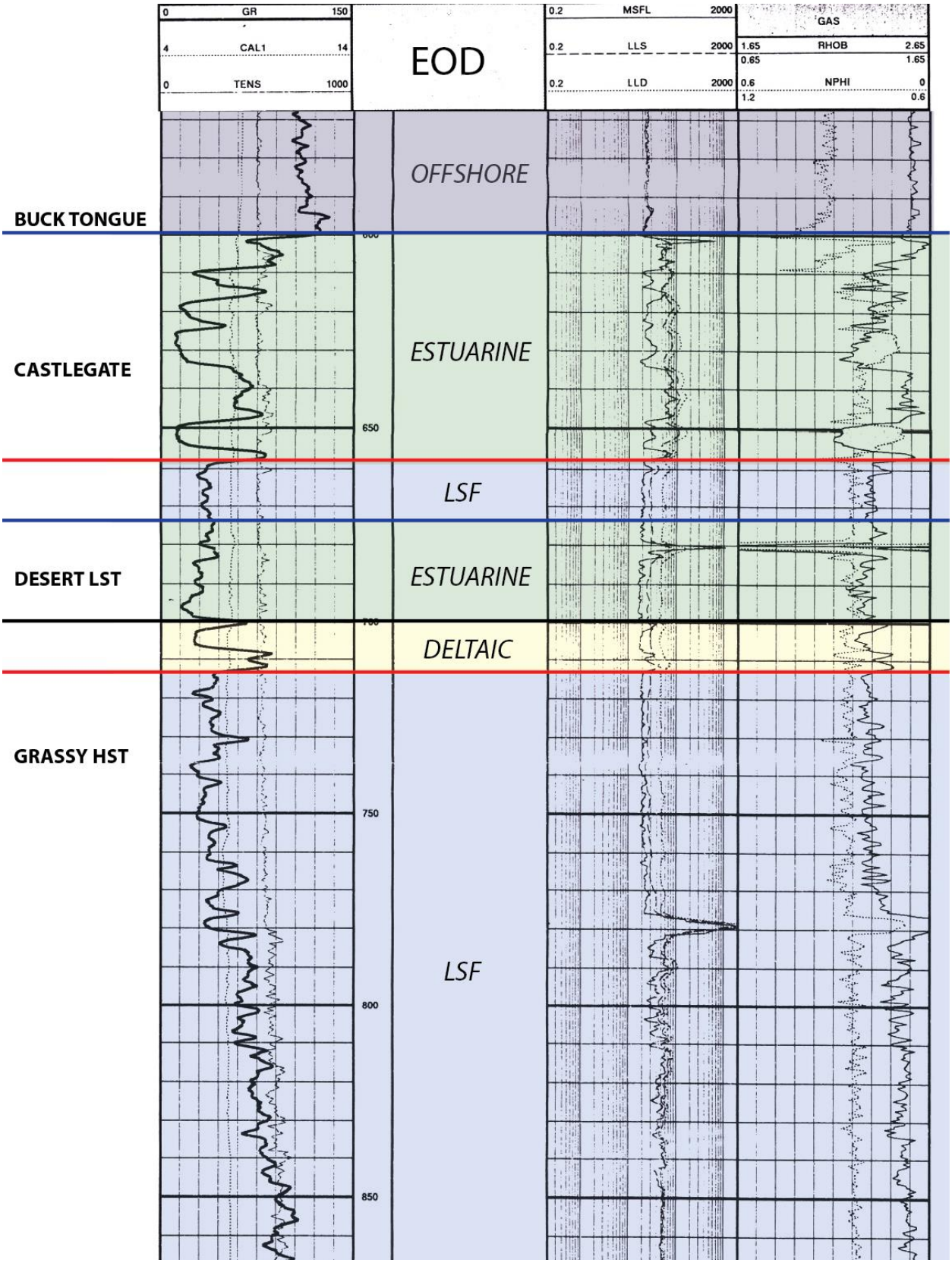
0 GR 150
4 CAL1 14
0 TENS 1000
EOD
0.2 MSFL 2000
0.2 LLS 2000
0.2 LLD 2000
GAS
1.65 RHOB 2.65
0.65 1.65
0.6 NPHI 0
1.2 0.6
OFFSHORE
BUCK TONGUE
ESTUARINE
CASTLEGATE
650
LSF
DESERT LST
ESTUARINE
DELTAIC
GRASSY HST
LSF
750
800
850

Figure 22: Interpreted Sego #2 well logs. My interpretations of environment of deposition (EOD) are based on core studies and log analysis. (Courtesy of ExxonMobil)

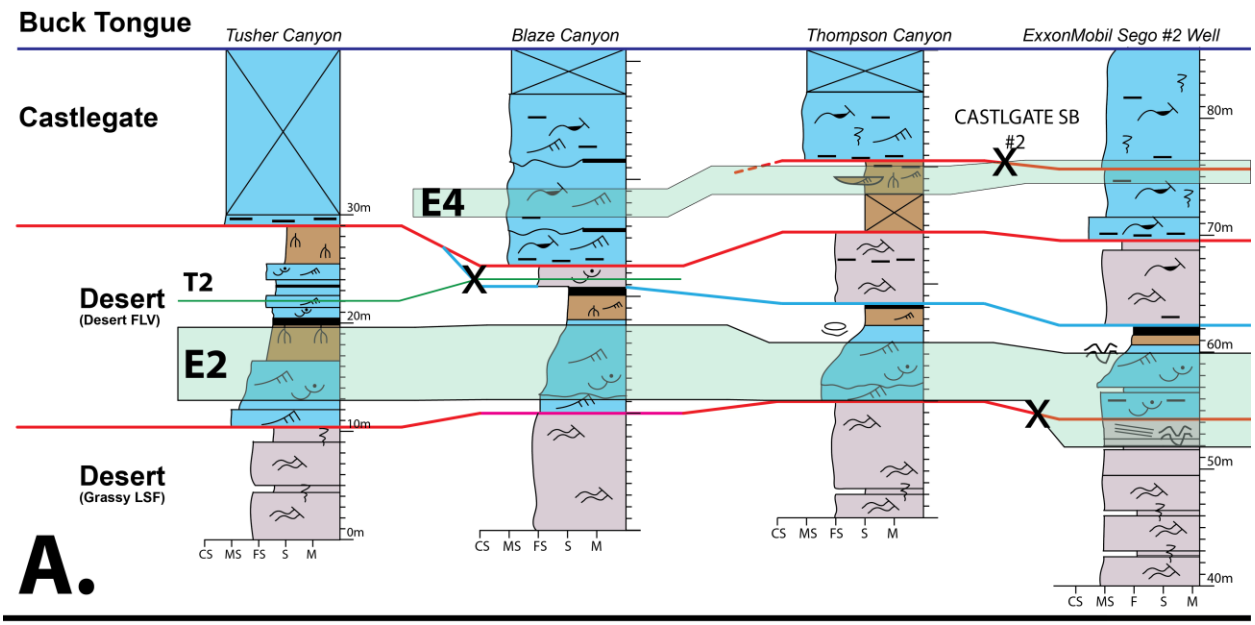
Buck Tongue
Tusher Canyon
Blaze Canyon
Thompson Canyon
ExxonMobil Sego #2 Well
Castlegate
CASTLGATE SB #2
E4
T2
Desert
(Desert FLV)
E2
Desert
(Grassy LSF)
30m
20m
10m
0m
80m
70m
60m
50m
40m
CS MS FS S M
CS MS F S M
A.

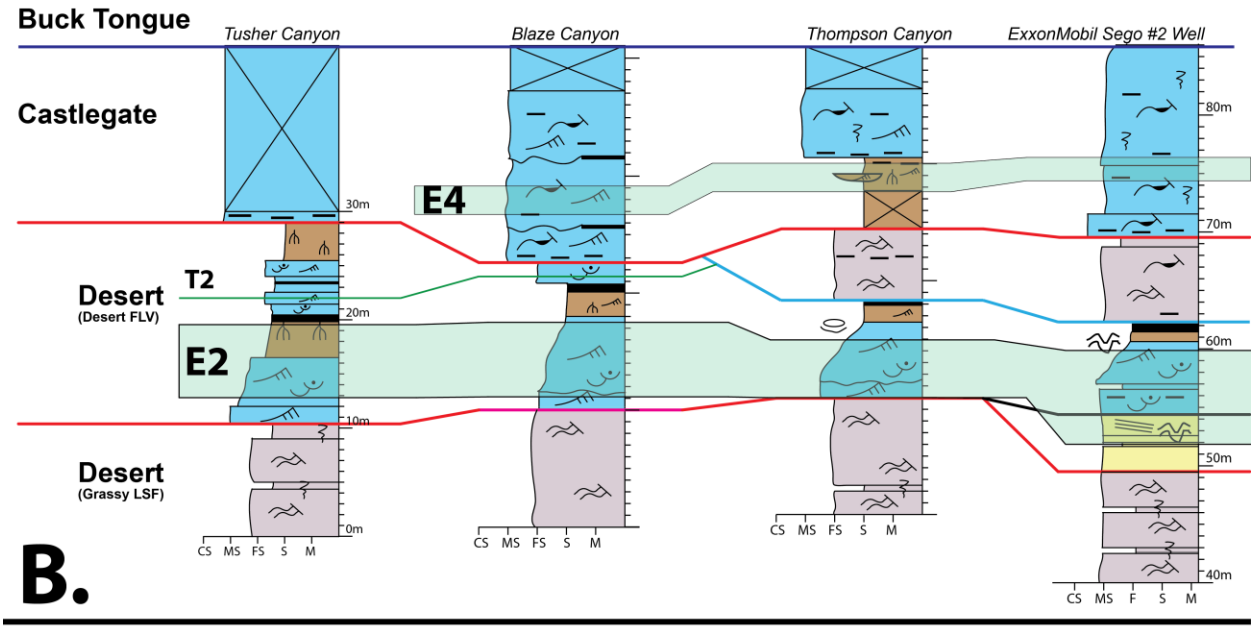
Buck Tongue
Tusher Canyon
Blaze Canyon
Thompson Canyon
ExxonMobil Sego #2 Well
Castlegate
E4
T2
Desert
(Desert FLV)
E2
Desert
(Grassy LSF)
30m
20m
10m
0m
80m
70m
60m
50m
40m
CS MS FS S M
CS MS F S M
B.

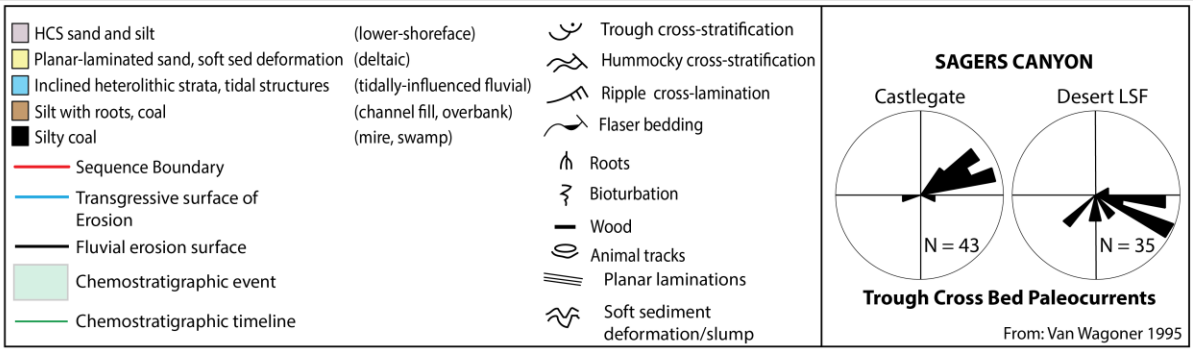
HCS sand and silt
Planar-laminated sand, soft sed deformation
Inclined heterolithic strata, tidal structures
Silt with roots, coal
Silty coal
Sequence Boundary
Transgressive surface of Erosion
Fluvial erosion surface
Chemostratigraphic event
Chemostratigraphic timeline
(lower-shoreface)
(deltaic)
(tidally-influenced fluvial)
(channel fill, overbank)
(mire, swamp)
Trough cross-stratification
Hummocky cross-stratification
Ripple cross-lamination
Flaser bedding
Roots
Bioturbation
Wood
Animal tracks
Planar laminations
Soft sediment deformation/slump
SAGERS CANYON
Castlegate
Desert LSF
N = 43
N = 35
Trough Cross Bed Paleocurrents
From: Van Wagoner 1995

Figure 23: Differing sequence stratigraphic and facies interpretations of my study area: A. Original interpretation by Van Wagoner (1995), B. New interpretation based on chemostratigraphy from this study. ~50-54m in Sego #2 has been reinterpreted as a deltaic deposit (yellow). In light of the chemostratigraphic time lines, and new facies interpretation, the sequence boundary has been shifted to the scour surface below the deltaic deposit. X's denote truncation of time lines and therefore invalidation of the sequence stratigraphic surface as a chronostratigraphic surface. Paleocurrent data comes from Sagers Canyon, which is located 7km SE of the sego #2 wellbore.

APPENDICES

Appendix A: Organic carbon and carbonate data collected from bulk sediments from Thompson Canyon

Depth (m)	Weight (mg)	Amplitude 44 (mV)	Area 44 (Vs)	δ^{13}C VPDB	TOC %	Carbonate %
0.0	37.824	2908	69.02	-26.84	0.06	8.3
0.2	38.429	2498	59.51	-25.73	0.05	11.1
0.4	35.355	2295	54.74	-26.59	0.05	9.7
0.6	39.606	2784	65.94	-26.95	0.05	9.1
0.8	33.804	1995	47.60	-26.20	0.04	8.5
1.0	41.403	3161	75.60	-27.02	0.06	10.4
1.2	37.993	2104	50.30	-26.43	0.04	10.5
1.4	32.565	2786	65.95	-26.49	0.06	10.3
1.6	33.176	2373	56.69	-26.49	0.05	12.0
1.8	9.299	6141	146.89	-26.30	0.48	17.7
2.0	32.203	4815	113.88	-26.61	0.11	10.9
2.2	38.123	2297	54.55	-25.91	0.04	13.5
2.4	38.434	2594	61.39	-26.50	0.05	14.4
2.6	38.257	2727	64.51	-26.63	0.05	10.4
2.8	39.880	2956	69.98	-26.92	0.05	10.2
3.0	31.292	2727	64.38	-25.62	0.06	10.6
3.0	31.700	1796	42.63	-26.68	0.04	10.6
3.2	41.252	2587	61.60	-26.45	0.04	10.4
3.4	34.592	2563	60.55	-27.03	0.05	10.8
3.6	33.622	2375	56.21	-26.15	0.05	11.8
3.8	37.945	2697	63.73	-26.15	0.05	13.7
4.0	37.195	3112	73.79	-26.04	0.06	12.8
4.2	41.973	2991	70.92	-25.59	0.05	12.9
4.4	38.577	2567	60.99	-25.17	0.05	9.8
4.6	41.052	13311	316.72	-24.73	0.24	9.9
4.8	31.220	2600	61.30	-27.05	0.06	12.6
5.0	35.405	4328	101.95	-25.90	0.09	12.2
5.2	41.013	3541	83.88	-27.55	0.06	9.3
5.4	37.340	3204	76.21	-27.32	0.06	8.1
5.6	41.859	3346	78.24	-26.43	0.06	8.1
5.8	36.458	3723	86.45	-27.40	0.07	6.9
6.0	33.637	4460	102.68	-26.86	0.09	8.9
6.2	34.352	3048	70.93	-26.38	0.06	9.7

Appendix A: Organic carbon and carbonate data collected from bulk sediments from Thompson Canyon

Depth (m)	Weight (mg)	Amplitude 44 (mV)	Area 44 (Vs)	δ^{13}C VPDB	TOC %	Carbonate %
6.4	33.636	3279	76.14	-26.03	0.07	7.2
6.6	28.030	3412	78.99	-25.63	0.09	9.4
6.8	36.495	4166	96.22	-26.26	0.08	8.8
7.0	35.058	4091	95.14	-27.24	0.08	8.7
7.2	34.388	2965	68.75	-26.81	0.06	11.0
7.4	37.065	4812	111.20	-26.68	0.09	8.0
7.6	41.945	3793	88.24	-27.19	0.06	8.1
7.8	40.831	2879	67.01	-27.12	0.05	7.4
8.0	41.583	2890	67.14	-25.55	0.05	8.7
8.2	30.716	3359	77.53	-26.41	0.08	12.6
8.4	31.300	2924	67.55	-26.34	0.07	11.2
8.6	40.974	3354	77.84	-25.86	0.06	11.6
8.8	37.751	4251	98.56	-25.95	0.08	12.0
9.0	34.726	3661	84.65	-26.63	0.07	11.8
9.2	38.610	3108	71.89	-26.54	0.06	11.6
9.2	37.473	2243	52.25	-26.15	0.04	11.6
9.4	34.830	1835	42.92	-25.25	0.04	9.3
9.6	34.930	3073	71.20	-25.16	0.06	9.5
9.8	36.575	4499	106.55	-24.69	0.09	10.0
10.0	3.715	3917	90.89	-24.46	0.74	29.7
10.2	21.990	7722	182.35	-23.61	0.25	28.7
10.4	36.595	3432	80.21	-25.61	0.07	1.5
10.6	29.038	1132	27.07	-25.84	0.03	3.0
10.8	30.838	2479	58.06	-25.39	0.06	6.1
11.0	37.834	2254	53.07	-25.80	0.04	2.3
11.0	38.424	2369	56.08	-26.71	0.04	2.3
11.2	38.478	2275	54.55	-26.06	0.04	4.9
11.4	39.062	1624	38.57	-26.26	0.03	5.4
11.6	24.346	1629	38.29	-24.76	0.05	4.6
11.8	38.465	1549	36.66	-26.80	0.03	4.8
12.0	37.326	1922	45.57	-26.32	0.04	5.2
12.2	36.079	2457	58.24	-26.00	0.05	7.0
12.4	37.361	1669	39.61	-25.91	0.03	5.2
12.6	29.130	1671	40.09	-25.63	0.04	6.5
12.8	26.519	1373	32.44	-25.65	0.04	7.9
12.8	27.253	1734	40.65	-25.99	0.05	7.9
13.0	17.177	8588	200.91	-24.68	0.35	12.6
13.2	28.458	1771	41.61	-26.48	0.04	10.8
13.4	30.588	2628	61.72	-26.06	0.06	13.3
13.6	23.613	1584	37.23	-25.45	0.05	33.7

Appendix A: Organic carbon and carbonate data collected from bulk sediments from Thompson Canyon

Depth (m)	Weight (mg)	Amplitude 44 (mV)	Area 44 (Vs)	δ^{13}C VPDB	TOC %	Carbonate %
14.0	2.765	3716	87.88	-24.78	0.99	26.0
14.2	32.871	3035	71.47	-25.58	0.07	9.7
14.4	17.172	2329	54.75	-25.13	0.10	9.4
14.6	5.701	7339	172.41	-24.99	0.93	23.4
14.8	5.092	1514	35.96	-25.20	0.22	14.7
15.0	3.388	2735	65.18	-24.97	0.59	21.2
15.2	19.790	1170	27.69	-23.21	0.04	8.4
15.4	28.200	2083	48.91	-26.04	0.05	13.0
15.6	2.424	4795	112.46	-25.25	1.41	23.9
15.8	3.170	2554	60.07	-24.35	0.58	15.7
16.0	20.170	5194	121.26	-25.76	0.18	12.8
16.2	34.938	2189	51.81	-27.05	0.05	1.4
16.4	33.450	4167	98.12	-26.64	0.09	2.2
16.6	22.374	2721	64.68	-26.08	0.08	2.7
16.6	32.843	2841	67.28	-27.25	0.05	2.7
16.8	2.182	3548	86.31	-25.03	1.01	4.7
17.0	2.084	4293	104.57	-25.18	1.27	5.0
17.2	0.759	5671	136.29	-25.84	4.48	6.3
17.4	0.224	1700	40.93	-25.25	4.99	7.6
17.6	0.413	2375	57.07	-25.57	3.64	12.4
17.8	0.520	2631	62.94	-25.66	3.17	8.7
18.0	0.202	2632	63.23	-25.44	8.17	12.6
18.2	0.241	8628	206.98	-25.64	21.24	18.4
18.4	2.654	8029	191.25	-25.15	1.79	7.9
18.6	2.358	3284	80.12	-25.66	0.87	17.8
18.8	19.512	3974	93.22	-25.64	0.12	5.6
19.0	32.389	4067	96.82	-23.21	0.08	5.3
19.2	32.767	2202	52.56	-26.40	0.04	5.1
19.4	35.132	2717	64.88	-26.44	0.05	6.6
19.6	33.984	2849	69.71	-25.75	0.05	7.0
19.8	37.703	3244	78.23	-26.52	0.05	6.6
20.0	38.496	6286	149.33	-24.87	0.10	6.8
20.2	37.862	4144	99.26	-27.28	0.07	7.4
20.4	35.229	6001	143.06	-25.31	0.10	6.0
20.6	41.261	3465	82.67	-28.15	0.05	6.7
20.8	42.746	3950	94.21	-26.03	0.06	5.9
21.0	41.616	4327	103.07	-25.86	0.06	8.5
21.2	36.260	2573	61.25	-27.02	0.04	8.7
21.4	37.648	5900	139.75	-25.75	0.09	8.5
21.6	32.899	3162	74.90	-26.44	0.06	8.4

Appendix A: Organic carbon and carbonate data collected from bulk sediments from Thompson Canyon

Depth (m)	Weight (mg)	Amplitude 44 (mV)	Area 44 (Vs)	δ^{13}C VPDB	TOC %	Carbonate %
21.8	40.806	3052	72.57	-26.51	0.05	9.0
22.0	29.535	3227	77.12	-26.27	0.07	11.0
22.2	35.087	2516	57.71	-26.14	0.06	10.1
22.4	35.675	2789	64.24	-26.55	0.06	10.4
22.6	40.149	2088	48.53	-25.84	0.04	7.4
22.8	39.914	3522	81.59	-27.13	0.07	0.0
23.0	44.210	2563	59.66	-27.14	0.05	10.5
23.2	42.392	3184	73.65	-25.53	0.06	11.3
23.4	35.907	1755	41.26	-26.17	0.04	6.9
23.6	39.291	2334	54.62	-26.71	0.05	8.8
23.8	45.713	2702	63.81	-27.49	0.05	7.0
24.0	41.116	1809	42.47	-25.48	0.03	8.9
24.2	42.708	2395	56.37	-26.09	0.04	9.2
24.4	38.943	2479	58.08	-26.15	0.05	12.1
24.6	36.547	3237	74.88	-26.64	0.07	15.4
28.0	2.706	6308	152.02	-26.23	1.91	33.0
28.2	2.513	7231	172.82	-26.12	2.35	46.7
28.4	2.297	5056	121.18	-25.96	1.79	39.1
28.6	3.654	3955	94.88	-25.17	0.88	31.5
28.8	2.560	4362	104.07	-25.42	1.37	34.3
29.0	1.981	4673	111.32	-25.66	1.90	31.8
29.2	2.452	5353	128.93	-25.90	1.78	38.7
29.4	2.511	4656	111.73	-25.34	1.51	40.4
29.6	2.545	23397	566.61	-26.53	7.63	46.3
29.8	0.547	20006	476.29	-26.14	29.77	30.8
30	1.030	20235	487.92	-25.50	16.19	15.3
30.2	37.582	1530	35.96	-26.54	0.03	1.0
30.4	41.260	1677	39.85	-26.85	0.03	1.2
30.6	2.119	1042	24.76	-23.81	0.38	2.2
30.8	2.721	1651	38.96	-24.33	0.47	2.3
31.0	43.570	2217	51.87	-26.14	0.04	6.2
31.2	31.967	3828	89.83	-25.42	0.09	2.3
31.4	6.500	6428	152.42	-25.36	0.75	1.7
31.6	29.921	1682	39.09	-24.68	0.03	1.8
31.8	18.480	10608	249.35	-25.83	0.44	4.8
32.0	41.233	2071	48.34	-24.74	0.03	3.3
32.2	42.917	1668	39.09	-24.86	0.02	3.1
32.4	39.450	1785	41.92	-24.54	0.03	3.9
32.6	2.958	5845	138.73	-25.10	1.49	3.8
32.8	9.244	1775	42.44	-23.86	0.12	10.8

Appendix A: Organic carbon and carbonate data collected from bulk sediments from Thompson Canyon

Depth (m)	Weight (mg)	Amplitude 44 (mV)	Area 44 (Vs)	δ^{13}C VPDB	TOC %	Carbonate %
33.0	13.773	3382	79.29	-24.63	0.17	3.1
33.2	32.079	1683	39.28	-25.89	0.03	10.1
33.4	32.690	1528	35.84	-25.24	0.03	9.0
33.4	28.174	1777	41.48	-23.86	0.04	9.0
33.6	41.186	2572	60.29	-26.04	0.04	9.5
33.8	41.305	2022	47.11	-23.81	0.03	10.4
34.0	41.086	3250	76.35	-22.20	0.06	11.2
34.2	46.051	2043	47.92	-24.62	0.03	12.2
34.4	36.521	2673	62.38	-25.12	0.05	14.2
34.6	37.169	2309	54.15	-23.92	0.04	13.1
34.8	39.277	2925	68.24	-27.26	0.05	14.1
35.0	39.789	2884	67.21	-25.48	0.05	12.0
35.2	38.707	2787	65.46	-26.71	0.05	17.2
35.4	35.035	2059	48.27	-26.09	0.04	18.5
35.6	41.942	3210	75.50	-24.95	0.05	16.0
35.8	39.359	3189	74.50	-22.85	0.06	16.9
36.0	35.746	1812	42.30	-25.81	0.03	17.0
36.2	40.505	2587	60.65	-25.82	0.04	18.0
36.4	35.880	2455	57.17	-26.52	0.05	17.6
36.6	36.945	2919	68.32	-26.56	0.05	16.6

Appendix B: Organic carbon and carbonate data collected from bulk sediments from Sego #2 Core

Depth (m)	Weight (mg)	Amplitude 44 (mV)	Area 44 (Vs)	δ^{13}C VPDB	TOC %	Carbonate %
0.0	7.373	2195	49.71	-26.09	0.44	14.0
0.2	6.629	2391	53.94	-26.08	0.53	14.9
0.2	6.240	2496	57.94	-25.79	0.61	14.9
0.4	9.151	5156	115.13	-25.70	0.80	13.9
0.4	8.492	4384	101.57	-25.71	0.79	13.9
0.6	8.966	4210	93.12	-25.89	0.66	15.6
0.6	10.340	5914	138.38	-26.08	0.88	15.6
0.8	7.212	2241	50.43	-26.08	0.46	13.7
0.8	10.045	2976	69.88	-25.98	0.46	13.7
1.0	10.378	2829	63.53	-26.07	0.40	16.4
1.0	11.060	3281	76.78	-26.19	0.46	16.4
1.2	9.925	6275	139.83	-25.87	0.89	16.8
1.4	8.159	2723	61.30	-26.28	0.49	15.8
1.60	3.540	4022	90.49	-25.67	1.63	13.3
1.60	9.934	3099	69.09	-26.26	0.45	13.3
1.8	10.240	5459	120.52	-25.62	0.75	14.4
2.0	11.882	2078	46.65	-27.17	0.26	17.0
2.2	9.990	3529	78.64	-25.93	0.51	14.8
2.4	9.753	4470	98.45	-26.03	0.65	14.4
2.6	12.266	3699	81.85	-26.47	0.43	13.7
2.8	6.642	9109	201.61	-25.60	1.92	16.4
3.0	11.238	4559	100.85	-26.08	0.57	12.6
3.2	13.912	6444	141.86	-26.17	0.65	13.9
3.4	9.567	5192	113.92	-26.04	0.76	13.5
3.6	8.196	3671	81.53	-26.41	0.65	12.0
3.8	9.639	3705	82.18	-26.09	0.55	13.8
4.0	12.609	7650	168.97	-25.97	0.86	14.0
4.2	6.176	2433	57.27	-25.91	0.72	13.4
4.4	5.933	5725	138.68	-25.34	1.84	17.3
4.6	10.046	5516	130.55	-25.43	1.02	17.8
4.8	5.810	3559	85.93	-25.76	1.16	15.2
5.0	11.559	9526	212.16	-26.13	1.17	15.7
5.2	10.416	7125	171.22	-25.22	1.29	15.1
5.4	7.760	4638	111.07	-25.75	1.12	11.0
5.6	4.118	5543	132.84	-25.20	2.53	14.7

Appendix B: Organic carbon and carbonate data collected from bulk sediments from the Sego #2 core.

5.8	18.540	7493	178.21	-25.70	0.76	12.5
6.0	13.057	11400	255.84	-26.02	1.24	12.1
6.2	8.581	4585	109.50	-25.66	1.00	15.6
6.4	6.705	4597	109.12	-25.64	1.27	14.8
6.6	14.155	9643	234.76	-25.32	1.30	14.9
6.8	6.198	4827	114.48	-25.26	1.44	16.9
7.0	12.752	6530	143.15	-26.10	0.72	13.0
7.2	9.952	6193	148.46	-25.41	1.17	11.6
7.4	10.102	8903	216.35	-25.30	1.68	11.3
7.6	8.468	4475	105.35	-25.63	0.97	10.2
7.8	9.018	4644	109.05	-25.59	0.94	11.1
8.0	13.500	6898	150.48	-25.85	0.72	13.3
8.2	4.035	4053	95.56	-25.57	1.84	12.0
8.4	7.863	3658	86.77	-25.62	0.86	9.6
8.6	9.014	5774	137.43	-25.43	1.19	14.1
8.8	12.735	4373	102.50	-25.58	0.63	12.7
9.0	13.057	7431	163.82	-25.80	0.81	14.4
9.2	13.817	6560	155.27	-25.35	0.88	13.2
9.4	27.551	5703	134.60	-25.70	0.38	14.9
9.6	9.936	6549	157.06	-25.35	1.24	0.0
9.8	9.212	4058	96.50	-26.06	0.82	0.0
10.0	11.823	5523	122.43	-23.90	0.67	14.1
10.2	10.674	4703	110.77	-25.75	0.81	0.0
10.4	14.346	7829	186.62	-25.49	1.03	0.0
10.6	12.590	6420	153.37	-25.59	0.96	0.0
10.8	12.425	3386	80.49	-26.30	0.51	0.0
11.0	10.644	4693	102.70	-26.00	0.62	14.0
11.2	16.327	7259	174.34	-25.74	0.84	11.6
11.4	12.104	5122	125.20	-25.98	0.83	11.7
11.6	16.945	7514	182.38	-25.90	0.86	10.5
11.8	14.908	7881	192.63	-25.72	1.03	10.4
12.0	8.522	16283	373.29	-25.94	2.74	21.0
12.2	11.672	6926	171.90	-25.73	1.17	10.9
12.4	13.574	6269	152.44	-25.83	0.89	12.4
12.6	18.058	5843	140.69	-26.14	0.62	10.6
12.8	17.051	7717	190.13	-26.05	0.89	11.2
13.0	9.866	7926	175.46	-25.88	1.12	12.6
13.2	10.983	11228	285.80	-25.45	2.08	13.4
13.4	8.022	7207	179.05	-25.70	1.78	13.8
13.6	11.543	9277	231.26	-25.77	1.60	12.9
13.8	11.366	3631	87.09	-26.33	0.61	14.0

14.0	7.868	2486	55.38	-26.46	0.45	11.8
14.2	10.097	5100	124.35	-26.03	0.98	11.9
14.4	19.200	8597	210.38	-25.79	0.88	12.7
14.6	17.589	4240	102.31	-26.34	0.46	13.6
14.8	15.675	3789	91.24	-26.54	0.46	10.9
15.0	7.627	4738	104.53	-26.18	0.88	12.0
15.2	28.997	4845	116.53	-27.33	0.32	10.8
15.4	34.454	5064	123.61	-27.44	0.29	11.8
15.6	6.406	6922	171.14	-25.59	2.14	14.1
15.8	4.712	4831	118.13	-25.84	2.00	14.1
16.0	13.321	6618	145.42	-26.56	0.70	21.8
16.2	10.958	5786	140.22	-26.20	1.02	31.6
16.4	21.030	2501	59.70	-27.58	0.23	12.3
16.6	3.597	2952	71.53	-25.77	1.58	19.4
16.8	14.675	4526	109.23	-26.43	0.59	14.7
17.0	13.502	3994	86.70	-26.60	0.41	17.5
17.2	38.058	3865	93.08	-28.05	0.19	9.2
17.4	25.066	5916	142.14	-27.46	0.45	14.3
17.6	29.220	9445	231.41	-27.25	0.63	17.9
17.8	32.519	6966	168.35	-26.97	0.41	14.1
18.0	7.694	7117	156.34	-26.17	1.30	22.6
18.2	38.604	6953	168.85	-27.40	0.35	22.8
18.4	16.306	9089	222.10	-25.99	1.09	12.2
18.6	13.642	3455	83.00	-26.75	0.48	14.3
18.8	11.276	3723	89.07	-26.21	0.62	11.5
19.0	8.761	5973	131.22	-26.04	0.96	14.5
19.2	18.617	2654	63.81	-26.95	0.27	17.4
19.4	5.243	3453	83.21	-25.78	1.24	24.2
19.6	32.832	3835	93.01	-27.78	0.22	22.4
19.8	4.876	8444	208.97	-25.64	3.39	17.2
20.0	4.418	5605	124.09	-25.98	1.81	17.3
20.2	14.289	3258	78.08	-26.73	0.43	16.8
20.4	5.923	6658	168.26	-25.78	2.24	16.8
20.6	13.189	8398	207.74	-25.86	1.25	19.6
20.8	5.591	5580	136.13	-25.64	1.92	18.0
21.0	4.497	2372	52.81	-26.08	0.77	22.6
21.2	21.680	3086	74.79	-27.35	0.27	12.0
21.4	13.264	1581	37.37	-26.48	0.21	20.2
21.6	24.730	1496	35.67	-26.84	0.11	11.3
21.8	19.038	2149	51.23	-26.40	0.21	12.8
22.0	9.322	6542	145.14	-26.21	1.00	14.6

Appendix B: Organic carbon and carbonate data collected from bulk sediments from the Sego #2 core.

22.2	8.910	4314	102.34	-25.72	0.90	14.2
22.4	7.349	438	10.46	-27.16	0.10	11.5
22.6	18.055	1890	45.46	-25.84	0.19	13.3
22.8	11.591	3881	92.68	-25.76	0.63	16.3
23.0	13.929	1792	39.61	-27.68	0.19	0.0
23.2	9.082	3347	79.12	-25.70	0.68	16.7
23.4	24.845	2473	58.56	-26.60	0.18	14.9
23.6	21.260	1225	29.35	-27.27	0.10	13.5
23.8	21.253	1546	36.66	-26.82	0.13	14.1
24.0	6.161	7008	154.47	-25.94	1.62	0.0
24.2	7.021	2472	58.67	-25.82	0.65	13.3
24.4	10.960	2305	54.09	-25.96	0.38	14.1
24.6	11.819	5902	140.45	-25.70	0.94	14.2
24.8	12.308	887	20.90	-27.30	0.13	16.5
25.0	11.549	6469	141.84	-26.08	0.80	0.0
25.2	31.659	2812	67.36	-27.04	0.17	11.9
25.4	33.437	1867	43.97	-27.21	0.10	14.4
25.6	10.591	3001	70.39	-25.92	0.52	15.4
25.8	9.814	1598	37.91	-26.17	0.31	18.5
26.0	10.590	8715	194.55	-26.40	1.18	0.0
26.2	12.982	2371	55.96	-26.28	0.35	14.1
26.4	9.748	7353	177.99	-25.76	1.48	15.0
26.6	7.469	6271	151.02	-25.73	1.64	15.9
26.8	16.357	1203	28.74	-27.27	0.14	12.9
27.0	12.673	5356	119.30	-26.45	0.61	13.0
27.2	14.989	1567	36.86	-26.83	0.20	15.9
27.4	11.673	4560	108.46	-26.46	0.76	15.4
27.6	9.937	5046	121.25	-25.81	0.99	15.6
27.8	7.458	3711	88.49	-25.84	0.96	20.3
28.0	10.488	5601	123.49	-26.41	0.77	13.9
28.2	11.134	2269	53.34	-26.16	0.39	18.3
28.4	9.717	5767	137.76	-26.04	1.16	18.5
28.6	8.000	9182	225.76	-25.94	2.31	18.9
28.8	14.522	1051	24.92	-27.11	0.14	17.4
29.0	13.347	4417	96.54	-26.78	0.47	16.7
29.2	17.857	1896	44.68	-26.74	0.20	13.1
29.4	16.498	1600	37.87	-26.71	0.18	14.9
29.6	29.549	8652	213.79	-25.64	0.59	15.9
29.8	22.139	1643	39.02	-27.29	0.14	17.0
30.0	13.942	1572	34.66	-27.33	0.17	15.3
30.20	3.853	2575	60.94	-26.53	1.28	21.1

Appendix B: Organic carbon and carbonate data collected from bulk sediments from the Sego #2 core.

30.4	17.021	6881	166.02	-25.93	0.80	14.9
30.6	30.970	7600	182.13	-26.36	0.48	36.5
30.8	17.778	1553	36.65	-27.25	0.16	55.0
31.0	13.402	2309	51.72	-28.47	0.26	34.6
31.2	17.058	2698	63.76	-26.48	0.30	52.0
31.4	20.244	21536	548.13	-26.79	2.22	53.3
31.6	28.084	10041	245.55	-26.58	0.72	54.6
31.8	21.359	20352	518.26	-27.29	1.99	54.4
32.0	14.841	2284	50.35	-27.73	0.22	17.8
32.2	35.788	1543	36.29	-27.34	0.08	13.8
32.4	41.869	1781	42.23	-27.74	0.08	12.3
32.6	26.736	1457	34.34	-27.37	0.10	10.2
32.8	40.879	1723	40.78	-27.43	0.08	11.0
33.0	22.949	1452	32.39	-27.99	0.09	46.6
33.2	16.039	767	18.07	-26.59	0.08	13.1
33.4	44.344	1401	33.04	-27.30	0.05	13.7
33.6	37.842	1425	33.37	-27.43	0.07	18.0
33.8	31.152	1140	26.69	-27.33	0.06	20.0
34.0	23.440	1333	30.00	-28.36	0.09	16.5
34.2	36.945	1481	34.64	-27.25	0.07	12.7
34.4	26.908	970	22.87	-27.14	0.06	12.6
34.6	40.901	1443	33.87	-27.42	0.06	12.0
34.8	27.674	1218	28.74	-27.41	0.08	12.4
35.0	20.164	2324	51.15	-27.75	0.17	9.1
35.2	40.998	2116	49.53	-26.80	0.09	8.3
35.4	14.449	3371	79.48	-26.46	0.42	11.5
35.6	39.454	1790	42.60	-26.83	0.08	9.5
35.8	26.932	1180	27.78	-27.00	0.07	8.5
36.0	2.725	10605	241.75	-26.33	5.80	12.3
36.2	29.897	1275	29.99	-27.27	0.07	6.6
36.4	28.968	986	23.22	-27.49	0.06	6.6
36.6	33.723	1875	44.34	-27.27	0.10	8.3
36.8	29.299	1693	39.98	-27.26	0.10	7.4
37.0	22.836	2116	47.45	-28.86	0.14	6.3
37.20	29.741	1109	26.32	-26.98	0.06	6.2
37.4	31.916	1302	30.75	-27.34	0.07	6.9
37.6	28.329	1488	35.30	-26.98	0.09	7.4
37.8	31.671	4023	95.76	-26.99	0.23	9.2
38.0	20.487	1914	42.40	-28.07	0.14	8.3
38.2	37.107	1388	32.85	-27.43	0.06	7.5
38.4	40.211	1384	32.96	-27.63	0.06	8.7

38.6	34.578	1344	31.92	-27.48	0.07	8.1
38.8	25.972	1207	28.45	-27.12	0.08	10.0
39.0	21.864	12625	279.15	-26.52	0.84	11.9
39.0	13.618	7155	165.91	-26.29	0.80	11.9
39.0	13.597	583	13.87	-27.20	0.06	11.9
39.2	14.591	611	14.30	-26.89	0.06	9.1
39.2	28.729	1015	24.01	-27.52	0.06	9.1
39.2	14.517	701	16.50	-27.03	0.07	9.1
39.4	15.444	664	15.41	-27.02	0.06	13.0
39.4	27.134	936	21.89	-27.55	0.06	13.0
39.4	15.696	971	22.74	-27.47	0.09	13.0
39.6	15.067	710	16.55	-27.19	0.07	9.9
39.6	38.250	1564	37.21	-27.61	0.07	9.9
39.6	16.709	1035	24.37	-27.58	0.09	9.9
39.8	18.805	1058	24.76	-26.91	0.08	10.6
39.8	31.731	1358	31.96	-27.68	0.07	10.6
39.8	17.555	1306	30.49	-27.38	0.11	10.6
40.0	22.302	1542	34.18	-28.36	0.10	8.7
40.0	18.762	1145	26.68	-27.73	0.09	8.7
40.0	15.745	781	18.31	-27.70	0.07	8.7
40.2	19.614	667	15.43	-27.13	0.05	14.6
40.2	38.309	1207	28.50	-27.73	0.05	14.6
40.2	18.737	990	22.95	-27.74	0.08	14.6
40.4	15.604	608	14.08	-27.58	0.06	11.0
40.4	23.212	2183	51.19	-27.57	0.07	11.0
40.4	13.976	1119	26.09	-27.63	0.12	11.0
40.6	24.049	2885	66.90	-27.47	0.08	11.6
40.8	30.314	4222	97.61	-27.33	0.10	12.2
41.0	20.223	2095	46.65	-28.65	0.15	11.5
41.2	34.989	20492	491.49	-26.73	0.42	16.9
41.4	31.622	4744	110.08	-27.56	0.10	22.3
41.6	27.252	3894	90.08	-27.55	0.10	18.8
41.8	24.360	2469	57.54	-27.33	0.07	14.6
42.0	21.830	1604	35.69	-28.05	0.11	9.9
42.2	30.222	3280	76.15	-27.09	0.08	12.2
42.4	27.871	2768	65.23	-27.49	0.07	19.1
42.6	23.499	12360	289.00	-26.04	0.37	10.9
42.8	24.028	3254	77.02	-27.53	0.10	8.1
43.0	19.901	1378	32.66	-25.84	0.11	8.8
43.2	31.466	2997	69.67	-27.94	0.07	8.0
43.4	33.864	3684	86.84	-28.02	0.08	8.4

43.6	38.116	3782	88.38	-28.15	0.07	8.5
43.8	31.009	4261	99.42	-27.91	0.10	11.1
44.0	22.824	1247	29.07	-27.56	0.08	7.6
44.2	37.027	3492	81.82	-27.86	0.07	8.1
44.4	33.441	3342	78.13	-28.27	0.07	8.3
44.6	28.744	5682	132.53	-27.64	0.14	8.0
44.8	27.219	3472	81.32	-27.72	0.09	7.9
45.0	20.520	1169	27.34	-27.73	0.09	8.5
45.2	38.416	4219	98.84	-27.84	0.08	8.8
45.4	35.226	5064	118.18	-27.86	0.10	8.7
45.6	34.227	4962	115.96	-27.78	0.10	8.5
45.8	16.815	5360	126.18	-26.70	0.23	8.7
46.0	3.259	13644	331.75	-25.93	6.65	11.0
46.2	13.411	2848	66.46	-25.13	0.15	8.2
46.4	24.852	4133	96.64	-27.81	0.12	8.4
46.6	30.185	4977	116.53	-27.63	0.12	9.1
46.8	28.107	4619	107.63	-28.08	0.11	9.0
47.0	18.570	1063	24.93	-27.55	0.09	9.0
47.2	30.208	4293	99.16	-27.75	0.10	8.9
47.4	24.456	4551	106.03	-27.50	0.13	9.5
47.6	33.308	4112	96.09	-28.08	0.07	8.6
47.8	30.571	4418	103.66	-28.21	0.09	8.3
48.0	20.271	1230	29.05	-27.91	0.09	8.7
48.2	26.587	3649	85.10	-27.83	0.08	8.3
48.4	30.011	4068	94.65	-28.12	0.08	7.5
48.6	31.439	4493	105.15	-28.21	0.09	8.1
48.8	35.929	5904	137.60	-28.35	0.10	10.8
49.0	20.362	1083	25.15	-27.47	0.08	7.5
49.2	23.745	7030	163.52	-27.25	0.19	7.8
49.4	37.192	11129	260.34	-28.18	0.20	6.5
49.6	32.325	3290	77.02	-28.03	0.06	6.4
49.8	40.945	12312	289.19	-27.99	0.20	14.9
50.0	16.455	2364	54.78	-27.18	0.22	13.1
50.2	39.133	4120	95.82	-28.03	0.06	1.4
50.4	28.133	3579	83.83	-27.97	0.07	2.4
50.6	39.100	4274	98.91	-27.73	0.07	1.4
50.8	24.214	2025	47.48	-27.04	0.04	1.9
51.0	21.987	804	19.11	-27.40	0.06	1.7
51.2	27.145	2942	68.04	-27.50	0.06	1.0
51.4	36.836	3689	85.72	-27.63	0.06	1.1
51.6	31.472	4300	100.40	-27.70	0.08	1.7

Appendix B: Organic carbon and carbonate data collected from bulk sediments from the Sego #2 core.

51.8	23.758	3676	85.46	-28.46	0.09	3.6
52.0	14.861	7069	166.64	-25.69	0.74	1.9
52.2	33.074	3762	86.82	-27.26	0.07	2.2
52.4	28.194	2321	54.22	-27.63	0.04	1.3
52.6	27.534	6581	152.60	-27.11	0.15	1.6
52.8	1.861	5263	123.36	-25.54	1.78	2.6
53.0	2.273	4954	120.04	-25.85	3.48	4.8
53.2	14.202	1377	32.41	-26.69	0.04	5.0
53.4	17.790	2093	49.06	-26.35	0.06	1.9
53.6	15.171	1783	41.55	-26.58	0.05	1.6
53.8	30.314	3214	74.29	-27.20	0.06	2.0
54.0	25.178	1097	25.69	-27.27	0.07	1.3
54.2	26.979	2148	50.03	-27.17	0.04	0.8
54.4	9.398	22728	535.47	-26.44	1.68	2.2
54.6	16.396	2352	54.97	-26.38	0.07	0.7
54.8	31.607	4110	95.93	-28.02	0.09	1.3
55.0	13.555	1874	43.58	-25.97	0.21	1.7
55.2	18.668	11274	262.00	-26.28	0.41	2.2
55.4	32.103	3650	85.73	-28.26	0.08	1.5
55.6	26.523	2798	65.64	-28.25	0.07	1.3
55.8	32.434	2678	62.65	-27.97	0.05	1.4
56.0	25.010	940	22.11	-27.33	0.06	1.4
56.2	17.410	9252	211.91	-26.40	0.36	4.0
56.4	34.615	2159	50.82	-27.96	0.04	1.3
56.6	14.741	2942	68.31	-26.76	0.13	1.3
56.8	27.256	2349	56.05	-27.48	0.06	1.8
57.0	25.345	684	15.92	-26.98	0.04	1.1
57.2	28.527	1555	36.65	-27.61	0.03	1.2
57.4	34.993	3054	71.44	-27.52	0.06	1.9
57.6	31.196	3384	78.51	-27.52	0.07	1.6
57.8	18.080	1853	43.52	-27.34	0.07	1.3
58.0	25.507	1129	26.44	-27.03	0.07	1.7
58.2	12.649	1694	39.97	-27.80	0.08	1.2
58.4	15.227	2929	67.91	-26.70	0.13	1.1
58.6	14.984	1537	36.21	-27.60	0.06	1.4
58.8	14.948	7898	182.39	-25.98	0.36	1.2
59.0	27.449	1155	27.21	-27.22	0.06	1.1
59.2	14.092	17123	398.92	-26.19	0.84	1.4
59.4	34.369	10033	231.87	-26.42	0.20	1.8
59.6	20.568	2661	62.22	-27.43	0.08	2.2
59.8	16.884	5930	137.51	-26.91	0.24	1.7

Appendix B: Organic carbon and carbonate data collected from bulk sediments from the Sego #2 core.

60.0	4.380	5174	123.08	-24.74	1.85	2.1
60.2	13.556	1525	36.14	-27.12	0.07	1.8
60.4	16.350	1863	43.99	-27.54	0.07	1.3
60.6	0.412	1996	47.08	-26.13	3.12	3.1
60.8	12.189	15380	360.71	-26.21	0.87	4.3
61.0	7.153	3209	74.98	-25.79	0.69	3.4
61.2	0.721	4725	110.67	-26.20	4.43	11.1
61.4	0.043	1978	46.33	-26.44	29.46	17.5
61.6	0.049	4254	100.46	-26.52	59.00	31.1
61.8	0.051	5078	119.88	-26.54	68.10	16.8
62.0	12.819	971	22.99	-27.22	0.12	9.7
62.2	27.350	3009	69.66	-27.40	0.06	10.1
62.4	34.252	3414	78.57	-27.56	0.06	9.5
62.6	28.690	1879	43.62	-28.08	0.03	9.9
62.8	28.466	3265	75.13	-27.28	0.07	10.4
63.0	20.197	984	22.89	-27.10	0.07	10.5
63.2	37.124	2696	62.15	-27.79	0.04	8.4
63.4	33.625	3298	75.73	-27.29	0.06	9.1
63.6	30.617	3098	71.19	-27.45	0.06	9.3
63.8	34.721	5891	137.26	-27.25	0.11	8.8
64.0	24.795	771	17.91	-27.17	0.05	7.7
64.2	33.765	3205	76.91	-26.90	0.06	8.0
64.4	29.253	2454	58.77	-26.84	0.05	8.7
64.6	34.653	4435	104.21	-26.70	0.08	10.3
64.8	34.026	3783	88.07	-26.98	0.07	10.1
65.0	25.803	1430	33.66	-27.11	0.09	10.7
65.2	31.407	4157	96.41	-27.29	0.08	8.4
65.4	31.234	3037	70.89	-27.24	0.06	8.7
65.6	31.772	3245	76.03	-27.49	0.06	10.5
65.8	26.728	2686	62.85	-27.24	0.06	10.2
66.0	26.771	1119	26.29	-26.99	0.06	9.2
66.2	21.188	4198	101.17	-28.65	0.13	10.4
66.4	25.183	2766	65.73	-26.86	0.06	9.7
66.6	34.507	4311	101.36	-27.01	0.08	9.7
66.8	32.237	2633	62.03	-27.20	0.05	9.3
67.0	27.363	1573	36.62	-27.00	0.09	9.8
67.2	29.055	2823	66.28	-27.20	0.06	9.6
67.4	29.492	2895	68.53	-27.39	0.06	10.8
67.6	26.440	3461	80.89	-27.30	0.08	23.6
67.8	28.068	7200	165.14	-27.71	0.16	29.1
68.0	24.775	1389	32.49	-27.28	0.09	22.5

68.2	35.671	4082	97.07	-27.41	0.07	16.7
68.4	25.391	4069	97.65	-27.45	0.10	17.0
68.6	22.726	6167	149.43	-26.99	0.18	19.7
68.8	8.193	6621	158.94	-26.08	0.54	15.0
69.0	6.765	7624	182.22	-26.01	1.78	18.2
69.2	8.630	4990	119.58	-26.38	0.37	21.0
69.4	20.306	1245	29.42	-27.49	0.04	9.7
69.6	20.388	1243	29.40	-26.99	0.04	9.4
69.8	21.631	1390	32.64	-26.94	0.04	8.2
70.0	22.669	524	12.23	-27.14	0.04	6.9
71.0	35.239	730	17.01	-27.27	0.03	6.6
71.2	22.617	4621	107.38	-26.22	0.14	9.2
71.4	11.233	4011	92.73	-26.18	0.25	14.5
71.6	3.470	13911	334.08	-25.89	2.87	18.5
71.8	3.638	6015	142.03	-25.77	1.16	14.7
72	7.214	13248	322.12	-26.20	2.86	12.8
72.2	12.576	2278	54.33	-27.09	0.13	18.9
72.4	2.086	4575	107.42	-25.46	1.52	17.8
72.6	42.837	4457	104.24	-27.29	0.07	10.9
72.8	3.462	11585	278.74	-26.26	2.39	10.9
73.0	6.122	2264	52.98	-25.93	0.55	15.3
73.2	11.768	12814	301.29	-26.06	0.76	17.2
73.4	5.384	11338	267.40	-25.94	1.48	14.3
73.6	2.237	5818	134.75	-25.35	1.78	20.6
73.8	4.698	8950	211.12	-25.72	1.34	18.8
74.0	9.155	3641	85.48	-25.69	0.60	19.6
74.2	2.537	7822	184.58	-25.04	2.16	17.4
74.4	5.629	9884	233.96	-25.85	1.23	16.2
74.6	22.236	12198	293.81	-27.09	0.39	13.6
74.8	1.879	2516	59.87	-25.70	0.94	15.1
75.0	9.753	7825	184.81	-25.90	1.22	15.4
75.2	4.442	7917	187.63	-25.84	1.25	17.8
75.0	4.661	4340	102.00	-25.88	0.65	13.0
75.6	12.745	2684	62.96	-26.70	0.15	2.9
75.8	37.353	2016	46.92	-27.70	0.04	26.6
76.0	14.263	565	13.19	-26.56	0.06	5.1
76.2	14.581	6437	150.40	-26.27	0.31	1.9
76.4	11.530	1639	38.14	-26.50	0.10	2.5
76.4	29.576	4648	107.61	-26.65	0.11	2.5
76.6	38.300	7138	165.69	-26.56	0.13	2.3
76.6	40.203	6591	154.45	-26.62	0.12	2.3

Appendix B: Organic carbon and carbonate data collected from bulk sediments from the Sego #2 core.

76.8	35.235	1821	42.90	-27.81	0.04	3.9
76.8	38.278	2137	50.21	-27.20	0.04	3.9
77.0	24.486	571	13.14	-27.36	0.03	3.4
77.2	32.976	1987	46.77	-27.94	0.04	5.3
77.2	34.466	1873	44.17	-27.88	0.04	5.3
77.4	36.739	4509	104.90	-27.19	0.08	5.7
77.4	40.302	3989	93.82	-27.25	0.07	5.7
77.6	35.849	3493	82.38	-28.29	0.07	2.6
77.8	37.450	15299	360.04	-26.49	0.30	3.4
78.0	20.154	3189	74.86	-26.85	0.24	2.8
78.2	37.083	4966	116.57	-31.32	0.10	2.7
78.4	40.920	5101	119.80	-26.96	0.09	2.0
78.6	37.873	8986	210.62	-26.56	0.17	2.5
78.8	27.702	14866	348.43	-26.23	0.40	2.2
79.0	28.461	1137	26.25	-28.66	0.06	4.9
79.2	0.603	20969	509.88	-25.04	26.75	12.6
79.4	0.412	8596	206.55	-25.57	15.77	
79.6	35.778	7523	179.59	-27.03	0.16	
79.8	25.294	6912	164.53	-27.18	0.20	
80.0	25.153	20237	481.76	-26.22	0.61	
80.2	0.544	15568	377.61	-25.85	22.09	
80.4	26.600	5406	128.68	-26.82	0.15	
80.6	32.592	20111	476.27	-32.98	0.47	
80.8	28.296	2395	56.93	-28.60	0.06	
81.0	33.531	2600	61.32	-29.81	0.06	
81.2	1.424	10417	250.04	-25.77	5.55	
81.4	2.146	5110	122.62	-26.59	1.78	
81.6	1.431	6491	154.63	-26.15	3.38	
81.8	1.713	4588	108.56	-26.23	1.96	
82.0.	3.612	19946	514.64	-26.82	4.53	
82.2	33.347	4566	109.00	-26.76	0.10	
82.4	4.473	9911	236.92	-26.04	1.66	
82.6	30.111	8953	209.84	-26.63	0.22	
85.0	4.960	8943	201.86	-26.68	2.68	28.3
86.0	4.806	5151	119.82	-27.31	1.63	8.6
87.0	3.655	3113	70.60	-27.00	1.27	6.7
88.0	4.394	2932	66.34	-26.69	0.99	11.4
89.0	3.820	2758	61.78	-26.75	1.06	9.4
90.0	3.614	2732	60.50	-26.79	1.10	10.5
91.0	3.830	3572	81.31	-26.64	1.39	10.2
92.0	3.960	3418	75.50	-26.66	1.24	13.4

93.0	3.339	3458	76.80	-26.73	1.50	10.3
94.0	4.926	4445	100.28	-26.81	1.34	8.8
95.0	3.832	3292	74.46	-26.79	1.27	9.3
96.0	5.689	6307	141.51	-26.91	1.63	9.4
97.0	5.989	5950	134.34	-26.91	1.47	9.5
98.0	5.526	6043	133.49	-26.81	1.58	10.3
99.0	6.569	7732	174.69	-26.86	1.74	10.0
100.0	5.471	4172	91.82	-26.73	1.10	10.2
101.0	4.733	4571	103.14	-27.33	1.43	8.4
102.0	3.413	3525	80.40	-27.27	1.55	7.3
103.0	4.056	3396	74.64	-27.33	1.20	10.4
104.0	3.719	3010	67.21	-27.22	1.19	8.6
105.0	5.124	4565	103.35	-27.12	1.32	9.4
106.0	4.701	3371	75.32	-26.89	1.05	11.4
107.0	4.204	3985	88.34	-27.34	1.37	12.3
108.0	5.487	4685	103.97	-27.21	1.23	11.5
109.0	6.936	5607	122.81	-27.03	1.16	10.2
110.0	6.933	5724	126.48	-27.29	1.20	13.8
111.0	5.988	5339	118.45	-27.17	1.29	10.0
112.0	5.730	4147	94.02	-26.97	1.05	8.4
113.0	6.107	5503	124.62	-27.02	1.31	11.9
114.0	8.087	8184	186.79	-27.18	1.48	9.5
115.0	4.766	4966	112.29	-26.86	1.53	7.5
116.0	3.905	4732	107.23	-26.95	1.78	14.0
117.0	4.391	4061	93.33	-26.85	1.38	42.1
118.0	3.438	4773	108.22	-26.96	2.04	10.1
119.0	3.468	4929	110.51	-26.83	2.07	11.5
120.0	5.763	7020	160.10	-27.02	1.81	8.2
121.0	5.008	6146	138.84	-26.90	1.81	10.1
122.0	3.618	3917	87.59	-26.39	1.59	13.2
123.0	3.773	4571	102.91	-26.80	1.79	9.9
124.0	6.508	8512	193.20	-27.06	1.95	13.5
125.0	6.660	9282	212.74	-27.11	2.10	11.9
126.0	5.703	6252	139.72	-26.93	1.62	12.1
127.0	4.967	6348	144.30	-27.01	1.92	9.9
128.0	4.555	6523	149.45	-27.16	2.17	11.2
129.0	5.759	6236	141.55	-27.08	1.62	8.4
130.0	4.755	4918	110.31	-27.01	1.53	10.5
131.0	5.402	5933	134.73	-26.99	1.65	9.1
132.0	4.841	6508	147.58	-27.01	2.02	8.9
133.0	8.260	6103	138.03	-27.18	1.10	12.6

134.0	11.007	6869	152.86	-27.06	0.92	11.5
135.2	10.649	13218	303.19	-27.18	1.88	10.3
136.0	7.009	5225	116.95	-26.89	1.10	10.9
137.0	6.155	1812	40.62	-26.44	0.44	11.4
138.0	7.078	3617	80.36	-26.50	0.75	11.5
139.0	9.320	4960	110.09	-26.61	0.78	14.1
140.0	10.123	7127	159.43	-26.81	1.04	16.8
141.0	7.201	8144	183.84	-26.63	1.64	13.7
142.0	7.985	3951	87.53	-26.79	0.71	17.3
143.0	9.566	2256	49.73	-26.78	0.34	13.4
144.0	6.122	9751	221.50	-26.67	2.34	11.5
145.0	7.497	6598	148.46	-26.43	1.29	13.6
146.0	9.757	5001	111.70	-26.65	0.75	15.0
146.0	11.425	5133	121.39	-26.78	0.32	15.0
146.2	4.971	4442	114.42	-26.96	0.94	13.8
146.4	4.367	11974	290.52	-26.79	2.11	10.2
146.6	9.317	5402	128.23	-26.99	0.42	18.4
146.8	7.826	16429	394.66	-26.64	1.62	13.4
147.0	14.036	12368	297.27	-26.65	0.67	14.3
147.2	2.402	5059	128.31	-26.85	2.21	14.3
147.4	9.699	7463	176.54	-26.82	0.57	13.9
147.6	9.342	22629	544.50	-26.31	1.86	9.9
147.8	7.253	14481	349.03	-26.64	1.53	10.4
148.0	5.098	28270	703.84	-26.55	4.44	7.7
148.2	9.182	2463	60.69	-26.74	0.24	25.5
148.4	4.454	20195	492.56	-26.37	3.53	9.9
148.6	10.113	8612	204.64	-26.75	0.63	11.6
148.8	5.203	24270	601.19	-26.48	3.70	10.1
149.0	3.957	26891	686.09	-26.66	5.54	9.6
149.2	2.690	21932	568.13	-26.14	9.40	9.8
149.4	18.024	7310	182.49	-26.77	0.31	23.8
149.6	15.806	4724	121.69	-25.32	0.24	7.5
149.8	11.554	1544	37.67	-26.26	0.08	6.9
150.0	12.589	2220	54.46	-25.80	0.12	7.8
150.2	8.202	1326	33.16	-25.28	0.12	4.4
150.4	11.558	2239	54.26	-26.17	0.13	5.1
150.6	7.624	16630	405.84	-26.64	1.59	13.4
150.8	9.193	9139	221.16	-26.54	0.71	4.4
151.0	10.317	1742	42.22	-25.01	0.11	3.8
151.2	5.821	5271	134.31	-26.55	0.95	7.4
151.4	12.162	2114	51.34	-25.16	0.11	9.2

Appendix B: Organic carbon and carbonate data collected from bulk sediments from the Sego #2 core.

151.6	13.065	3921	93.54	-25.96	0.20	4.9
151.8	6.726	2560	63.35	-26.29	0.26	18.1
152.0	9.044	1546	37.93	-25.68	0.11	4.4
152.2	1.996	1506	37.91	-25.64	0.59	
152.4	9.115	18252	446.48	-26.79	1.48	
152.6	13.060	1886	45.43	-25.98	0.09	3.3
152.8	7.687	27593	679.00	-26.60	2.71	9.0
153.0	9.486	1857	45.42	-25.15	0.12	3.9
153.2	5.929	5830	147.41	-26.50	1.04	5.6
153.4	4.552	13916	336.72	-26.69	2.23	7.0
153.6	6.549	3624	87.96	-26.11	0.38	6.3
153.8	14.993	1823	43.83	-26.40	0.08	4.1
154.0	10.278	3789	89.81	-26.35	0.25	5.8
154.2	10.059	1268	31.29	-26.50	0.09	5.1
154.4	6.089	12897	308.98	-26.38	1.54	6.1
154.6	6.988	11459	273.21	-26.13	1.17	4.2
154.8	5.309	7838	187.23	-26.19	1.05	5.8
155.0	5.688	17666	426.83	-26.45	2.27	5.1
155.2	2.232	11996	317.61	-26.49	6.22	6.8
155.4	3.820	26622	667.07	-26.49	5.32	5.1
155.6	6.533	49973	1439.69	-104.52	6.82	
155.8	4.984	26372	646.95	-26.45	3.96	
156.0	10.821	2048	50.85	-26.21	0.13	
156.2	13.525	2492	59.65	-25.46	0.13	
156.4	4.155	3745	90.15	-25.86	0.62	
156.6	5.519	11064	265.35	-26.18	1.47	
156.8	3.521	49981	1288.94	-80.58	11.37	
157.2	5.982	28290	698.63	-25.74	3.76	
158.2	10.022	33117	815.56	-25.55	2.63	
159.2	6.342	879	22.49	-26.63	0.08	
160.2	21.011	1937	46.61	-27.06	0.06	
161.2	10.241	5084	121.56	-26.25	0.36	
162.2	10.784	2297	56.63	-24.81	0.15	
163.2	10.325	1075	26.99	-26.09	0.06	
164.2	4.122	5856	141.17	-26.15	1.05	
165.2	4.158	3016	75.25	-26.64	0.69	8.2
166.2	3.061	5405	136.25	-26.36	1.84	
167.2	9.858	1647	40.34	-26.60	0.13	
168.2	11.405	990	24.62	-26.86	0.05	
169.2	16.441	1530	37.66	-27.07	0.07	
170.2	15.574	1517	37.15	-27.32	0.07	4.6

Appendix B: Organic carbon and carbonate data collected from bulk sediments from the Sego #2 core.

171.2	6.309	10368	261.40	-26.36	1.79	9.2
172.2	5.995	6271	156.53	-26.35	1.09	8.2
173.2	17.541	1116	27.51	-27.33	0.04	5.7
174.2	5.439	8967	221.54	-25.88	1.74	7.1
175.2	10.395	812	19.93	-27.11	0.03	6.8
176.2	20.653	1282	31.13	-27.33	0.04	9.8
177.2	8.664	6868	169.35	-26.80	0.82	3.4
178.2	11.830	1075	26.58	-26.18	0.06	
179.2	32.989	1740	42.46	-27.69	0.04	
180.2	10.461	1205	29.45	-26.73	0.08	
181.2	5.725	11796	296.11	-26.32	2.24	
182.2	10.082	3575	88.40	-26.52	0.34	
183.2	4.758	21969	575.55	-25.83	5.34	
184.2	7.427	2445	59.52	-26.19	0.23	
185.2	5.413	9412	224.28	-26.28	1.31	
186.2	4.400	6722	160.91	-26.37	1.14	
187.2	3.137	7649	182.96	-26.35	1.82	
188.2	11.044	5332	126.78	-26.58	0.35	

Appendix C: Organic carbon and carbonate data collected from bulk sediments from Blaze Canyon

Depth (m)	Weight (mg)	Amplitude 44 (mV)	Area 44 (Vs)	δ^{13}C VPDB	TOC %	Carbonate %
0	31.867	2905	68.70	-27.82	0.08	17.51
0.2	42.014	1874	44.02	-26.70	0.04	2.23
0.4	38.129	15268	368.18	-25.77	0.34	8.80
0.6	5.142	12935	309.52	-24.75	2.09	8.89
0.8R	3.395	15537	369.09	-25.75	3.77	27.22
1.0R	7.208	12226	287.30	-25.18	1.38	27.60
1.2R	4.113	2740	63.97	-22.33	0.54	28.69
1.4R	43.112	4882	108.46	-26.63	0.09	16.89
1.6R	44.770	2313	54.00	-26.12	0.04	11.59
1.8R	39.001	1872	44.07	-25.78	0.04	10.21
2.0R	42.081	2218	52.13	-26.33	0.04	11.57
2.2R	37.911	1903	44.76	-26.14	0.04	15.56
2.4	42.298	3500	82.09	-25.29	0.07	15.30
2.6R	19.724	11895	280.84	-25.66	0.49	28.94
2.8	10.644	5309	125.16	-25.59	0.41	33.02
3.0	44.003	8985	211.61	-25.72	0.17	27.76
3.2	9.828	12891	313.94	-26.03	1.10	25.55
3.4	4.541	32399	807.71	-26.04	6.11	20.29
3.6	4.442	10649	256.00	-26.37	1.98	19.73
3.8	4.909	18206	436.95	-26.34	3.05	18.50
4.0	9.035	13925	336.49	-26.42	1.28	17.01
4.2	12.987	18260	444.29	-26.31	1.17	17.31
4.4	9.190	7834	189.18	-25.94	0.70	16.30
4.6	4.228	13324	318.22	-25.37	2.59	19.34
4.8	8.932	14329	351.83	-26.38	1.35	21.65
5.0	18.253	13402	325.11	-26.38	0.61	15.09
5.2	12.982	11060	267.33	-26.36	0.71	19.02
5.4	13.155	9956	233.74	-26.00	0.61	12.51
5.6	10.005	7071	169.97	-25.89	0.58	17.84
5.8	3.679	2245	53.16	-25.19	0.41	14.52
6.0	6.279	4235	98.74	-25.94	0.49	13.04
6.4	4.140	6009	142.60	-26.16	1.12	20.29
6.6	3.020	2469	59.12	-25.38	0.56	20.80
6.8	4.193	2851	67.90	-25.54	0.48	17.89
7.0	4.297	2761	66.22	-25.25	0.45	15.54
7.2	3.436	3445	82.37	-25.68	0.73	17.80

7.4	3.383	1126	26.26	-23.87	0.16	17.59
7.6	3.595	1024	24.20	-23.90	0.13	9.61
7.8	3.626	1545	36.02	-24.42	0.24	14.17
8.0	4.813	1271	29.53	-23.85	0.14	11.56
8.2	1.490	1469	34.63	-24.88	0.55	14.21
8.4	1.776	2083	48.96	-25.20	0.75	13.01
8.6	3.795	4464	105.73	-26.27	0.88	15.34
8.8	2.473	3204	76.41	-25.95	0.92	3.57
9.0	3.087	5310	126.37	-26.36	1.30	2.30
9.2	1.407	1908	45.58	-25.10	0.86	1.85
9.4	3.552	3364	79.27	-25.81	0.67	1.91
9.6	1.986	1693	40.35	-24.75	0.51	1.50
9.8	2.919	3515	83.19	-25.89	0.86	3.04
10.0	2.233	2498	59.92	-25.42	0.76	2.88
10.2	0.215	15014	355.66	-27.62	55.72	9.47
10.4	0.231	16284	389.97	-27.18	56.90	8.47
10.6	23.393	2906	67.77	-25.93	0.08	2.29
10.8	31.987	2015	47.57	-26.02	0.04	1.11
11.0	22.660	1344	31.70	-24.93	0.03	1.19
11.2	20.481	4277	98.88	-25.83	0.15	2.78
11.4	9.008	1169	27.44	-24.81	0.06	1.42
11.6	6.507	1230	28.85	-23.65	0.09	2.22
11.8	9.411	1318	30.85	-25.38	0.08	3.39
12.0	9.071	632	14.97	-25.22	0.02	2.13
12.2	18.820	1088	25.37	-26.12	0.03	4.21
12.4	13.037	2118	48.91	-24.79	0.11	3.36
12.6	71.991	4686	112.88	-23.51	0.05	2.98
12.8	75.410	2126	51.72	-24.38	0.02	1.39
13.0	75.396	2696	65.98	-24.05	0.03	5.12
13.2	71.482	3758	90.67	-24.85	0.04	13.09
13.4	74.809	3722	90.76	-25.18	0.04	5.14
13.6	77.645	3276	78.77	-24.07	0.03	5.93
13.8	73.622	4010	98.21	-23.80	0.04	6.61
14.0	9.363	1002	23.56	-24.58	0.05	7.80
14.2	72.769	4189	101.00	-24.65	0.05	8.10
14.4	71.655	2878	69.79	-22.89	0.03	5.33
14.6	78.940	2969	72.61	-23.80	0.03	7.76
14.8	72.369	3171	76.97	-26.12	0.03	6.47
15.0	73.742	3402	83.48	-25.23	0.04	1.77
15.2	6.713	1488	35.54	-23.79	0.14	1.13
15.4	11.629	1091	26.02	-25.41	0.05	2.48

15.6	0.521	20648	502.72	-25.25	33.39	18.52
15.8	3.502	1054	24.84	-24.40	0.16	3.30
16.0	10.162	3030	73.63	-24.20	0.23	8.79
16.2	54.203	6488	147.37	-26.36	0.13	0.80
16.4	46.700	5883	133.04	-26.44	0.13	5.46
16.6	47.427	3055	68.81	-26.77	0.06	8.38
16.8	54.265	6896	156.82	-26.40	0.13	8.45
17.0	45.482	2285	53.36	-25.78	0.05	16.93
17.2	48.906	2107	48.14	-25.50	0.04	7.46
17.4	45.574	4231	96.24	-25.11	0.10	5.43
17.6	53.968	2127	48.49	-25.43	0.04	3.75
17.8	47.814	3855	87.57	-25.55	0.08	7.17
18.0	46.947	8031	184.19	-25.48	0.18	5.63
18.2	41.619	18875	450.71	-26.70	0.51	15.71
18.4	44.821	1409	32.01	-26.06	0.03	5.47
18.6	53.479	3048	69.72	-25.81	0.06	8.12
18.8	43.545	2089	47.47	-26.66	0.04	6.42
19.0	44.589	1653	37.60	-27.29	0.03	5.85
19.2	48.520	1434	32.87	-26.38	0.03	7.22
19.4	42.882	1766	40.49	-26.43	0.04	10.91
19.4R	35.603	2022	45.72	-27.06	0.05	12.97
19.6	47.461	4652	107.41	-25.87	0.10	9.67
19.8	48.185	2833	64.67	-25.83	0.06	8.00
20.0	41.475	2223	50.44	-26.06	0.05	7.62
20.2	51.339	2364	54.09	-25.72	0.04	6.96
20.4	40.616	3472	79.52	-25.79	0.09	26.17
20.6	50.670	2610	59.44	-25.85	0.05	10.00
20.8	36.110	7541	172.18	-26.31	0.22	11.23
21.0	42.110	9778	227.44	-26.02	0.25	10.36
21.2	52.009	2497	57.10	-26.65	0.05	9.35
21.4	42.386	3156	72.07	-26.08	0.07	9.95
21.6	42.130	2809	64.30	-25.68	0.07	8.08
21.8	36.364	9639	221.11	-27.39	0.26	22.89
22.0	29.113	16608	393.70	-27.45	0.58	3.50
22.2	52.190	1718	39.01	-25.21	0.03	1.67
22.2R	46.935	3946	88.54	-24.84	0.08	1.27
22.4	58.260	1350	30.81	-26.53	0.02	1.19
22.6	55.236	1230	27.25	-26.09	0.02	2.54
22.8	43.363	1446	32.74	-26.66	0.03	5.25
23.0	42.369	1722	39.00	-26.73	0.03	10.08
23.2	45.265	3654	82.68	-25.50	0.07	12.46

23.4	36.279	1754	39.96	-26.49	0.04	15.66
23.6	44.293	1859	42.13	-26.73	0.03	17.71
23.8	38.013	9041	205.73	-23.47	0.23	19.49
24.0	49.890	3670	84.05	-26.95	0.07	18.69

Appendix D: Analytical methods at the Arizona LaserChron Center, (https://sites.google.com/a/laserchron.org/laserchron.com)

Zircon crystals are extracted from samples by traditional methods of crushing and grinding, followed by separation with a Wilfley table, heavy liquids, and a Frantz magnetic separator. Samples are processed such that all zircons are retained in the final heavy mineral fraction. A large split of these grains (generally thousands of grains) is incorporated into a 1" epoxy mount together with fragments of the LaserChron Center Sri Lanka standard zircon. The mounts are sanded down to a depth of ~20 microns, polished, imaged, and cleaned prior to isotopic analysis.

U-Pb geochronology of zircons is conducted by laser ablation multicollector inductively coupled plasma mass spectrometry (LA-MC-ICPMS) at the Arizona LaserChron Center (Gehrels et al. 2006, 2008). The analyses involve ablation of zircon with a Photon Machines Analyte G2 excimer laser using a spot diameter of 30 microns. The ablated material is carried in helium into the plasma source of a Nu HR ICPMS, which is equipped with a flight tube of sufficient width that U, Th, and Pb isotopes are measured simultaneously. All measurements are made in static mode, using Faraday detectors with $3x10^{11}$ ohm resistors for ^{238}U, ^{232}Th, ^{208}Pb-^{206}Pb, and discrete dynode ion counters for ^{204}Pb and ^{202}Hg. Ion yields are ~0.8 mv per ppm. Each analysis consists of one 15-second integration on peaks with the laser off (for backgrounds), 15 one-second integrations with the laser firing, and a 30 second delay to purge the previous sample and prepare for the next analysis. The ablation pit is ~15 microns in depth.

For each analysis, the errors in determining $^{206}Pb/^{238}U$ and $^{206}Pb/^{204}Pb$ result in a measurement error of ~1-2% (at 2-sigma level) in the $^{206}Pb/^{238}U$ age. The errors in measurement of $^{206}Pb/^{207}Pb$ and $^{206}Pb/^{204}Pb$ also result in ~1-2% (at 2-sigma level) uncertainty in age for grains

that are >1.0 Ga, but are substantially larger for younger grains due to low intensity of the ^{207}Pb signal. For most analyses, the cross-over in precision of ^{206}Pb/^{238}U and ^{206}Pb/^{207}Pb ages occurs at ~1.0 Ga.

^{204}Hg interference with ^{204}Pb is accounted for by measurement of ^{202}Hg during laser ablation and subtraction of ^{204}Hg according to the natural ^{202}Hg/^{204}Hg of 4.35. Hg correction is not significant for most analyses because our Hg backgrounds are low (generally ~150 cps at mass 204).

Common Pb correction is accomplished by using the Hg-corrected ^{204}Pb and assuming an initial Pb composition from Stacey and Kramers (1975). Uncertainties of 1.5 for ^{206}Pb/^{204}Pb and 0.3 %?? for ^{207}Pb/^{204}Pb are applied to these compositional values based on the variation in Pb isotopic composition in modern crystal rocks.

Inter-element fractionation of Pb/U is generally ~5%, whereas apparent fractionation of Pb isotopes is generally <0.2%. In-run analysis of fragments of a large zircon crystal (generally every fifth measurement) with known age of 563.5 ± 3.2 Ma (2-sigma error) is used to correct for this fractionation. The uncertainty resulting from the calibration correction is generally 1-2% (2-sigma) for both ^{206}Pb/^{207}Pb and ^{206}Pb/^{238}U ages.

Concentrations of U and Th are calibrated relative to the Laserchron Center Sri Lanka zircon, which contains ~518 ppm of U and 68 ppm Th. Uncertainties are shown at the 1-sigma level, and include only measurement errors. Analyses that are >20% discordant (by comparison of ^{206}Pb/^{238}U and ^{206}Pb/^{207}Pb ages) or >5% reverse discordant are not considered further.

Appendix E: Youngest Zircon Ages from University of Houston

Location	Unit	Zircon Id.	206Pb/238U	SD 2σ
Thompson Canyon	Sego (n=303)	070214-20_56	75.2	3.2
		070214-20_170	77.6	5.0
		070214-20_05	78.5	3.4
		070214-20_285	79.1	4.7
		070214-20_338	83.9	3.0
		070214-20_74	84.5	4.2
		070214-20_334	85.0	2.9
		070214-20_06	85.6	2.6
		070214-20_370	85.8	4.2
		070214-20_357	86.5	4.2
		070214-20_23	87.5	3.2
		070214-20_26	88.0	2.6
		070214-20_51	88.3	3.7
		070214-20_52	88.6	3.2
		070214-20_18	89.2	3.7
		070214-20_221	89.5	3.9
		070214-20_296	89.6	2.7
		070214-20_359	90.0	3.6
	U Blackhawk (n=306)	070314-21_60	76.9	4.9
		070314-21_250	90.6	3.1
		070314-21_07	91.7	2.8
		070314-21_220	93.0	2.9
		070314-21_206	93.2	5.0
		070314-21_273	93.6	2.8
		070314-21_277	94.7	3.3
		070314-21_70	95.0	2.7
		070314-21_348	96.2	2.9
		070314-21_344	103.2	3.8
		070314-21_345	107.4	3.1
		070314-21_371	108.4	3.4
Tusher Canyon	Farrer (n=316)	070514-27_14	72.2	3.2
		070514-27_03	73.2	5.9
		070514-27_376	74.0	5.7
		070514-27_103	74.6	4.9
		070514-27_142	75.2	5.3
		070514-27_174	75.7	6.9
		070514-27_105	76.9	3.1
		070514-27_49	78.1	3.5

	Bluecastle (n=333)	070514-28_396	72.9	2.4
		070514-28_76	74.2	3.9
		070514-28_245	82.9	5.2
		070514-28_152	91.1	3.8
		070514-28_355	92.4	3.8
		070514-28_29	95.4	2.4
		070514-28_16	98.4	3.2
		070514-28_339	98.6	3.3
	Sego (n=309)	070414-26_18	73.7	3.3
		070414-26_28	74.4	3.0
		070414-26_367	75.0	3.5
		070414-26_239	75.2	3.3
		070414-26_316	78.3	3.8
		070414-26_75	79.1	3.1
		070414-26_354	80.6	3.0
		070414-26_176	83.5	5.7
		070414-26_36	85.4	3.8
		070414-26_374	87.3	3.6
		070414-26_165	88.5	3.5
		070414-26_396	89.8	3.4
		070414-26_110	90.0	4.0
	L Castlegate (n=327)	070414-25_243	94.2	6.8
		070414-25_213	101.6	4.2
		070414-25_357	164.0	8.4
		070414-25_140	200.6	7.2
	U Blackhawk (n=304)	070514-30_324	71.9	4.6
		070514-30_154	78.5	3.1
		070514-30_54	81.5	3.7
		070514-30_95	88.7	2.5
		070514-30_303	92.6	3.7
		070514-30_182	92.9	3.5
		070514-30_226	98.5	4.2

Appendix F: Blackhawk Formation, Zircon Ages from ExxonMobil Upstream Research

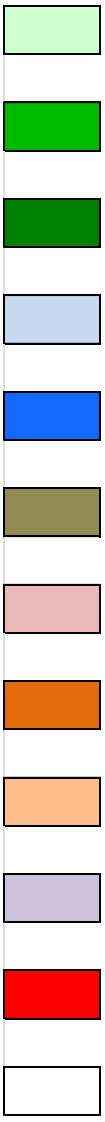

Cretaceous Western Cordillera

Jurassic Western Cordillera

Triassic Western Cordillera

Appalachian-Taconic-Acadian-Alleghanian (~290-500 Ma)

Appalachian-Gondwanan (500-700 Ma)

Grenville (950-1300 Ma)

Mid-Continent Granite-Rhyolite Province (1300-1500 Ma)

Yavapai-Mazatzal Orogens (1600-1800 Ma)

Penokean-Trans Hudson Orogens (1800-2000 Ma)

Appalachian-Gondwanan? (2000-2200 Ma)

Archaean Shield (>2400 Ma)

unknown

Appendix F: Blackhawk Formation, Youngest Zircon Ages from ExxonMobil Upstream Research

Formation: Blackhawk							
Location: Horse Canyon				Location: Tusher Canyon			
Unit: Upper Blackhawk		**Unit: Upper Blackhawk**		**Unit: Grassy LSF**		**Unit: Desert FLV**	
ID: BC-10		ID: BC-11		ID: BC-01		ID: BC-03	
206Pb/238U	SD 2σ	206Pb/238U	SD 2σ	206Pb/238U	SD 2σ	206Pb/238U	SD 2σ
76.0	2.8	76.2	3.0	81.9	2.3	79.3	3.9
76.6	3.4	77.1	2.5	88.5	1.7	78.5	3.6
76.9	3.5	77.3	3.3	89.6	3.4	78.8	2.6
77.0	3.1	77.3	3.7	90.2	4.0	79.3	1.6
77.4	6.5	80.7	2.4	90.7	3.2	79.5	3.1
77.5	1.2	85.9	2.8	91.5	3.0	79.8	4.9
79.2	1.6	88.9	1.1	91.6	2.6	79.9	1.7
89.8	0.8	90.9	1.4	91.8	1.9	80.5	1.8
95.0	2.6	91.5	1.9	95.6	5.1	93.5	3.0
109.5	0.8	92.0	5.3	96.5	1.9	93.9	1.4
162.5	2.5	92.9	1.0	96.6	3.5	95.7	3.2
187.5	8.7	93.3	1.7	97.2	3.4	95.8	1.5
213.2	9.4	93.6	4.7	97.4	7.5	95.9	1.6
244.9	5.4	93.8	6.3	100.2	2.8	96.7	1.6
260.4	7.1	93.8	3.2	100.4	6.2	98.2	3.3
311.1	15.4	94.0	1.6	100.7	1.4	98.2	1.3
315.5	4.3	97.2	3.4	101.5	3.7	98.4	1.9
360.6	6.9	97.3	4.2	157.2	4.7	98.6	3.4
410.6	8.1	97.6	1.7	306.5	5.6	98.6	2.0
417.6	8.7	97.6	2.8	317.1	5.2	98.8	1.8
424.2	11.5	97.7	1.2	332.4	8.3	99.1	2.1
454.5	10.8	97.7	1.4	358.3	12.1	99.7	1.1
459.4	6.0	97.9	3.0	360.4	16.7	101.2	1.8
468.4	13.0	98.0	3.5	370.9	8.1	103.2	1.2
589.3	20.6	99.8	3.1	375.1	9.2	105.2	2.3
625.4	7.4	101.8	5.8	380.5	7.6	110.7	1.4
949.5	24.5	102.6	2.7	402.6	10.3	113.0	3.0
1003.2	69.6	103.5	2.3	404.7	9.6	166.8	1.9
1036.1	14.1	107.9	3.9	407.6	9.2	168.3	4.8
1037.8	6.7	156.4	1.9	411.5	12.1	175.3	2.9
1046.1	18.9	159.3	3.0	419.1	4.4	216.6	6.2
1048.2	36.8	165.3	9.4	420.8	9.9	224.0	19.7

Appendix F: Blackhawk Formation, Youngest Zircon Ages from ExxonMobil Upstream Research

1050.3	22.2	168.9	12.8	427.2	23.3	237.5	1.6
1051.2	126.8	246.2	11.0	429.0	6.8	254.7	5.2
1055.0	37.2	262.1	2.3	429.2	6.1	268.7	3.2
1058.8	39.6	290.4	5.7	431.4	4.5	294.3	15.2
1060.1	100.2	335.8	6.5	433.8	10.7	308.6	3.5
1061.0	22.3	340.0	8.4	437.1	9.2	330.9	13.6
1061.9	23.0	396.6	12.9	446.5	8.7	359.5	8.5
1062.9	40.7	407.7	6.9	447.3	24.0	380.9	4.3
1065.6	7.3	408.8	5.9	447.9	13.8	404.6	8.3
1070.8	63.0	411.7	8.9	472.9	6.5	407.0	6.5
1071.1	19.2	416.0	13.7	481.1	15.7	413.5	7.8
1072.0	43.4	419.7	4.2	500.6	17.8	415.2	6.0
1072.3	31.4	425.1	11.9	501.4	7.2	418.1	5.0
1073.8	18.7	426.3	4.0	520.2	17.4	420.5	5.2
1074.7	34.2	445.3	13.3	538.5	6.3	421.3	5.4
1075.7	14.4	447.7	11.2	555.3	8.3	422.2	6.6
1075.8	43.6	472.3	29.3	575.9	22.2	424.6	3.5
1077.6	126.1	482.4	13.6	585.1	8.2	434.3	10.0
1079.3	17.6	486.5	7.1	599.9	13.8	438.0	14.0
1083.0	78.4	514.4	13.5	629.6	10.1	440.7	5.5
1083.4	20.8	575.2	19.2	659.7	14.3	452.3	2.6
1084.6	41.3	575.7	9.4	689.4	15.1	469.5	30.6
1084.7	64.2	600.5	9.0	917.0	62.1	525.2	6.4
1084.8	25.1	633.3	10.2	937.5	31.3	542.7	8.1
1087.8	24.8	641.5	18.2	946.9	92.3	560.2	3.3
1094.1	10.6	935.6	81.8	967.0	65.3	618.4	7.9
1094.7	24.1	957.7	48.9	969.1	59.2	652.8	17.9
1096.6	53.4	961.4	11.1	976.4	58.6	1018.0	14.7
1098.2	14.3	1029.7	124.5	1004.0	49.7	1028.8	22.5
1099.0	42.9	1035.0	101.2	1005.4	59.0	1037.5	17.5
1099.6	8.7	1045.3	9.3	1020.2	7.4	1037.8	55.6
1101.9	95.8	1053.1	9.9	1021.7	93.3	1059.2	26.2
1105.1	68.6	1062.2	44.0	1033.2	13.4	1060.0	57.3
1106.3	32.6	1069.6	53.7	1036.2	57.9	1064.2	17.0
1107.3	27.4	1070.4	6.3	1038.2	18.1	1071.4	20.6
1109.1	18.1	1070.9	40.1	1039.4	19.9	1087.1	15.1
1113.4	87.1	1103.8	145.8	1040.9	30.6	1092.9	29.2
1116.8	19.3	1121.2	24.3	1046.0	13.2	1099.4	30.3
1117.2	12.5	1132.8	47.3	1050.3	104.7	1101.5	15.4

1119.1	19.9	1133.5	12.7	1064.0	23.1	1104.3	16.5
1122.6	38.6	1135.2	36.9	1068.4	51.1	1112.9	56.9
1123.2	16.1	1139.7	16.9	1076.8	32.9	1127.0	18.3
1123.5	64.0	1141.1	19.9	1080.5	22.2	1130.5	36.7
1126.0	18.1	1146.8	9.7	1085.1	45.6	1138.9	50.9
1126.1	26.4	1215.9	16.9	1104.0	16.5	1142.7	23.6
1129.9	131.1	1220.7	94.8	1110.4	52.6	1174.5	28.2
1130.6	18.9	1245.1	99.5	1114.4	65.3	1192.5	29.6
1133.5	77.0	1250.3	24.3	1132.2	34.6	1193.9	10.1
1134.2	68.2	1286.7	50.3	1150.8	25.5	1200.9	26.0
1134.6	16.8	1317.1	66.4	1167.2	21.2	1214.4	18.9
1150.5	54.0	1329.1	16.2	1168.0	35.0	1269.9	25.2
1150.7	74.4	1369.8	32.8	1168.9	17.4	1293.3	25.4
1155.4	144.1	1370.5	10.9	1176.1	7.3	1305.7	14.1
1155.8	46.6	1378.0	9.7	1218.3	16.1	1320.3	33.7
1179.1	31.1	1380.8	18.1	1237.5	13.8	1325.3	28.6
1183.1	21.2	1386.6	11.9	1243.3	22.5	1370.5	19.9
1190.9	40.8	1416.6	46.0	1267.2	17.3	1371.0	7.6
1193.9	54.8	1425.2	22.8	1269.9	32.1	1375.8	11.9
1196.9	23.0	1434.7	29.7	1302.9	34.1	1387.8	5.0
1206.7	19.9	1435.0	11.8	1316.4	46.8	1389.4	20.9
1207.8	13.9	1444.1	32.8	1322.3	21.9	1389.8	36.7
1212.0	82.0	1454.1	14.5	1331.8	26.7	1411.7	6.7
1230.0	18.3	1501.6	12.2	1332.2	62.2	1418.4	13.2
1244.5	13.1	1502.3	30.5	1336.4	11.9	1419.5	34.1
1288.9	11.7	1510.5	19.6	1357.1	44.5	1431.3	4.6
1291.0	75.9	1513.7	50.1	1367.6	19.1	1434.1	4.2
1362.4	34.6	1580.0	37.7	1394.3	39.0	1434.4	15.9
1362.6	114.2	1611.6	16.0	1395.2	49.2	1435.1	14.3
1365.1	22.3	1625.1	8.0	1474.1	35.9	1441.3	34.0
1368.2	78.1	1638.4	8.4	1477.0	4.6	1443.2	61.2
1382.7	22.5	1642.1	22.7	1521.9	23.0	1444.1	6.7
1384.9	45.3	1649.2	10.2	1546.0	19.2	1447.4	34.7
1388.9	23.9	1651.1	31.3	1549.3	10.9	1458.9	10.4
1419.3	33.5	1656.8	16.0	1583.3	6.7	1472.8	32.0
1422.0	19.8	1664.7	12.0	1593.9	19.4	1493.5	9.7
1430.4	40.7	1669.1	7.5	1602.7	11.6	1566.2	6.7
1430.7	16.7	1695.2	11.6	1622.9	13.8	1576.6	29.6
1433.3	17.6	1706.9	19.9	1630.9	19.6	1621.9	5.1

Appendix F: Blackhawk Formation, Youngest Zircon Ages from ExxonMobil Upstream Research

1434.0	20.5	1717.5	3.3	1632.7	4.7	1626.8	4.9
1434.6	13.3	1719.6	2.9	1642.2	11.7	1629.4	11.8
1438.9	17.7	1726.0	5.4	1646.0	10.8	1667.2	14.3
1439.6	12.0	1734.5	11.6	1648.8	14.3	1672.4	12.0
1440.1	17.9	1759.9	26.8	1651.1	19.2	1687.6	5.9
1440.5	27.9	1788.9	18.2	1651.8	38.4	1694.0	4.8
1440.6	13.2	1789.5	16.9	1653.4	15.8	1707.0	5.0
1442.7	23.2	1808.4	4.8	1653.6	6.6	1737.3	28.2
1444.8	6.5	1814.6	20.0	1660.0	29.2	1747.2	22.0
1445.5	11.4	1856.2	7.2	1662.3	23.0	1752.8	5.3
1445.6	11.7	1891.0	9.2	1684.4	13.6	1755.5	4.2
1448.2	16.5	1892.6	6.3	1709.4	5.3	1778.6	10.2
1449.5	10.6	1948.7	2.6	1721.8	20.2	1781.0	4.0
1450.8	19.3	1959.4	9.0	1728.1	15.0	1785.3	4.9
1452.2	13.7	1987.9	6.1	1734.0	7.9	1787.7	5.1
1452.4	20.4	2079.2	32.3	1741.9	8.1	1791.5	4.5
1476.7	33.4	2173.3	22.5	1743.0	172.6	1802.0	5.2
1510.9	15.9	2444.2	7.3	1789.3	4.2	1804.6	4.7
1519.6	49.2	2448.1	5.5	1798.7	11.0	1834.5	9.6
1520.6	25.9	2588.6	9.9	1810.7	3.5	1862.8	18.2
1548.3	29.0	2605.2	55.4	1829.7	5.3	1926.5	3.7
1607.8	10.1	2633.0	2.7	1864.1	6.9	2452.8	5.0
1617.1	38.0	2857.9	5.8	1865.0	20.4	2509.6	6.3
1633.8	12.5	2858.0	2.8	1916.7	15.9	2672.9	3.0
1672.3	14.0	2949.5	3.2	1938.4	38.5	2687.7	13.0
1676.7	44.6	2963.4	5.2	2630.7	1.8	2719.1	5.1
1682.3	6.6	3126.1	7.4	2726.0	7.6	2858.6	6.8
1684.3	6.4			2748.6	13.4		
1688.2	27.6			2772.2	4.6		
1688.4	16.4			2832.6	8.3		
1692.2	19.4			2851.8	3.1		
1693.7	6.6			2873.7	59.8		
1694.5	16.0			2879.4	12.9		
1696.5	13.8			3203.8	3.7		
1698.3	26.2						
1699.4	8.9						
1699.8	9.0						
1701.6	17.4						
1706.7	16.1						

1707.8	15.7						
1711.3	11.2						
1714.8	8.3						
1714.9	13.9						
1719.2	13.6						
1720.1	6.5						
1729.0	15.6						
1743.5	21.3						
1765.8	7.1						
1766.8	33.9						
1775.0	8.6						
1779.0	11.0						
1787.7	8.1						
1793.5	9.7						
1793.8	10.3						
1825.3	4.4						
1827.9	14.0						
1832.2	18.8						
1837.0	17.8						
1844.0	11.7						
1844.9	13.7						
1851.4	31.2						
1868.8	16.9						
1877.6	20.0						
1902.3	8.9						
1916.4	9.6						
1925.8	7.0						
1933.6	11.2						
1936.0	19.6						
1955.9	15.3						
2001.4	8.4						
2053.2	4.6						
2533.8	6.8						
2565.4	18.9						
2680.3	9.2						
2689.1	5.1						
2700.1	10.3						
2805.0	10.4						
2954.5	10.1						

Appendix F: Blackhawk Formation, Youngest Zircon Ages from ExxonMobil Upstream Research

Appendix G: Castlegate Sandstone, Zircon Ages from ExxonMobil Upstream Research

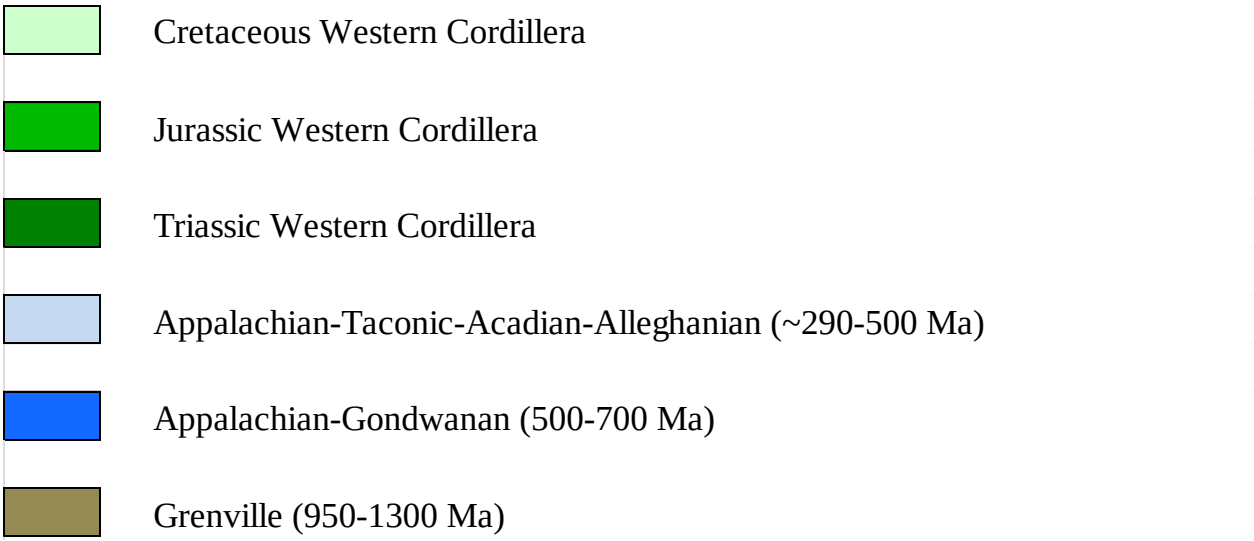

Formation: Castlegate Sandstone									
Location: Horse Canyon						Location: Tusher Canyon			
Unit: Upper Castlegate Fluvial		Unit: Middle Castlegate Fluvial		Unit: Lower Castlegate Fluvial		Unit: Castlegate Fluvial		Unit: Lower Sego Fluvial-IHS	
ID: BC-09		ID: BC-07		ID: BC-08		ID: BC-05		ID: BC-06	
206Pb/238U	SD 2σ	206Pb/238U	SD 2σ	206Pb/238U	SD 2σ	206Pb/238U	SD 2σ	206Pb/238U	SD 2σ
72.6	3.9	171.0	9.3	62.4	1.4	90.1	2.2	79.2	3.6
74.1	7.3	241.5	3.8	86.6	1.6	95.9	1.2	80.8	3.6
74.2	6.3	262.5	11.5	92.2	4.3	197.2	9.0	88.1	0.6
74.7	3.4	284.6	18.3	92.7	3.6	220.9	2.9	88.4	3.0
75.5	2.3	307.7	8.4	93.5	1.3	226.0	3.3	89.6	2.5
75.6	3.3	363.4	5.7	93.5	4.6	226.2	5.2	90.5	1.5
75.7	3.4	369.7	13.4	93.6	1.4	226.2	4.0	91.6	3.4
75.7	4.9	375.2	8.9	93.9	1.5	230.0	16.7	93.5	1.7
76.4	4.2	380.9	5.3	94.0	1.7	242.8	5.9	94.2	2.2
76.6	2.2	387.2	10.0	95.1	4.5	271.2	5.9	95.0	6.0
77.9	8.1	400.1	15.3	95.5	2.0	313.0	16.2	95.0	2.5
78.1	3.2	412.0	8.6	96.3	2.9	346.3	10.7	95.1	3.9
78.3	4.1	412.7	31.7	97.6	3.4	356.6	7.1	95.2	5.5
86.9	2.6	413.8	11.8	97.7	4.4	364.9	10.3	95.7	1.9
88.4	1.8	430.3	7.2	99.0	5.9	377.9	8.6	95.8	2.2
92.3	4.9	433.1	8.9	99.1	2.0	399.6	14.7	96.3	1.7
97.4	5.2	441.6	6.1	99.2	3.0	415.2	8.6	96.8	1.4
99.1	2.4	447.6	5.5	100.2	3.0	415.3	6.2	96.9	1.2
112.8	2.0	450.7	6.1	102.3	3.7	415.4	9.0	97.9	3.0
163.3	4.7	458.8	12.1	103.3	2.0	419.7	8.0	98.0	1.4
212.7	6.6	533.7	5.7	103.4	2.7	423.6	6.1	98.0	2.2
222.3	5.4	558.8	14.8	107.8	1.3	426.5	6.4	98.6	3.2
229.1	7.6	565.3	19.0	120.4	5.1	430.1	8.9	101.0	2.7
238.4	13.3	627.1	9.6	145.6	2.6	432.7	5.0	152.1	3.5
239.6	4.8	653.5	8.6	156.8	1.6	438.0	5.1	159.9	2.1
243.0	5.7	701.1	20.7	156.8	1.7	440.3	8.1	243.7	3.2
246.5	7.9	992.7	41.9	157.8	4.5	442.8	5.2	310.2	7.5
251.1	4.1	1017.4	49.7	157.8	5.2	463.8	9.3	315.7	6.9
265.3	12.0	1044.2	44.0	159.1	2.5	463.9	6.5	325.5	6.6
287.6	4.0	1047.1	67.6	159.4	3.1	469.4	9.8	372.5	21.9
419.5	14.8	1049.2	140.2	159.6	4.4	476.7	12.0	386.1	16.4
421.4	3.1	1057.6	41.4	159.7	1.5	553.3	10.0	408.7	4.0
432.2	11.7	1059.0	42.5	160.9	3.4	557.3	3.7	409.6	4.7
437.0	16.1	1067.1	32.8	161.2	4.2	557.6	26.4	418.9	2.7
467.1	8.1	1075.9	13.5	161.5	3.3	586.7	17.2	422.0	8.9
519.3	9.1	1077.6	14.9	161.8	3.3	591.7	10.5	430.3	8.1
627.6	30.8	1078.7	11.2	163.1	3.6	610.3	10.9	435.8	5.8
710.3	6.9	1080.7	20.4	235.3	5.0	619.4	5.7	440.3	8.0

960.3	102.6	1082.3	28.4	247.1	2.8	627.9	6.2	447.6	7.8
985.3	58.5	1085.6	40.4	265.0	5.2	628.6	4.8	454.5	33.8
988.9	41.5	1086.0	23.8	362.2	31.0	640.9	10.6	454.6	8.1
999.7	159.3	1090.0	35.7	422.2	9.1	991.6	77.4	456.7	11.0
1003.2	56.9	1091.5	40.5	426.8	4.7	997.3	108.7	513.3	8.3
1003.7	59.6	1091.5	53.9	433.8	4.7	1011.2	44.0	529.7	3.9
1016.3	22.6	1094.5	71.1	435.9	13.9	1019.3	28.6	628.5	6.5
1022.3	30.2	1094.7	59.2	436.0	11.6	1040.7	103.6	660.9	12.5
1026.3	10.4	1098.1	85.4	441.3	5.8	1046.6	18.1	678.8	4.7
1028.7	64.1	1105.7	68.0	459.6	6.4	1051.5	16.2	732.0	16.4
1029.9	52.0	1113.3	11.7	460.2	16.6	1052.1	61.6	998.4	32.1
1030.0	25.7	1114.1	30.1	517.0	6.7	1053.4	11.5	1007.1	40.0
1030.4	63.5	1120.2	49.3	523.7	12.8	1053.9	91.7	1009.0	22.4
1032.4	32.6	1124.6	91.7	524.5	9.5	1054.2	18.6	1028.0	30.4
1040.7	18.9	1127.2	41.2	541.6	6.9	1058.3	39.1	1033.0	26.8
1041.5	12.6	1130.7	27.0	552.5	7.6	1059.7	19.4	1037.1	8.2
1046.4	93.6	1158.7	12.3	559.8	11.0	1068.5	37.4	1038.6	18.9
1046.7	33.4	1165.8	20.5	609.5	5.7	1073.6	76.5	1039.1	24.3
1047.6	33.3	1195.4	144.2	612.0	13.6	1073.6	39.5	1042.0	24.9
1049.3	62.0	1201.6	126.1	626.8	15.7	1074.8	69.5	1058.6	34.3
1055.8	156.0	1256.4	42.0	631.9	12.3	1076.5	147.3	1073.6	49.9
1055.9	75.5	1262.9	17.8	735.6	12.4	1078.5	58.0	1132.5	15.5
1059.1	40.8	1280.5	40.0	773.4	11.8	1085.1	11.3	1132.8	22.8
1063.1	26.8	1329.2	3.1	877.7	16.3	1086.5	73.7	1169.5	94.8
1069.5	77.8	1352.7	42.2	945.0	11.9	1087.5	31.5	1218.5	53.0
1074.0	44.4	1354.1	76.0	964.4	22.9	1087.6	20.1	1261.7	75.5
1074.5	27.1	1357.8	28.3	999.3	43.6	1088.1	14.9	1306.9	49.4
1076.9	36.0	1374.6	23.1	1004.7	18.3	1095.5	47.6	1374.2	21.2
1077.6	78.1	1384.3	21.5	1006.7	13.6	1100.1	71.6	1380.8	16.2
1080.9	146.1	1392.6	20.0	1010.4	45.0	1101.1	136.0	1383.7	18.1
1082.3	111.7	1417.1	48.7	1025.2	54.1	1106.9	14.5	1385.8	13.8
1084.9	28.9	1432.7	9.4	1040.9	28.8	1108.7	193.4	1429.5	27.2
1087.6	16.2	1435.2	27.8	1041.4	138.9	1111.3	19.2	1431.6	9.1
1088.1	119.4	1437.0	6.1	1042.8	36.0	1114.8	13.8	1432.0	9.2
1088.6	17.1	1437.6	20.2	1043.5	63.1	1116.2	38.3	1443.2	19.8
1091.8	24.1	1439.2	19.7	1048.7	17.2	1116.6	38.9	1446.9	11.6
1091.9	31.8	1442.3	46.9	1074.0	15.1	1119.5	53.9	1448.8	33.3
1094.3	6.3	1450.4	18.8	1083.3	42.1	1127.4	7.2	1450.2	3.6
1095.2	8.9	1452.0	35.2	1096.9	29.3	1130.3	50.6	1467.5	4.6
1097.2	13.4	1452.0	24.8	1108.0	71.1	1130.8	54.2	1486.4	5.1
1098.8	26.0	1452.6	31.3	1120.0	23.8	1133.0	28.7	1497.5	8.8
1099.0	10.1	1455.9	19.7	1124.8	59.7	1135.0	8.8	1515.4	25.8
1099.8	64.9	1479.5	23.6	1143.5	19.2	1136.6	71.0	1523.4	13.4
1100.9	62.8	1481.6	21.3	1158.6	211.7	1139.6	24.4	1526.4	30.5
1102.5	23.2	1501.3	6.0	1161.1	117.5	1142.0	34.0	1532.0	53.2
1106.4	29.2	1602.8	18.0	1209.7	13.3	1155.4	87.9	1551.2	39.3
1106.6	48.6	1605.0	9.5	1210.1	170.2	1155.7	8.7	1581.0	5.4
1107.2	38.7	1628.2	63.2	1275.7	53.7	1158.0	41.2	1616.1	69.7

1107.4	32.1	1631.9	36.8	1302.3	28.6	1159.1	15.1	1634.8	3.7
1108.2	27.8	1641.0	12.4	1357.5	25.4	1159.5	92.2	1653.1	18.9
1108.4	81.6	1646.2	28.2	1365.9	33.9	1171.0	24.8	1658.8	5.5
1109.9	18.6	1648.2	43.9	1366.8	11.3	1173.9	11.2	1665.5	13.4
1110.8	112.4	1650.4	21.3	1383.2	12.7	1183.6	23.4	1667.2	17.5
1111.6	42.0	1670.6	15.5	1385.3	10.8	1204.2	7.2	1668.2	6.7
1111.6	83.8	1681.6	13.0	1387.0	16.9	1239.6	10.4	1673.0	48.3
1111.8	78.2	1693.7	14.4	1391.6	24.6	1252.5	5.7	1673.1	20.0
1112.7	44.0	1694.1	19.3	1400.4	15.1	1268.6	203.9	1673.7	5.2
1115.4	74.1	1695.3	21.2	1415.2	39.6	1273.2	59.7	1683.5	6.9
1115.6	19.8	1695.8	27.9	1417.1	18.9	1290.1	29.5	1688.9	14.7
1115.6	17.4	1703.2	6.4	1420.6	19.3	1295.0	173.2	1699.6	13.0
1117.7	52.7	1719.2	5.3	1432.9	12.7	1334.4	5.5	1701.9	17.8
1121.7	11.6	1720.0	22.9	1436.6	29.8	1339.6	23.5	1705.2	11.5
1124.9	48.7	1720.2	12.2	1439.2	10.7	1366.2	48.0	1708.6	8.6
1125.7	51.0	1720.9	82.0	1446.8	30.2	1369.5	20.9	1709.6	9.1
1130.1	43.3	1722.6	13.1	1449.1	23.7	1376.0	26.4	1717.9	4.5
1133.1	38.0	1733.4	12.7	1453.1	54.1	1380.8	31.4	1718.1	9.2
1133.9	37.7	1752.9	8.1	1468.4	11.9	1381.1	6.9	1718.3	3.2
1139.5	52.7	1759.8	9.9	1495.5	8.4	1381.3	23.7	1722.1	10.9
1141.1	37.9	1782.8	82.4	1500.8	11.0	1392.5	8.2	1723.0	12.0
1141.2	44.4	1786.6	4.2	1601.6	6.2	1395.6	11.7	1723.9	6.2
1147.2	36.5	1833.6	19.9	1630.3	5.9	1410.7	45.1	1728.5	12.9
1149.3	74.4	1834.4	14.9	1646.8	7.6	1416.4	8.7	1730.6	10.4
1154.9	151.0	1838.6	9.1	1659.9	3.3	1440.0	8.1	1732.1	4.8
1155.1	108.4	1850.9	13.9	1659.9	11.6	1441.1	9.6	1733.4	12.1
1172.1	88.4	1874.0	33.8	1668.2	5.8	1442.7	12.1	1735.2	9.1
1175.3	49.2	1904.2	73.6	1669.6	12.9	1444.1	6.0	1739.7	7.0
1182.6	50.2	1927.8	5.9	1689.3	22.9	1445.3	9.8	1744.3	6.8
1184.2	78.6	2070.3	33.6	1696.4	6.1	1449.5	5.1	1746.5	13.5
1197.0	85.2	2073.6	24.9	1705.6	8.3	1487.1	24.7	1754.9	14.0
1228.1	28.2	2178.3	57.8	1706.3	12.7	1497.6	32.4	1781.4	15.4
1228.2	64.7	2250.6	13.8	1709.6	6.7	1505.4	5.1	1782.9	35.0
1229.8	35.8	2585.8	18.6	1717.7	12.4	1528.5	18.5	1798.4	5.4
1242.0	44.2	2695.2	9.0	1770.2	8.8	1578.7	54.8	1824.3	7.2
1310.8	35.1	2721.4	10.1	1778.4	3.6	1606.4	25.9	1834.7	15.2
1355.4	105.8	2760.5	21.9	1779.3	7.2	1628.6	9.6	1868.6	7.6
1373.2	44.0	2773.0	5.5	1781.5	5.8	1629.5	53.9	1895.6	12.3
1378.5	17.5	2986.2	5.2	1782.8	6.6	1641.4	6.4	1943.8	10.5
1379.2	9.2	3220.7	2.7	1787.4	15.4	1644.0	11.8	1978.8	6.2
1379.6	13.5	3622.0	5.1	1804.3	10.2	1644.9	3.8	2028.7	7.5
1383.3	45.7			1824.3	9.3	1682.3	31.5	2052.6	11.7
1383.9	22.0			1835.9	18.0	1684.9	21.8	2076.7	9.2
1404.0	28.6			1857.5	29.1	1686.8	13.3	2415.3	6.7
1405.8	15.2			1865.1	21.7	1697.6	11.6	2470.6	8.1
1407.0	22.2			1876.6	13.2	1709.3	9.1	2556.3	3.8
1409.1	48.2			1877.5	28.4	1732.3	5.6	2624.6	87.1
1415.3	17.6			1895.9	38.8	1734.3	35.7	2627.1	0.9

1415.3	23.1			1918.2	7.5	1739.5	16.0	2646.3	5.7
1418.7	61.7			1922.0	16.3	1746.1	9.6	2691.8	4.7
1420.2	24.1			1933.8	19.1	1749.7	11.1	2727.3	3.8
1427.3	13.4			1964.0	9.1	1749.9	4.2	2769.9	3.7
1428.4	27.3			1998.0	4.3	1776.6	4.6	2771.5	5.7
1429.1	36.0			2106.1	7.6	1781.5	7.5	2776.8	2.7
1429.5	11.4			2171.2	7.1	1786.5	7.0		
1433.3	11.4			2229.1	12.7	1801.2	13.7		
1434.3	7.5			2264.8	38.5	1813.6	46.2		
1435.2	21.8			2311.8	18.5	1834.6	12.2		
1436.4	16.6			2347.4	5.4	1835.8	43.6		
1437.8	20.5			2361.9	26.9	1835.9	16.8		
1440.2	10.0			2382.5	4.6	1836.6	18.9		
1442.6	11.2			2441.8	8.1	1843.8	8.8		
1443.6	12.0			2699.4	3.0	1845.3	11.8		
1447.0	10.7			2728.7	12.4	1850.8	8.9		
1448.1	11.6			2755.2	5.4	1912.3	57.6		
1449.2	8.7			2837.5	18.5	1921.3	11.9		
1450.4	9.0			2956.8	21.7	1926.5	28.6		
1479.2	35.9					1927.5	7.4		
1511.9	69.2					1961.4	9.9		
1662.8	17.5					1963.2	10.1		
1663.8	15.4					1991.3	2.3		
1684.9	10.1					2002.7	5.1		
1688.4	10.1					2085.4	6.4		
1690.1	12.5					2090.0	20.1		
1693.1	13.0					2271.0	38.1		
1693.2	17.6					2703.1	6.5		
1695.2	46.9					2703.7	5.3		
1700.8	17.1					2717.4	6.5		
1701.1	40.8					2732.7	4.6		
1706.1	22.4								
1707.8	11.7								
1708.3	11.1								
1711.1	22.6								
1712.3	24.6								
1712.8	15.3								
1718.2	8.4								
1718.2	16.1								
1757.0	30.6								
1774.3	26.0								
1775.2	33.6								
1775.4	14.8								
1778.0	15.5								
1780.0	25.0								
1781.6	7.9								
1782.4	14.2								
1782.8	16.5								

1783.8	20.4								
1817.9	45.9								
1831.3	21.1								
1837.9	7.7								
1838.8	9.7								
1843.8	25.5								
1846.3	7.8								
1857.1	14.8								
1889.2	55.9								
1911.3	55.1								
1924.9	29.5								
1933.9	7.1								
1939.4	50.3								
1946.4	19.5								
2032.8	40.6								
2075.7	39.0								
2098.1	9.5								
2111.4	8.4								
2627.9	2.7								
2658.2	8.4								
2713.6	4.5								
2769.2	7.7								
2801.9	9.5								